STUDY OF DIELECTRIC PROPERTIES OF DOPED BARIUM TITANATES

M. Phil. Thesis
(Physics)

By

MOHAMMED KAMRUL HAQUE BHUIYAN
Roll No. 040214022F
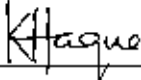Session: April 2002

#103153#

DEPARTMENT OF PHYSICS
BANGLADESH UNIVERSITY OF ENGINEERING AND TECNOLOGY (BUET)
DHAKA-1000, BANGLADESH.

CANDIDATE'S DECLARATION

It is hereby declared that this thesis or any part of it has not been submitted elsewhere for the award of any degree or diploma.

Date: 19 February, 2007
BUET, DHAKA
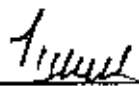
(Mohammed Kamrul Haque Bhuiyan)

BANGLADESH UNIVERSITY OF ENGINEERING AND TECHNOLOGY
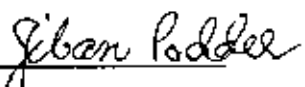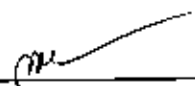## Department of Physics, Dhaka-1000, Bangladesh

Certification of Thesis Work

The thesis titled "STUDY OF DIELECTRIC PROPERTIES OF DOPED BARIUM TITANATES" submitted by Mohammed Kamrul Haque Bhuiyan , Roll No: 040214022F, Session: April/2002, has been accepted satisfactory in partial fulfillment of the requirement for the degree of Master of Philosophy in Physics on 19 February, 2007.

Board of Examiners

1.

Dr. Mominul Huq   Chairman
Professor, Department of Physics, BUET, Dhaka
(Supervisor)

2.

Dr. Jiban Podder   Member (Ex-Officio)
Professor and Head
Department of Physics, BUET, Dhaka

3.

Dr. Md. Abu Hashan Bhuiyan   Member
Professor, Department of Physics, BUET, Dhaka

4.

Dr. Md. Tafazzal Hussain   Member (External)
Professor
Department of Physics
University of Dhaka

Acknowledgements

Md. Kamrul Haque Bhuiyan
Dhaka
February, 2007.

ABSTRACT

In the present research work the doped $BaTiO_3$ were prepared by conventional mixed oxide method. The doping elements were Calcium, Strontium, Chromium and Vanadium. The doping levels were 0.1 and 0.025 mole fraction. The samples were sintered at 1300°C. Effect of doping, concentration and milling procedure on the dielectric properties of $BaTiO_3$ based ceramics were studied. The dielectric constant and dielectric loss were measured in the frequency range of 0.5 kHz to 13 MHz at room temperature. The highest value of the dielectric constant for sample $Ba(Ti_{.975}Cr_{.025})O_3$ was found 2729 and the lowest value for the sample$Ba_{.9}Sr_{.1}$ $(Ti_{.975}V_{.025})$ was found 14.57. The value of dielectric constant was found higher at low frequency and almost the same at 100 KHz, the dielectric constant is lower at high frequencies.Pure$BaTiO_3$ exhibits the curie temperature at 65°C.Thesample $Ba(Ti_{.975}Cr_{.025})O_3$, $Ba_{.9}Sr_{.1}$ $(Ti_{.975}Cr_{.025})O_3$, $Ba_{.8}Ca_{.1}Sr_{.1}(Ti_{.975}Cr_{.025})O_3$ and $Ba_{.8}Ca_{.1}Sr_{.1}(Ti_{.975}V_{.025})O_3$ exhibits the curie temperature 80°C at fixed frequency 1 MHz. The sample $(Ti_{0.975}V_{0.025})O_3$ exhibits the maximum curie temperature 110°C at fixed frequency1MHz. The sample $Ba_{.9}Sr_{.1}$ $(Ti_{.975}V_{.025})O_3$ exhibits the dielectric constant 90°C. The maximum dielectric loss was 2.74 for the sample $Ba_{.8}Ca_{.1}Sr_{.1}(Ti_{.975}Cr_{.025})O_3$ the minimum dielectric loss was 0.034 for the sample $Ba_{.9}Sr_{.1}(Ti_{.975}Cr_{.025})O_3$ at 13 MHz. Dielectric measurement also indicates that curie temperature for doped sample is larger than the pure undoped $BaTiO_3$ sample. From the present investigation it is observed that the substitution of dopant having larger ionic radius increases the dielectric constant. Dielectric constant has dependence on the grain size thereby ball milling time. It is observed that dielectric constant is higher for 24 hours ball milling samples.

CONTENTS

List of Figures

List of Tables

CHAPTER 1

Introduction

The ferroelectric and dielectric properties of BaTiO$_3$ with the perovskite structure are of utmost importance in the electronic industry [1]. Barium titanate was the first piezoelectric ceramic developed and is still widely used [2]. Ferroelectric materials play an essential role in the technological development. These materials offer a very high resistance to the passage of electric current under the action of the applied voltage and therefore sharply differ in their basic electric properties from conducting materials. They are chemically more stable than other dielectric material and have the obvious advantage of easy manufacture by ceramic technique. BaTiO$_3$ based ceramics have been studied for their applications in multilayer capacitors transducer, Positive Temperature Coefficient Resistor, thermistor, Non Volatile Free Random Access Memory, Dynamic Random Access Memory, etc [3].

1.1 Scope of this study

In this research the dielectric properties of Vanadium, Calcium, Strontium and chromium doped BaTiO$_3$ and BaTiO$_3$ are studied to see the effect of the dopant. Since dielectric properties depend on the ionic size and polarizibility, the dielectric properties of the doped BaTiO$_3$ are studied in the light of these parameters at different frequencies and temperatures. The effect of milling procedures is also investigated. Finally the change of the dielectric properties due to the milling procedure is discussed. The aims of the research are to determine the optimum milling time of the sample to obtain the best value of dielectric constant and to find out the appropriate composition. Undoped BaTiO$_3$ was also prepared to compare the properties of each composition are explained. The XRD studies are done to identify the homogeneity and SEM are taken to examine the surface morphology.

CHAPTER 2

Historical background of piezoelectric Ceramics

Barium titanate is a ferroelectric material belongs to the subclass of piezoelectric material. Piezoelectricity is the ability of certain crystalline materials to develope an electric charge proportional to a mechanical stress. The creation of useful piezoelectric by treatment of a polycrystalline material depends on a single crystal, Rochelle salt [4] although for this crystal, piezoelectricity is quite strong even without ferroelectricity. Ferroelectricity is the presence of a spontaneous electric moment in a crystal, which can be changed in its orientation between two or more distinct crystallographic directions by applying an external electric field. Prior to about 1940 only two types of ferroelectric's were known. The first linking of unusual dielectric properties in refractory oxides amenable to ceramic preparation came out of work by Thurnauer and Deaderic [5,6] on a barium oxide titanium oxide composition in 1940. The existence of barium titanate as a perovskite had long been known [7].

It is apparent that as with many of the important advances that troubled times, this high dielectric constant of barium titanate was discovered independently in several different part of the world. There were three basic steps in the discovery and understanding of piezoelectricity in ceramics.

1) The first of these was the discovery of the high dielectric constant.
2) The second step was the realization that the cause of the high dielectric constant was ferroelectricity.
3) The third significant step was the discovery of the Poling process.

The first commercial piezoelectricity devices were phonograph pickups marketed by Sonoton Corporation about 1947. Rapid development of barium titanate piezoelectric followed. Compositional modifications were found desirable to improve the temperature stability or to give moderate improvements in voltage out put.

CHAPTER 3

Literature Review

3.1 Electronic Ceramics - Classification

Properties of material have its origin in the crystal structure. Having identical chemical composition may yield entirely different properties owing to the difference in crystal structure and vice versa. A property of ceramics is dictated by its crystal structure and so its classification is based on symmetry element of crystal. The seven crystal systems can be classified into 32-point group according to symmetry. The thirty-two point groups can be further classified into (a) crystals having a center of symmetry and (b) crystals that do not possess a center of symmetry. Crystals with a center of symmetry include the 11 point groups labeled as centrosymmetric. These point groups do not show polarity. The remaining 21 point groups do not have a center of symmetry (i.e. non-centrosymmetric) possesses one or more crystallographically unique directional axes. All non-centrosymmetric point groups show piezoelectric effect along unique directional axes. The following classification, based on the symmetry of crystals, is useful in considering electronic ceramics.

3.2 Piezoelectric Ceramic

Crystals that lack center of symmetry of ion distribution are electrically polarized (i.e. they develop surface charges) when they are mechanically stressed. This is the definition of piezoelectricity. The most important piezoelectric ceramics are those that are also ferroelectric. This means that the ferroelectric (and therefore also piezoelectric) domains within a polycrystalline sample of material can be reoriented ("poled") under the influence of an external electric field, and the reorientation is permanent. Thus, polycrystalline piezoelectric transducers can be produced. One very important application of piezoelectric ceramics transducers for the conversion of electrical energy into mechanical vibration, as in ultrasonic cleaners, ultrasound generators (imaging devices, detection devices) and for the conversion of mechanical vibration into electrical signals, as in ultrasonic sensors.

3.3 Pyroelectric Ceramic

Some of crystals that lack center of symmetry of ion distribution, (i.e. piezoelectric) can also spontaneously develop electric dipoles (polarize), with the degree of polarization

dependent on temperature. This is called the pyroelectric effect, which was first discovered in tourmaline by Teophrast in 314 B.C. and so named by Brewster in 1824 [2]. The spontaneous polarization is given by the value of the dipole moment per unit volume or by the value of the charge per unit area on the surface perpendicular to the axis of spontaneous polarization. The axis of spontaneous polarization is usually along a given crystal axis. Although a crystal with polar axes (20 non-centrosymmetric point groups) shows the piezoelectric effect, it is not necessary for it to have a spontaneous polarization vector. It could be due to the canceling of the electric moments along the different polar axes to give a zero net polarization. Only crystals with a unique polar axis (10 out of 21 non-centrosymmetric point groups) show a spontaneous polarization P_s vector along this axis and its value depends on the temperature. The pyroelectric effect can be described in terms of the pyroelectric coefficient π. A small change in the temperature ΔT, in a crystal, in a gradual manner, leads to a change in the spontaneous polarization vector ΔP_s given by.

$$\Delta P_s = \pi \, \Delta T \qquad --- \qquad \{1\}$$
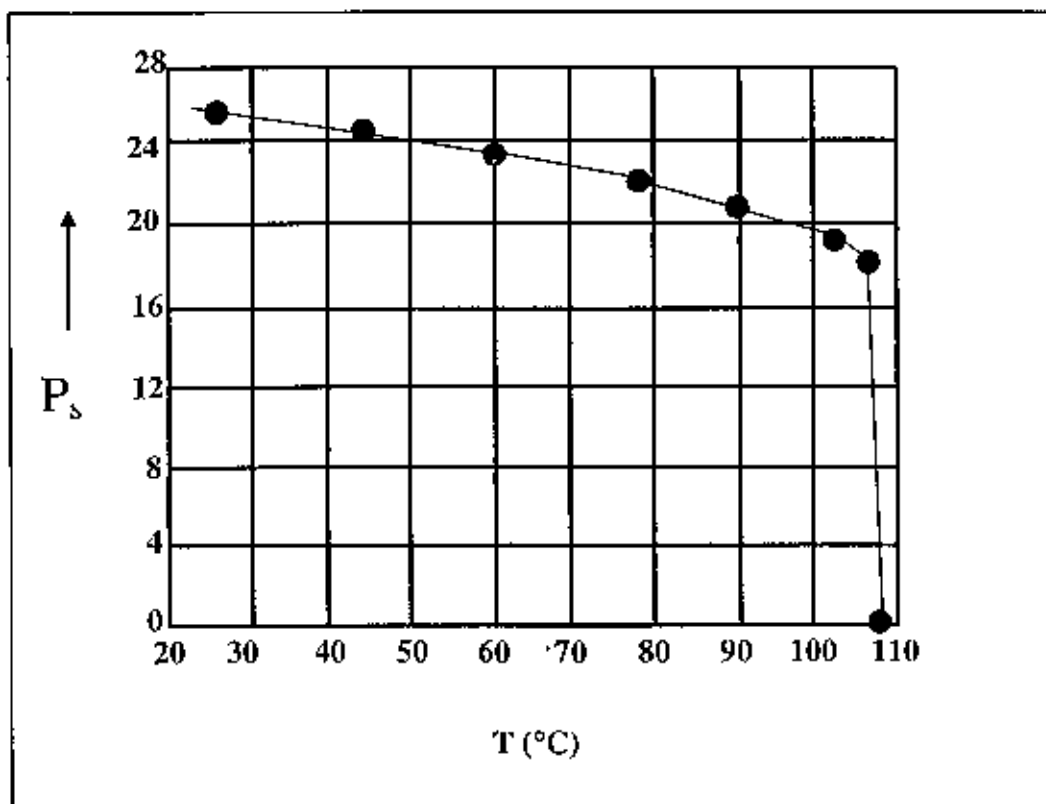
Figure 3-1 : The temperature dependence of spontaneous polarization P_s for BaTiO$_3$ ferroelectric crystal [8].

polarization BaTiO$_3$ has a negative pyroelectric coefficient. The polarization suddenly falls to zero on heating the crystal above T$_c$ [8].

3.4 Ferroelectric ceramics

A subgroup of pyroelectrics has an unusual property of spontaneous alignment of the electric dipoles within domains (~1μ m) and the polarization direction can change under the influence of an electric field. This is the definition of ferroelectricity. The spontaneous alignment of electric dipoles (in a pyroelectric material) by their mutual interaction results in the high dielectric constant and P-E$_c$ hysteresis loop. All ferroelectrics are pyroelectrics and piezoeletric, but not vice versa. For example, tourmaline shows pyroelectricity but is not ferroelectric. The alignment of electric dipoles is opposed by thermal vibrations and at the Curie temperature T$_c$ the alignment disappears. For T > T$_c$, Curie-Weiss law holds:

$$\chi = \frac{P}{(\varepsilon.E)} = \frac{\varepsilon}{\varepsilon_o} - 1 = K' - 1 = \frac{3T_c}{(T - T_c)} \quad \text{------------}\{2\}$$

χ Represent the electrical susceptibility, P represents polarization, E electric field, ε and ε_o, permittivity of material and vacuum respectively and k' represents dielectric constant.

The classic example of a ferroelectric ceramic is BaTiO$_3$. A relatively small Ti^{4+} ion is located in a large octahedral site, with some room for free movement. The rattling Ti hypothesis suggests that there are minimum energy positions for Ti off center, by less than 0.01 nm, giving an electric dipole in each unit cell.

Because of spontaneous alignment of the dipoles, the dielectric constant (k'= $\varepsilon/\varepsilon_o$) for barium titanate exceeds 2000 at room temperature. The largest dielectric constant is achieved when critical temperature is approached, at T = T$_c$ = 125°C, k' = 12,000. However, structural modifications of the classic BaTiO$_3$ are required if variations in dielectric constant vs temperature and polarization voltage are of concern.

3.5 Ferroelectric Domains

Ferroelectric crystals possess regions with uniform polarization called ferroelectric domains. Within a domain, all the electric dipoles or the polar axis transformation occur and spontaneous polarization takes place. The electrical stray field energy caused by the

non-compensated polarization charges is reduced by the formation of ferroelectric domains as shown in Figure 3-2. The configuration of the in cubic crystals the polarization may be orientated in any of the six-pseudo cubic <001> directions. Therefore, the polar axis may be aligned orthogonally (90° domains) and anti-parallel (180° domains) with respect to each other (Figure 3-3)
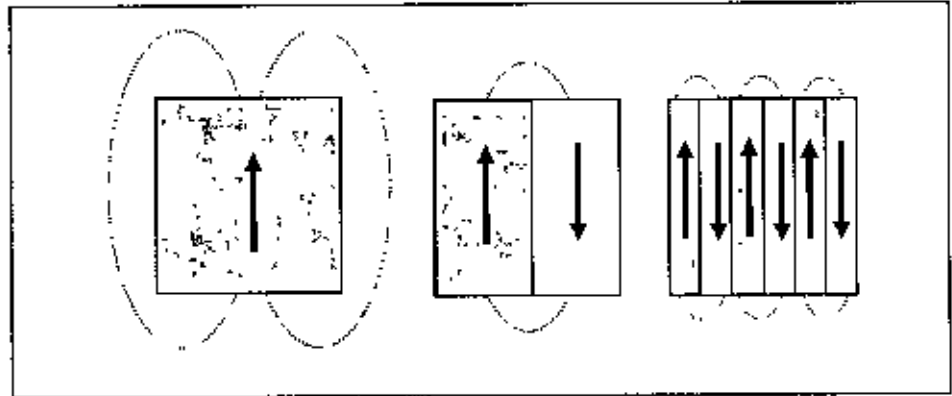
Figure 3-2: Reduction of electrical energy by domain formation [9]

domains follows a head-to-tail condition in order to avoid discontinuities in the polarization at the domain boundary.
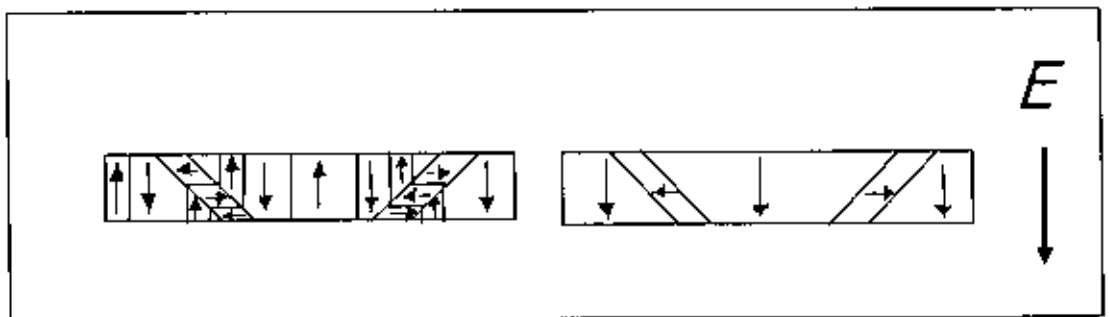
Figure 3-3 : Domain polarization direction changed by poling [9]

A single domain can be obtained by domain wall motion made possible by the process called poling. An appropriate electric field is applied to the sample at a temperature slightly below the T_c. Overall performance of the ferroelectric material greatly influenced by the nature of domain and its movement. Many researches are on going to

characterize the domain and its activities. The 180° domains are easily removed by polling as illustrated in Figure 3-3. The 90° domains are difficult to remove because the surface strain generated during cooling and the crystal fabrication restrict the motion of the domain. Mechanical force is used by many researchers [10] to pole 90° domain and recently Chen [11] described a new technique. There may be many domains in a crystal separated by interfaces called domain walls. These walls have a thickness of only 100 nm or less [12]. Muller [13] described a new laser technology that provides information about domain structure, their nucleation, and their dynamics.

Atomic force microscopy [14] and TEM [15] was used to characterize domain. A very strong field could lead to the reversal of the polarization in the domain, known as domain switching [16]. Domains can be observed under the optical microscope and in SEM after the polished sample being etched with concentrated HCl [17]. The relationships between etch pattern and the domain orientation in $BaTiO_3$ crystal in tetragonal state had been described by Hooton [18]. During etching processing the positive ends of the electric dipoles etch rapidly, forming a rough surface, the negative ends etch slowly, forming smooth surface and the sides (dipoles parallel to the surface) etch at an intermediate rate, forming a semi smooth surface.

The built-up of domain wall, elastic stress fields as well as free charge carriers counteracts the process of domain formation. In addition, an influence of vacancies, dislocations and dopants exits [19].

3.6 Ferroelectric Hysteresis Loop

The main difference between pyroelectric and ferroelectric materials is that the direction of the spontaneous polarization in ferroelectrics can be switched by an applied electric field.
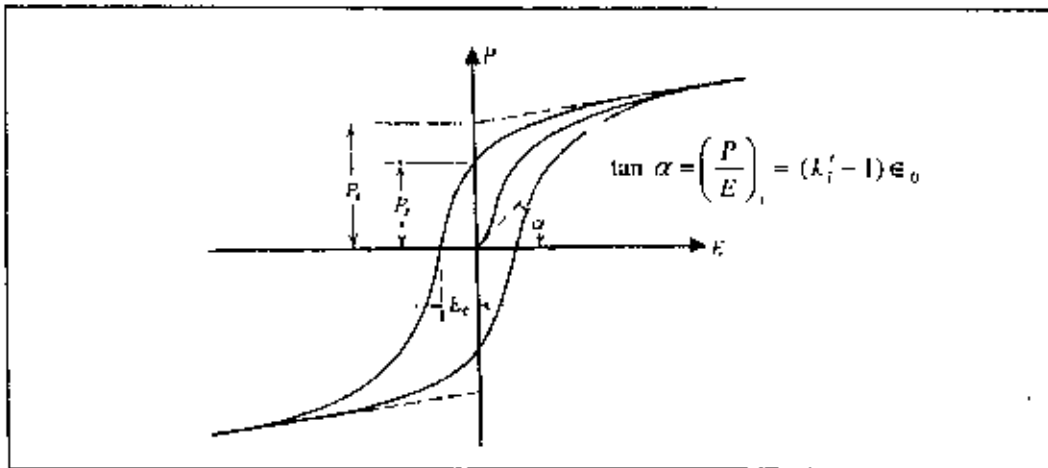
Figure 3-4 A Polarization vs. Electric Field (P-E) hysteresis loop for a typical ferroelectric crystal. [20]

The polarization reversal can be observed by measuring the ferroelectric hysteresis (analogous to ferromagnetic behavior) as shown in Fig. 2-4. As the electric field strength is increased, the domains start to align in the positive direction giving rise to a rapid increase in the polarization. At very high field levels, the polarization reaches a saturation value (P_{sat}). The polarization does not fall to zero when the external field is removed. At zero external field, some of the domains remain aligned in the positive direction, hence the crystal will show a remnant polarization P_r. The crystal cannot be completely depolarized until a field of magnitude is applied in the negative direction. The external field needed to reduce the polarization to zero is called the coercive field strength E_c. If the field is increased to a more negative value, the direction of polarization flips and hence a hysteresis loop is obtained. The value of the spontaneous polarization P_s is obtained by extrapolating the curve onto the polarization axes.

The ferroelectric hysteresis originates from the existence of irreversible polarization processes by polarization reversals of a single ferroelectric lattice cell. However, the exact interplay between this fundamental process, domain walls, defects and the overall appearance of the ferroelectric hysteresis is still not precisely known. The separation of the total polarization into reversible and irreversible contributions might facilitate the understanding of ferroelectric polarization mechanisms. Especially, the irreversible processes would be important for ferroelectric memory devices, since the reversible processes cannot be used to store information. For ferroelectrics, mainly two possible mechanisms for irreversible processes exist. First, lattice defects, which interact with a domain wall and hinder it from returning into its initial position after removing the

electric field that initiated the domain wall, motion ("pinning"). Second, the nucleation and growth of new domains that do not disappear after the field is removed. In ferroelectric materials, the matter is further complicated by defect dipoles and free charges that contribute to the measured polarization and can also interact with domain walls [13].

Reversible ferroelectrics are the basic requisite of dielectric materials for application such as capacitors. Reversible contributions in ferroelectrics are due to ionic and electronic displacements and to domain wall motions with small amplitude. These mechanisms are very fast. The reorientation of dipoles and/or defect or free charges also contributes to the total polarization. These mechanisms are usually much slower, but they also might be reversible (relaxation). Remnant polarization and coercive voltage are of critical importance to the design of external circuits of FeRAMs or DRAMs

3.7 Curie Point and Phase Transitions

All ferroelectric materials have a transition temperature called the Curie point (T_c). At a temperature $T > T_c$ the crystal does not exhibit ferroelectricity, below Tc it is ferroelectric. On decreasing the temperature through the Curie point, a ferroelectric crystal undergoes a phase transition from a non-ferroelectric phase to a ferroelectric phase. If there are more than one ferroelectric phases, the temperature at which the Crystal transform from one ferroelectric phase to another is called the transition temperature.
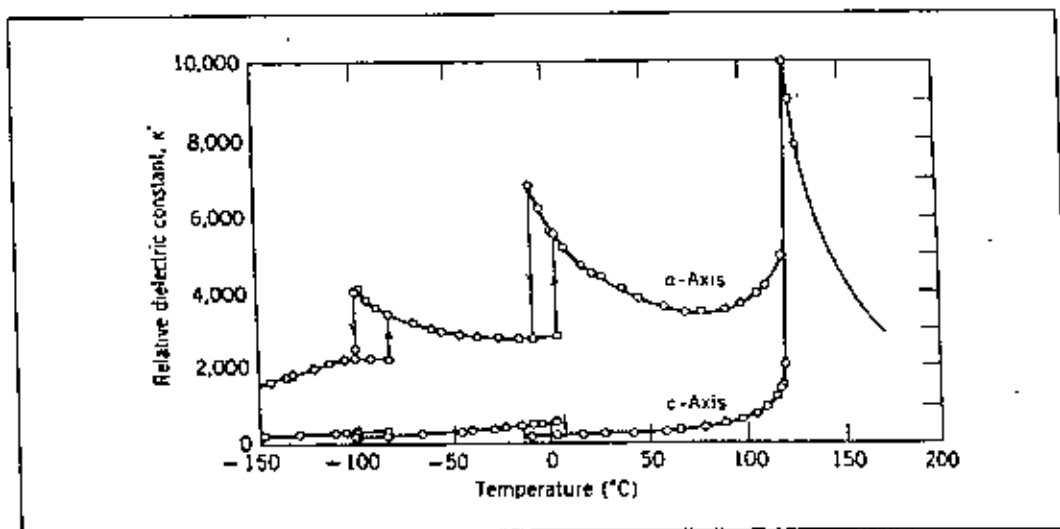
Figure 3-5: Variation of dielectric constants (a and c axis) with temperature for $BaTiO_3$. [21]

The phase transition in BaTiO$_3$ is of first order, and as a result, there is a discontinuity in the polarization, lattice constant, and many other properties clear in Figure 3-6. It is also clear in the figure that there are three phase transitions in barium titanate having the following sequence upon heating: rhombohedral, orthorhombic, tetragonal and cubic. There is a small thermal hysteresis of the transition temperature, which depends on many parameters such as the rate of temperature change, mechanical stresses or crystal imperfections.

From a crystal chemical view, the Ba-O framework evokes an interstitial for the central Ti^{4+} ion, which is larger than the actual size of the Ti^{4+} ion. As a result, the series of phase transformations takes place to reduce the Ti cavity size. Certainly, the radii of the ions involved impact the propensity for forming ferroelectric phases; thus both PbTiO$_3$ and PaTiO$_3$ have ferroelectric phases, while BaTiO$_3$ and SrTiO$_3$ do not [22]. Early research works on ferroelectric transitions have been summarized by Nettleton [23, 24]. Figure 3.6 shows the variation of the relative permittivity E with temperature as a BaTiO$_3$ crystal is cooled from its paraelectric cubic phase to the ferroelectric tetragonal, orthorhombic, and rhombohedral phases. Near the Curie point or transition temperatures, thermodynamic properties including dielectric and thermal constants show an anomalous behavior. This is due to a distortion in the crystal as the phase structure change. The temperature dependence of the dielectric constant above the Curie point ($T > T_c$) in ferroelectric crystals is governed by the Curie-Weiss law mentioned in section 3.1.3
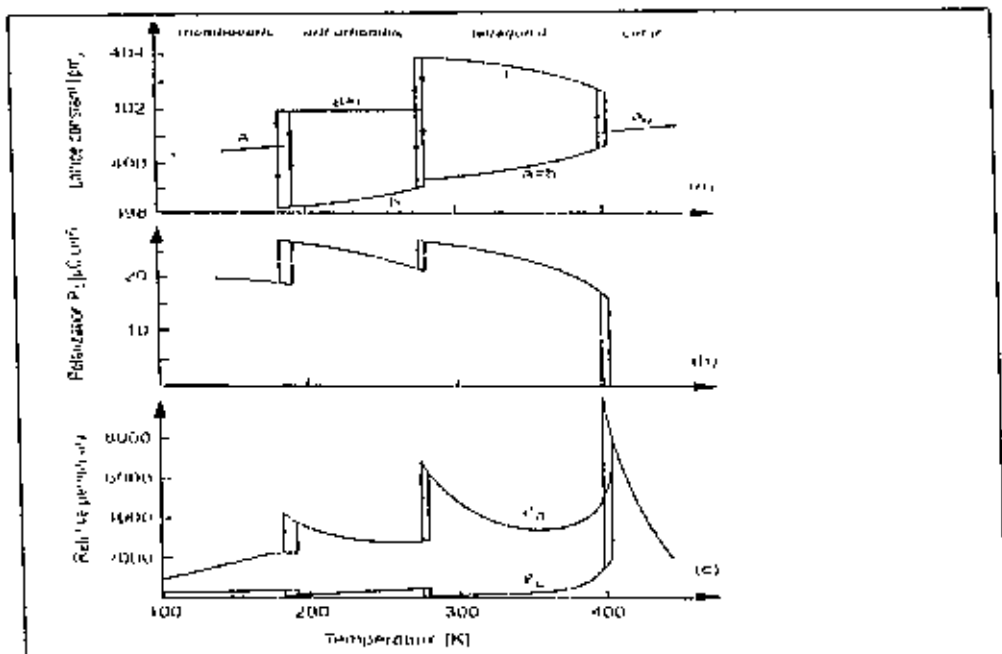
Figure 3-6: Various properties of BaTiO$_3$ as function of phase transformation

3.8 Type of Ferroelectric materials

Ferroelectric materials can be grouped according to their structure, into four main types. These are the corner sharing oxygen octahedra, compounds containing hydrogen bonded radicals, organic polymers and ceramic polymer composites. Corner sharing octahedra can be classified into perovskites (ABO_3), tungsten bronze type compounds ($K_x WO_3$, x< 1, such as $PbNb_2O_6$), Bismuth oxide layer structured (such as $Bi_4Ti_3O_{12}$) and Lithium Niobate & Tantalate. Hydrogen bonded ferroelectric usually water-soluble made in single crystal. Rochelle salt ($NaKC_4H_4O_6$, $4H_2O$) is one example of this type and this was the first ferroelectric material discovered. Phase are now gradually replaced by ceramic ferroelectrics. Interesting type of ferroelectric material are organic polymers for medical applications. These piezo-polymers have some properties, which make them better suited for use in medical imaging applications. The density of these polymers is very close to that of water and the human body tissues, hence there is no acoustic impedance mismatch with the body. Polyvinylidene fluoride (PVDF, $(CH_2-CF_2)_n$) and copolymers of PVDF with trifluoroethylene {P(VDF-TrFE)} have found applications as piezoelectric and pyroelectric materials. The drive for piezoelectric composites stems from the fact that desirable properties could not be obtained from single phase materials such as piezoceramics or piezopolymers. Piezoelectric composites are made up of an active ceramic phase embedded in a passive polymer, The properties of the composite depend on the connectivity of the phases, volume percent of ceramic, and the spatial distribution of the active phase in the composite. The concept of connectivity developed by Newnham et al. [25] describes the arrangement of the component phases within a composite.

3.9 Corner Sharing Octahedra and Perovskite

A large class of ferroelectric crystals are made up of mixed oxides containing corner sharing octahedra of O_2. Ions schematically had shown in Figure 3.7 Inside each octahedron is a cation B^{b+} where 'b' varies from 3 to 6. The spaces between the octahedra are occupied by A^{a+} ions where 'a' varies from 1 to 3. In prototype forms, the geometric centers of the A^{a+}, B^{b+} and O^{2-} ions coincide, giving rise to a non-polar lattice. When polarized, the A and B ions are displaced from their geometric centers with respect to the O^{2-} ions, to give a net polarity to the lattice. These displacements occur due to the changes in the lattice structure when phase transitions take place as the temperature is

changed. The formation of dipoles by the displacement of ions will not lead to spontaneous polarization if a compensation pattern of dipoles are formed which give zero net dipole moment. Perovskite is a family name of a group of materials and the mineral name of calcium titanate ($CaTiO_3$) having a structure of the type ABO_3. A wide variety of cations can be incorporated into perovskite structure as long as they obey the relationship:

$$t = (R_A + R_B)/ 2(R_B + R_0)$$
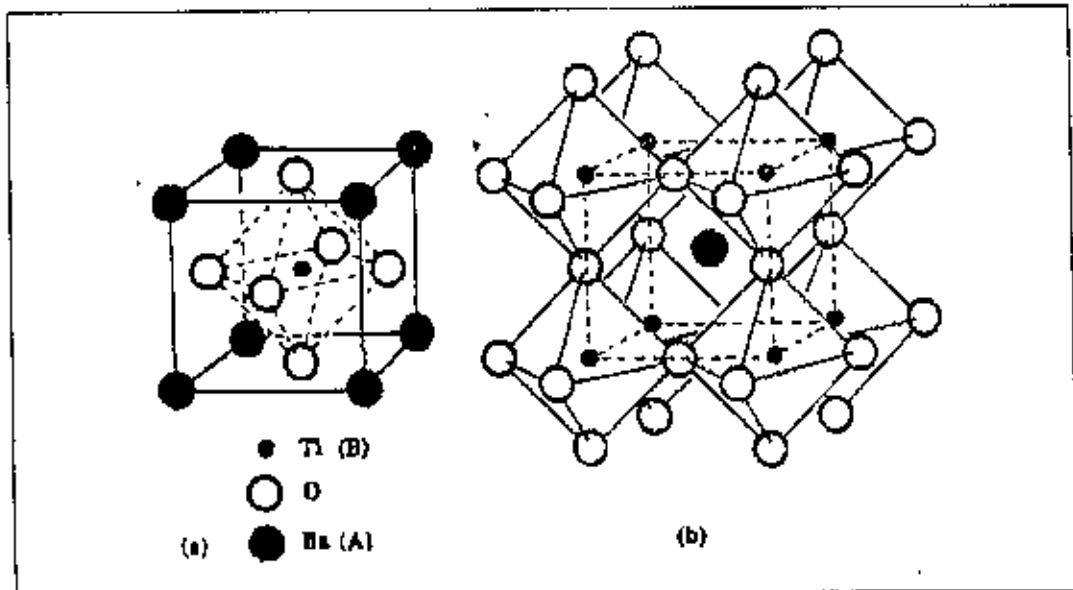
Figure 3-7 (a) A cubic ABO_3 ($BaTiO_3$) perovskite-type unit cell and (b) three dimensional network of corner sharing octahedra of O^{2-} ions [21].

For an ideal perovskite structure $t = 1$, and R_A, R_B and R_0 the ionic radius of large cation, small cation and oxygen [26]. The structure takes cubic from with the t value between 0.95 to 1.0; lower this slightly distorted cubic but not ferroelectric but slightly above 1.0 tends to be ferroelectric [27]. Many piezoelectric (including ferroelectric) ceramics such as Barium Titanate ($BaTiO_3$), Lead Titanate ($PbTiO_3$), Lead Zirconate Titanate (PZT), Lead Lanthanum Zirconate Titanate (PLZT), Lead Magnesium Niobate (PMN), Potassium Niobate ($KNbO_3$), Potassium Sodium Niobate ($K_xNa_{1-x}NbO_3$), and Potassium Tantalate Niobate ($K(Ta_xNb_{1-x})O_3$) have a perovskite type structure.

3.10 Electrical Properties

Ceramics are mostly covalently bonded material hence electrically non- conductive or insulator. Importance of particular property depends on the application demand. For instance, dielectric strength is an important parameter for application of ceramic as

insulators used in power transmission line, load bearing general insulators, in house hold appliances, etc. In this kind of applications where frequency does not exceed 1 kHz, the breakdown strength, measured in kV/cm, and mechanical strength are prime important factors. The dielectric constant (k′) or loss factor (k″) does not matter much. On the other hand, for capacitor and electronics applications just the opposite is required. The values of k′ and k″ are of prime importance, not only their room temperature values but also as function of temperature and frequency. These are intrinsic properties of material, can be modified by doping, micro structural variation, etc. $BaTiO_3$ is used extensively as a principal ingredient for multi layer ceramic capacitor (MLCC) manufactured commercially in billions. In the following sections basic concept and factors governing dielectric constant, dielectric losses are discussed. Materials are treated as polycrystalline and linear dielectric.

3.11 Dielectric constant

The overall Dielectric constant (k′) of an insulator material is given by the relation

$$D = \varepsilon E = \varepsilon_0 k' E \qquad \text{------- (2)}$$

D represents the electric displacement, E the electric fields in the dielectric, k′ the dielectric constant and permittivity of vacuum. The electric displacement describes the extent to which the electric field has been altered by the presence of the dielectric material. The dielectric constant k′ is an intrinsic property of a material and a measure of the ability of the material to store electric charge relative to vacuum. It is measured indirectly from the capacitance of a capacitor in which the material is used as electrode separator or dielectric. From equation- 2 and the capacitive cell illustrated in Figure 2-8 the dielectric constant k′, total charge Q (coulombs) and capacitance C (farads) can be developed as follows:

$$k' = \frac{D}{\varepsilon_o E} = \frac{Q/A}{\varepsilon_o V/d} \qquad \text{--------- (3)}$$

Therefore, $\quad Q = \varepsilon_0 k' \frac{A}{d} V = CV \quad \text{---------(4)}$

Where, $\quad C = \varepsilon_0 k' \frac{A}{d} \quad \text{---------------- (5)}$

$$C_o = \varepsilon_0 \frac{A}{d} \quad \text{------------(6)}$$

and
$$k' = \frac{C}{C_o} \simeq \frac{\varepsilon}{\varepsilon_n} \quad \text{--------------(7)}$$

Here, A represents the area of the capacitive cell, d its thickness (or gap between the electrodes)
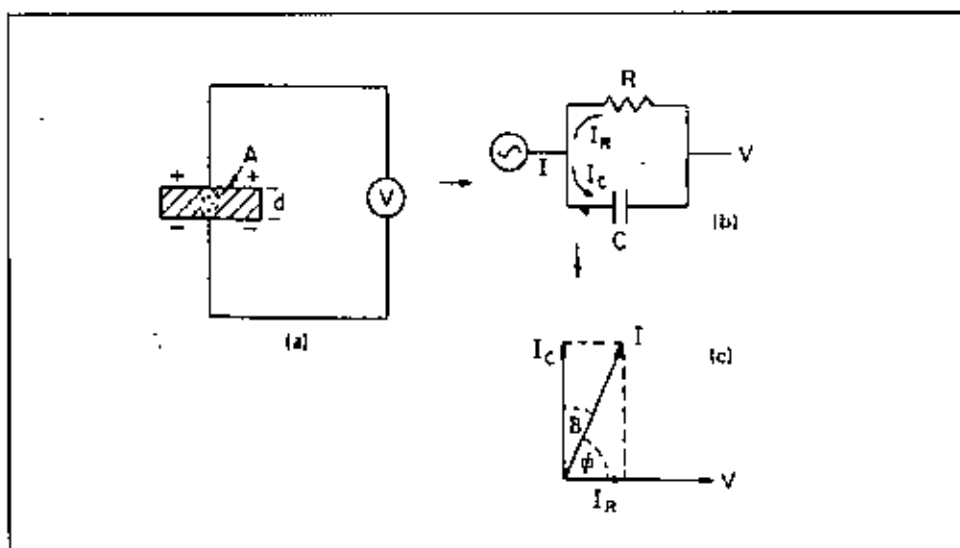
Figure 3-8: Equivalent circuit diagrams a) Capacitive cell, b) Charging and loss current c) loss tangent

between the electrodes), Co and C the respective capacitance of the capacitor with air and material, V the voltage across the cell and E the material permittivity (F/m). Thus k' represents the ratio of the permittivity or charge storage capacity relative to air or vacuum as dielectric. It is clear from equation-5 that for a given size capacitor and applied voltage the higher the k' the higher the capacitance of the capacitor. This is the only variable left with the material scientist to increase the capacitance unit volume value of capacitor for modern electronics applications.

3.12Dielectric Loss

An ideal dielectric would allow no flow of electronic charge, only a displacement of charge via polarization. If a plate of such ideal material were placed between the capacitate cell shown in Figure 3-9 (a) and a dc voltage was applied, the current through the circuit would decay exponentially to zero with time. But this would not be case if an

alternating (sine wave) electric field was applied. In this case the equation-4 may be written as:

$$Q = CV_0 e^{i\omega t} \quad ----(8)$$

Therefore, $\quad I = \dfrac{dQ}{dt} = i\omega CV = i\omega C_o \, \varepsilon_o k \, 'V ------(9)$

here, I represents the current flow on discharge of the capacitor in time T. For real dielectric material, the current I has two vector components, real I_R and imaginary I_c. The condition of a loss (not so good) dielectric illustrated in Figure 3-9 (c) as an equivalent circuit analogous of a resistance in parallel with the capacitor. The current I_c represents a (watt less) capacitive current proportional to the charge stored in the capacitor. It is frequency dependent and leads the voltage by 90°. On the other hand the current I_R is an ac conduction current in phase with the voltage V. which represents the energy loss or power dissipated in the dielectric. The resultant angle between the current and the voltage is ϕ somewhat less than 90°. Ideal dielectric under this circumstance would not absorb any power and the capacitor would have zero loss. The current would lead the voltage exactly 90°. The current in real capacitor lags slightly behind what it would be in an ideal capacitor. The angle of lag is defined as δ and the amount of lag becomes tan δ or loss tangent.

Equation- 9 can be written for real and imaginary part,

$$I = I_c + I_R ------------(10)$$

$$= i\omega C_o \, \varepsilon_o k \, 'V + i\omega C_o \, \varepsilon_o k''V ------(11)$$

By definition, $\tan\delta = \left| \dfrac{I_R}{I_c} \right| = \dfrac{k''}{k'} ------------(12)$

Dielectric loss often attributed to ion migration, ion vibration & deformation and electronic polarization. Ion migration is particularly important and strongly affected by temperature and frequency. The losses due to ion migration increase at low frequency and the temperature increases.

3.13 Material Aspect

Intrinsic properties such as k' and k'' can be explained in terms of chemical composition and structure. Material behavior in a dielectric field is a direct result of three vector quantities a) dielectric displacement D, b) electric field E, and c) polarization P

$$D = \varepsilon_o k'E = \varepsilon_o E + P$$

Affect of dielectric in capacitor illustrated in Figure 2-9. The contribution of vacuum is the term $\varepsilon_o E$ and is the electrical polarization contribution of the dielectric.

Therefore, $\qquad$ $P = \varepsilon_o (k'-1) E = \varepsilon_o \chi E$ --- ---------- [14]

It is clear from equation. [1] and {14} polarization is the key factor attributing to the dielectric property of material. Low ceramic material, polarization can be further described in terms of a volume charge density related to the concentration of dipole per unit volume N and the local field E' in the dielectric:
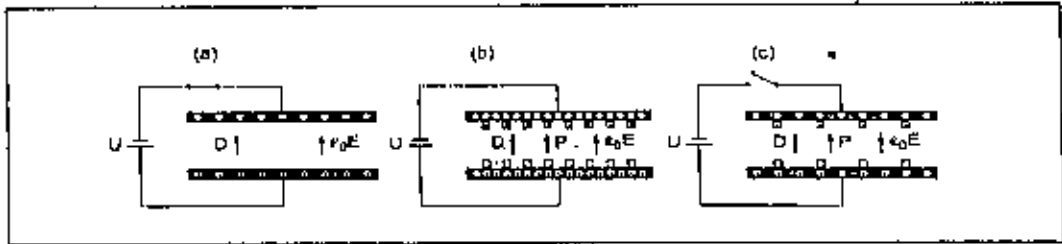
Figure 3-9: Parallel plate capacitor: (a) without dielectric (b) with dielectric E constant, c) with dielectric with D constant

$$P = \alpha\, NE' \text{-------------}(15)$$

and $\qquad$ $E' = \dfrac{k'+2}{3} E$ -----------(16)

Where, α represents the polarizability, arising from different polarization mechanism of the material:

$$\alpha = \bar{\alpha_e} + \alpha_i + \alpha_o + \alpha_s \text{--- ---} (17)$$
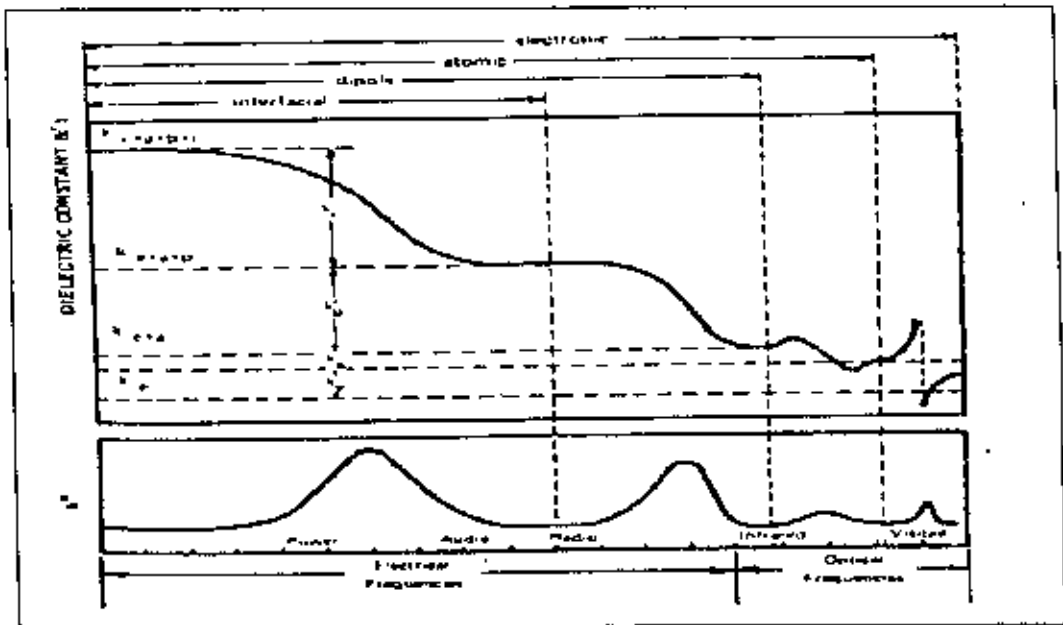
Figure 3-10: Frequency dispersion behavior of dielectric material as function of frequency

representing the susceptibility associated with electronic, ionic, orientational and space charge polarization, respectively. Mechanism of polarization described in the following section. For cubic structures and for induced dipoles (ionic and electronic polarization), the calculation reveals a relation between the atomic polarizability and the macroscopic permittivity $\epsilon = \epsilon_0 \epsilon_r$ which is referred to the Clausius-Mossotti equation [28].

$$\varepsilon = \frac{\varepsilon_o + 2N\alpha}{\varepsilon_o - N\alpha} \quad ----------(18)$$

In Figure 3-10, the frequency dependence of k' and associated polarization mechanism are illustrated. Affect of different polarization mechanism to the overall dielectric constant is related to the composition, frequency and temperature of the dielectric material. In general, increases with ion concentration, ion size and ion polarizability, hence ions like Ba^{2+}, Pb^{2+} La^{3+} are used in order to achieve a higher dielectric constant and refractive index. In ionic solids (such as MgO, Al_2O_3) is the predominant polarization mechanism, where ion size and separation have the significant effect. For ceramic materials with mobile ion, the orientational polarization can be a factor. This can be attributed to ion jump polarization, where

$$\alpha_o = \frac{p^2}{3kT} \quad \text{and} \quad \alpha_j = \frac{(ezd)^2}{3kT} \quad ----------(19)$$

$p = ezd$, represents the dipole moment associated with the jump of an ion of charge ez through a distance d. The relaxation time T and the number of successful ion jumps per second are given in Arhenius form:

$$\tau = \tau_o \, e^{\mu/kT} \quad \text{and} \quad n = n_o \, e^{-\mu/kT} \quad ----------(20)$$

here, μ is the activation energy, k Boltzman constant and T absolute temperature. In other word, for ceramic r decreases with temperature, the relaxation move to higher temperature with increasing frequency and n increases with the temperature. Hence it is normally observed that at a given frequency k' increases with the temperature and at a given temperature k' decreases as frequency increased.

3.14 Mechanism of Polarization

In general, there are five different mechanisms of polarization, which can contribute to the dielectric response [29].

Electronic polarization exists in all dielectrics. It is based on the displacement of the negatively charged electron shell against the positively charged core. The electronic polarizability is approximately proportional to the volume of the electron shell. Thus, in

general α_e is temperature-independent, and large atoms have a large electronic polarizability. Ionic polarization is observed in ionic crystals and describes the displacement of the positive and negative sublattices under an applied electric field.

➤ Orientation polarization describes the alignment of permanent dipoles. At ambient temperatures, usually all dipole moments have statistical distribution of their directions. An electric field generates a preferred direction for the dipoles, while the thermal movement of the atoms perturbs the alignment. The average degree of orientation is given by the Langevin function $<\alpha_0> = p^2/(3k\ T)$ where k denotes the Boltzmann constant and T the absolute temperature.

➤ Space charge polarization could exist in dielectric materials which show spatial inhomogeneities of charge carrier densities. Space charge polarization effects are not only of importance in semiconductor field-effect devices, they also occur in ceramics with electrically conducting grains and insulating grain boundaries (so-called Maxwell-Wagner polarization).

➤ Domain wall polarization plays a decisive role in ferroelectric materials and contributes to the overall dielectric response. The motion of a domain wall that separates regions of different oriented polarization takes place by the fact that favored oriented domains with respect to the applied field tends to grow.

3.15 Processing of Barium Titanate ceramic

Property of the final product depends on the processing from raw material to the final sintering.
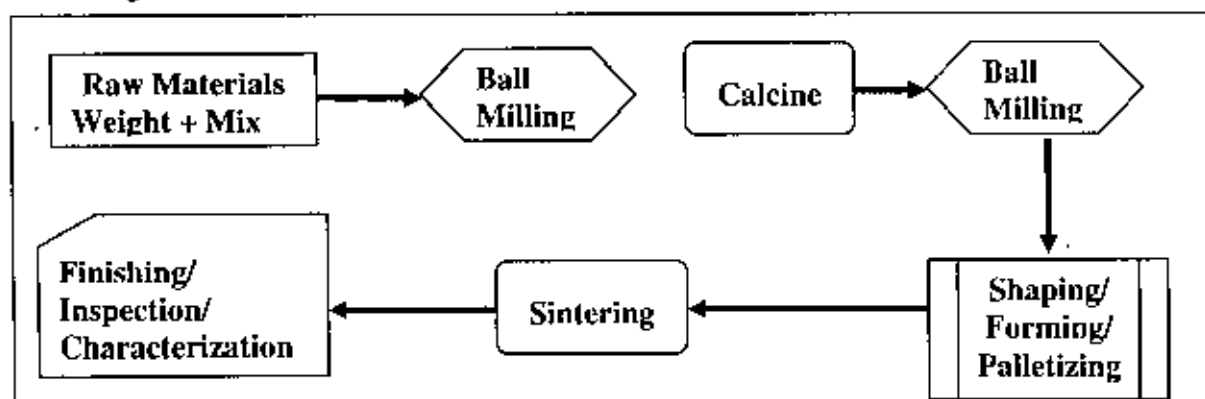
Figure 3-11: Flow chart of Mixed Oxide route

Every step in the process chain has its own influence on the successive step and the final product. Many methods are used to syntheses $BaTiO_3$, a) conventional mixed oxide, b) sol-gel, c) chemical precipitation, d) hydrothermal and e) combustion reaction. Choice of route depends on the application. Nanopowders are prepared using the electrophoretic (EPD) method for making films. Even thin film was prepared from bulk single crystal using ion slicing method [29]. Ultra fine $BaTiO_3$ powder obtained by combustion reaction are used to make bulk material was described as relatively efficient method [32]. By far the first method is widely in the industrial application as well as at laboratories. However, powder obtained in other routes is superior in terms of homogeneity and fineness. This method also known as solid state method was used to prepare sample in this study.

Processing route of this method illustrated in Figure 3-11. In the following sections important steps were discussed briefly with their influence on dielectric property of $BaTiO_3$ ceramics. The raw materials $BaCO_3$ and TiO_2 (rutile or anatase) are first weighed according to the stoichiometric Formula. The raw materials should be of high purity.

3.16 Ball Milling

The weighted powders are mixed mechanically by either ball milling or attrition milling. Milling is carried out to reduce the particle size of the powders to the micron range for the ease of solid phase reactions to occur by atomic diffusion.
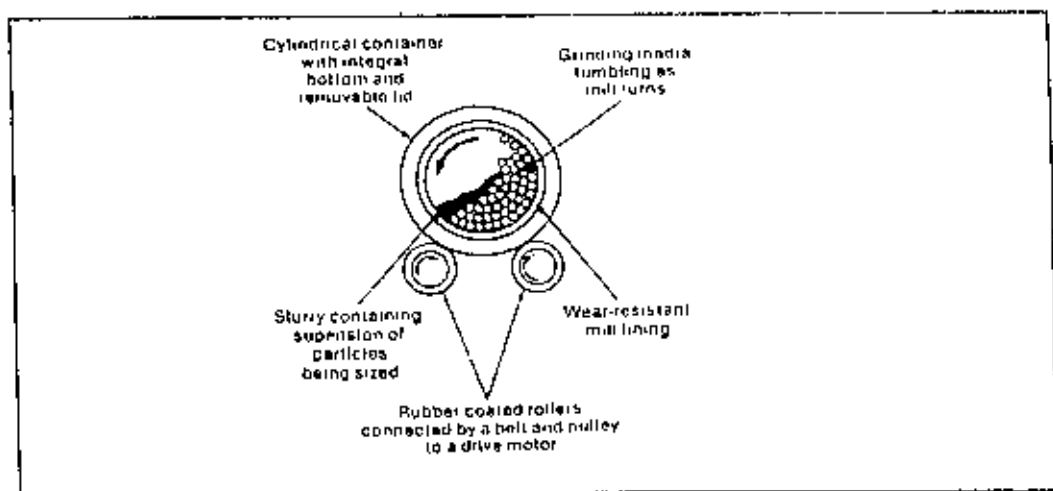
Figure 3-12 Schematic of a Ball Mill

The schematic of a ball mill is illustrated in Fig 3-12. Size and distribution of the ball is an import factor determining the product quality. Particle size is reduced by the action of impact and friction of balls with the powder. Thumb rule is, smaller the size of balls finer the particle but it take longer time to break down big particles, hence use mix of different size balls. Motion of ball is controlled by the rotation speed of the mill. At higher speed balls cling at the inner side of the mill due to centrifugal force, too low speed would set the balls almost stationary at the bottom. In both case insufficient friction between balls and particle would not break down the particle. Optimum speed is achieved when balls are in circular motion and roll back to bottom from about three quarter way to the top as shown in Figure 3-12.

Media is another important consideration for two reasons. It must not react with the ball, the container, or the powder. Secondly, must avoid decrease of colloidal stability. For instance, milling of $BaTiO_3$ in water media set of tribochemical reaction. The reaction forms strongly alkaline $Ba(OH)_2$ which upset the PH balance, decreasing the colloidal stability of the suspension [30]. Either non-polar liquid such as acetone, alcohol, is used or polyelectrolyte stabilizers are used with water. Usually the same set up is used for milling the calcined powder. Finer particle can lower the sintering temperature and firing time significantly. Extent of ball milling is usually assessed by particle size analysis.

3.17 Calcination

Chemically as well as ceramic point of view, this is an important step. Desired compound are formed and necessary reactions are accomplished. During the calcination step the mixed powder is exposed to high temperature at a specified atmosphere and time. The purposes of calcinations are -

a)   To remove residual media form milling process

b)   To remove water of hydration, carbon dioxide forming oxide, and any volatile impurities.

c)   To effect solid phase reaction between the constituents giving the desired phase or solid solution.

d)   The reaction would reduce the volume shrinkage in the final sintering. The calcination of $BaTiO_3$, starting raw materials $BaCO_3$ and TiO_2 are mixed.

$$BaCO_3 \rightarrow BaO + CO\uparrow$$

$$BaO + TiO_2 = BaTiO_3$$

in the molar ratio of 1:1, ball milled, then calcined in ambient air at 1000°c to obtain the perovskite phase through the diffusion controlled reaction [31]. Degree of calcinations can be assessed by weight loss of CO_2 as a function of time and temperature using TGA. Under isothermal condition, the reaction obeys a parabolic time law. Newnham [22] has detailed the model of kinetic of solid state reaction between spherical particles. According to him, the reaction rate is inversely proportional to the square of the particle radius. Importance of milling before calcinations is realized and so is the fineness of the powder.

3.18 Formation of phases and Phase Diagram

$BaTiO_3$ formed during reaction above through formation number of intermediate phases. Templeton [32] detected the intermediate second phases Ba_2TiO_4, $BaTi_4O_9$ and $BaTi_3O_7$. The final conversion to monophase $BaTiO_3$ determined by decomposition of the intermediate phases, ie, the diffusion exchange between Ba and Ti rich region in the powder. The calcinations temperature and the amount of intermediate phases critically depends on the morphology and degree of mixing of the raw material. During ball milling this is an important point aimed to accomplish. According to Bauger [31], during this solid-solid reaction BaO act as the mobile agent. At the contact interface BaO is formed which diffuses into the TiO_2 forming as intermediate layer of Ba_2TiO_4, which slowly reacts with the residual TiO_2 to form $BaTiO_3$. Hence, particle size is an important factor especially the size of TiO_2 as it determines the particle size of $BaTiO_3$.

The phase diagram of $BaO-TiO_2$ is shown in Figure 3-13. As per phase diagram, stoichometric $BaTiO_3$ can accommodate little more TiO_2 with the compound. Formation of Ba_2TiO_4 is inhibited below 1100°C by the presence of a CO_2 atmosphere. This phase is particularly harmful, since it is hygroscopic and decomposed with swelling in slightly moist air. Incomplete mixing and reaction will yield small amounts of Ba_2TiO_4 and $BaTi_3O_7$ and other intermediate phases. The same kind of harmful phases may also occur when alkaline earth oxides, such as Ca, Sr used in substituted $BaTiO_3$. Effect of calcination temperature was studied by Maison et *al* [33] suggest at 700°C tetragonal $BaTiO_3$ do not form whereas at 100°C it does at the expenses of particle agglomeration.

Dopent and other additives are added at this stage of processing. A great advantage of this method is that dopes and additives can be homogeneously incorporated into the perovskite lattice during calcinations [34].
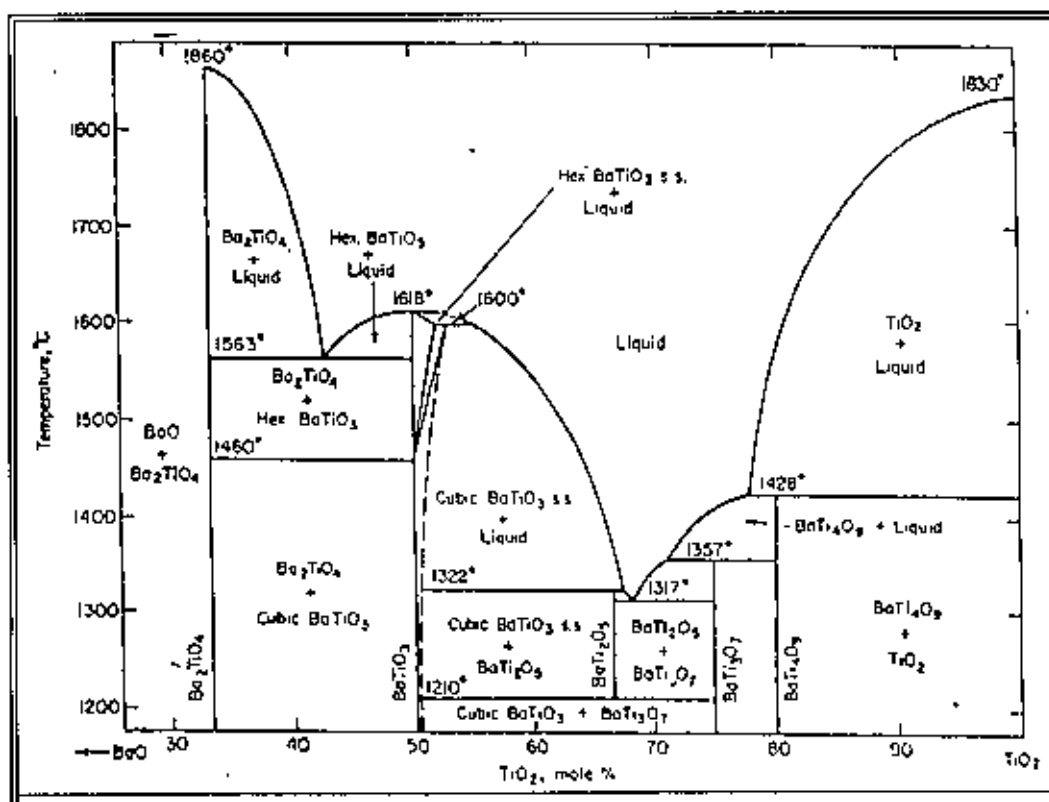
Figure 3-13: Phase Diagram of BaO - TiO_2 system

The calcining temperature is important as it influences the density and hence the electromechanical properties of the final product. The higher the calcination temperature, the higher the homogeneity and density of the final ceramic product. Many calcination temperature and time scheme has been suggested. Higher temperature and longer time usually yield completely reacted powder but coarser particle size posing difficulties during subsequent milling. So, proper calcination at the right temperature is necessary to obtain the best electrical, mechanical properties and minimizing the presence of harmful phases.

3.19 Effect of particle size

Reaction kinetics greatly influenced by the fineness of the particle size. Henning *et al* [34] studies the effect of grain size of particle on the reaction during sintering and the final product using TGA. They concluded that the decomposition temperature of $BaCO_3$ in mixtures with TiO_2 is largely independent of the particle size of $BaCO_3$. However, the

particle size of TiO_2 widely determines the grain size of $BaTiO_3$. This is in good agreement with diffusional solid state reaction suggested where BaO act as a mobile agent. Sub micron sized $BaCO_3$ however, strongly inhibits the formation of harmful phase Ba_2TiO_4. The Ba/Ti atomic ratio has a strong influence on the calcination temperature. Higher temperature required for Ba rich composition.

3.20 Shaping and drying

After calcining, the lumps are ground by milling as described previously. The milled powder ready for further processing is commonly referred at green body. The green bodies should have a certain minimum density before they can be sintered. Common practice is to achieve 60% of the theoretical density (during shaping and pre-sintered state. The desired shape and a minimum green density can be provided by various techniques including powder compaction, slip-casting, extrusion, doctor banding, dipping, etc. Hot pressing (both axial and isotactic), although expensive method, is becoming popular for better quality ceramic material used in high-end application. The choice of the method depends on the type of powder used, particle size distribution, state of agglomeration, desired shape, and thickness of the part. Hydraulic or mechanical presses are used to press powder in to desired shape at the pressure of ~100 to 300MPa. Owing to the nature of this process, only simple and symmetric shape can be prepared. No sintering aid or liquid is added to the powder for solid phase sintering route. Hence, strength of the green powder compact is achieved through addition of a suitable binder such as PVA, glycol phthalate, etc.

After shaping, the green bodies are heated very slowly to between 400-600°C in order to remove any binder present. Initial heating rate to burnout the binder is about ~1 -2°C/mm in order to allow the gases to come out slowly without forming cracks and blisters in the ceramic part. After the binder burnout is over, the samples are taken to a higher temperature for sintering to take place.

3.21 Sintering

In this step, powder so prepared finally transforms to usable ceramic body. In ceramic industries, this step is also known as firing. $BaTiO_3$ matures in the 1350°C to 1450°C range [35]. This is the most important processing step in making of ceramic material. All properties of ceramic depends on the sintered body which is the direct result of the

sintering parameter such sintering temperature, hold time, atmosphere, thermal profile, etc. There are many sintering methods used but this discussion would be limited to solid phase method.

Heat causes the powder particles to develop inter granular bonds by surface diffusion and other physical driving force, Mechanism of sintering and allied topics detailed elsewhere [36]. The typical green density of ceramic body at the start is about 60% of TD. Strength starts to develop gradually as more and more particles bond. At about —80% to 90% density the pores are still open and the ceramic has a typical "chalky" appearance. The dielectric constant is usually low and the T is not pronounced strongly. The pores of a ceramic are generally closed at ~95% of TD. Additional heat work causes grater densification as trapped gasses diffuse out along grain boundaries. At densities below 95% of TD the presence of open pores would cause the dielectric loss and undoubtedly inferior dielectric properties.

Setting of sintering temperature is not that straight Forward. Low temperature sintering results in ceramic of poor density and formation of Ba_2TiO_4. On the other hand, too high temperature and long hold time may cause open structure with low density [35]. Also, at high temperature grain growth is accelerated resulting in low dielectric properties. Another harmful hexagonal phase of $BaTiO_3$ may form at the temperature higher than 1460°C (Figure 3-10). The sintering temperature and time should be optimum for proper densification to occur without abnormal grain growth. This is best done by trail and error for particular material, volume and other process parameters.

In MLC manufacturing industries, sintering high temperature such as 1300°C is not practicable, due to use of low melting point electrode material. Commercial formulation is aimed to lower temperature (~1100°C) sintering with the addition of many sintering and dopents.

3.22 Properties of BaTiO₃

Ferroelectric ceramics and dielectric behaviors were discussed in length in the previous sections. Ferroelectric nature of $BaTiO_3$, the mechanism of superior dielectric properties, factors affecting properties discussed in the following sections. Effect of doping, process

variables such as ball milling practice, calcination thermal profiles, sintering temperature and hold time on the dielectric properties discussed.

3.23 Crystal Structure and Phase Transformation

Different phase transformations and cell dimensions of $BaTiO_3$ are illustrated in figure 2-14. $BaTiO_3$ has a paraelectric cubic phase above its Curie point of about 1 30°C. In the temperature range of 1 30°C to 0°C the ferroelectric tetragonal phase with a $\frac{c}{a}$ ratio of ~1.01 is stable. The spontaneous polarization is along one of the [001]
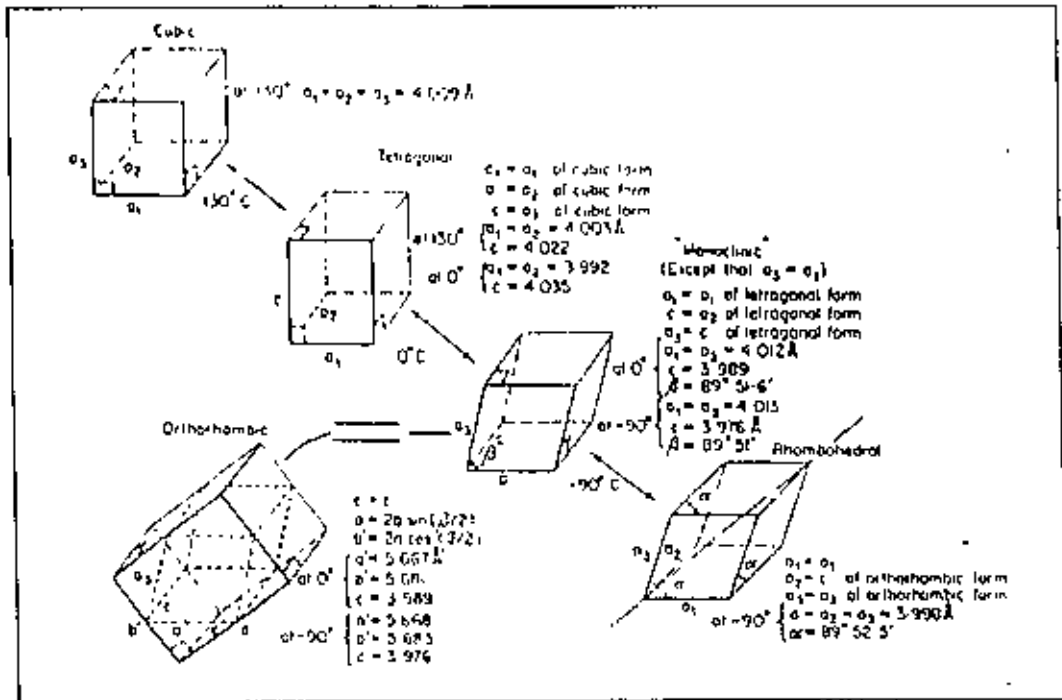
Figure 3-14: Different Phases, transformation and cell dimension of $BaTiO_3$

directions in the original cubic structure. Between 0°C and -90°C, the ferroelectric orthorhombic phase is stable with the polarization along one of the [110] directions in the original cubic structure. On decreasing the temperature below -90°C the phase transition from the orthorhombic to ferroelectric rhombohedral phase leads to polarization along one of the [111] cubic directions.

On cooling from high temperatures, the permittivity increases up to values well above 10,000 at the phase transition temperature T_c. The inverse susceptibility as well as the dielectric permittivity follows a Curie-Weiss law. The appearance of the spontaneous polarization is accompanied with a spontaneous (tetragonal) lattice distortion. The phase

transition in barium titanate is of first order, and as a result, there is a discontinuity in the polarization, lattice constant, and many other properties, as becomes clear in Figure 3-6.

3.24 Significance of tetragonal phase

The phase of ferroelectric interest is the tetragonal existing between 1 30°C (T_c) to 0°C. The extent of tetragonality i.e. c/a ratio can be calculated from XRD pattern. Separation of (002) and (200) peak is a good indication of formation of tetragonal BaTiO$_3$ as indicated in Figure 2-15 for sample calcined at 700°C, 900°C and 1100°C
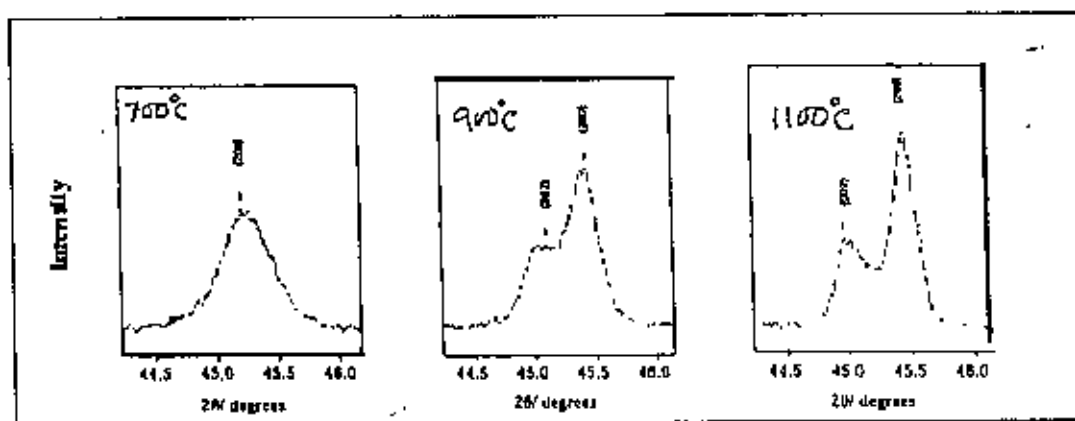
Figure 3-15 : XRD pattern showing separation of (002) and (200) peaks

[37], The JCPDS file for tetragonal and cubic phase are 5-626 and 31-174 respectively. The lattice parameters are given as a_0=3.994A and c_0 = 4.038A for tetragonal phase and a_0 = 4.031A for cubic phase. The c/a ratio was also increased from 1 .0065 to 1 .010 for calcination at 900 °C and 1100 °C respectively. Extreme anomalies of properties at T_c are associated with the extent of tetragonality of BaTiO$_3$ ceramic. On the other hand, ferroelectric properties will diminish with the absence of tetragonal phase.

3.25 Factors influencing tetragonal phase

Apart from the calcination temperature of BaTiO$_3$ formation the other major factor is the Ba/Ti molar ratio. Lee [21] reported the extent of dielectric peak at T_c lowed as Ba/Ti ratio increased. Impurities such as Fe, Cr, Mn present also suppress tetragonal phase. Curie point also suppressed in ultra fine-grained ceramic. Arlt et al [35] shown the dependence of lattice constants (c/a − 1)% of tetragonal BaTiO$_3$ ceramic on average grain size as illustrated in Figure 3-16. With the change of grain size different ferroelectric phases coexist at room temperature. At grain size above 1μm normal tetragonal XRD reflection occur for (004) and (400) planes. As the grain size is reduced

to 0.84µm these peaks shift closer and a third pseudo cubic reflection of (040) appear within. This pseudo cubic Phase most probably ascribed to the orthorhombic phase that exits below 10°C.
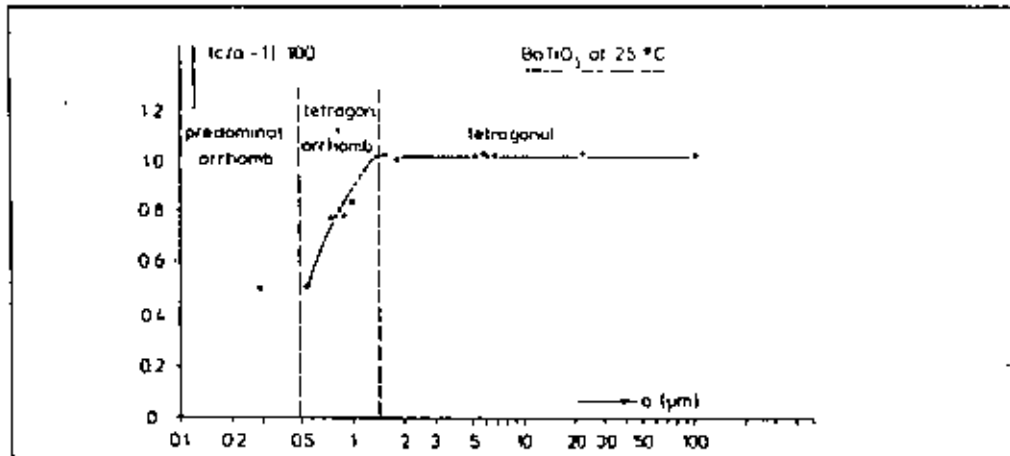
Figure 3-16: Ratio of the lattice constants as a function of grain size

At grain size of 0.28µm only two reflections are observed which cannot be ascribed to any know ferroelectric phases of BaTiO$_3$ [38].
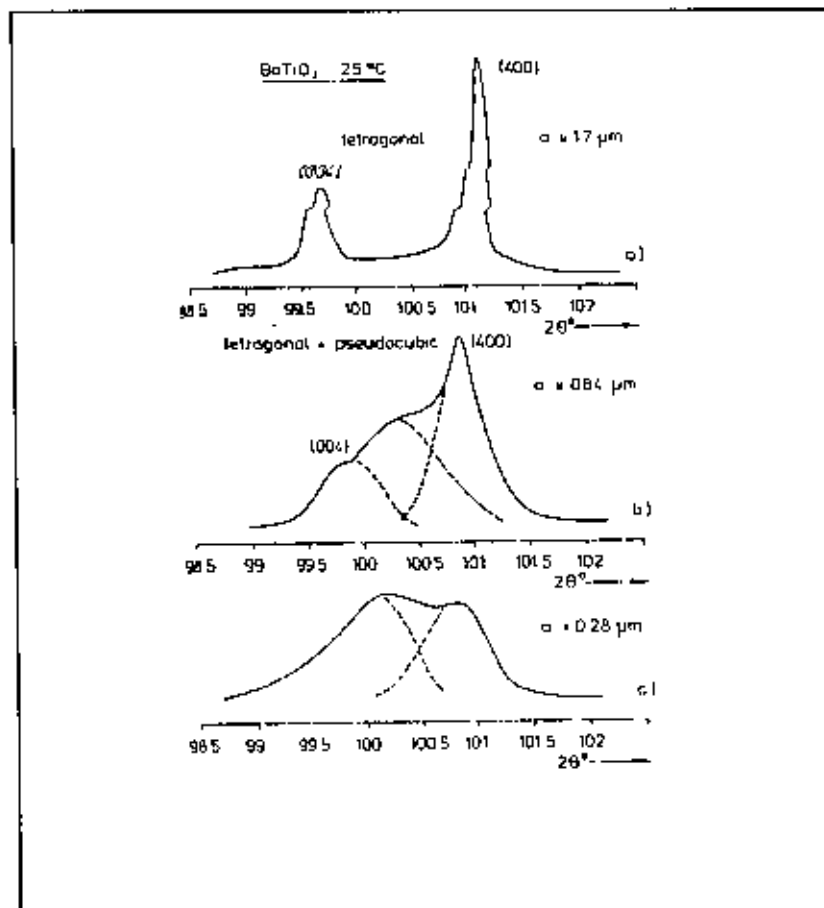
Figure 3-17: Deformation of the tetragonal (400)/(004) x-ray diffraction peaks due to grain size [38]

3.4.1.3 Displacement of ion off center dimension of atoms with in the unit cell of $BaTiO_3$ is given in figure
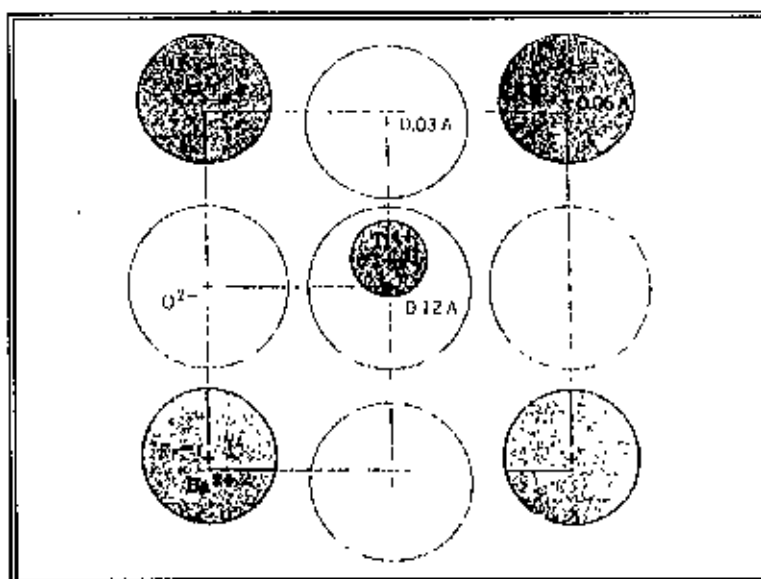
Fig: 3-18 Displacement ions in unit cell of $BaTiO_3$

3-18. Titanium ion is displaced by $0.12Å$ towards oxygen ion in [001] direction and that oxygen ion also displaced by 0.03 Å towards [001] titanium atom. Barium ion also displaced by 0.06 Å towards [001] direction. Under the influence of electric field of opposite direction the displacement will be towards opposite direction. On cooling below the Curie point T_c, the tetragonal structure so develops where the center of Ba^{2+}/c and Ti^{4+} ions are displaced relative to the O^{2-} ions, leading to the formation of electric dipoles. Spontaneous polarization developed is the net dipole moment produced per unit volume for the dipoles pointing in a given direction [17].

Large octagonal space compared to Ti atom size is responsible for this displacement. This is the basis of spontaneous polarization of $BaTiO_3$ or ferroelectric ceramic. This large octagonal hole is also the reason of $BaTiO_3$ undergoing many phase transformation at different temperatures. The relative displacement of ions in a unit cell illustrated in Fig: 3-18.

3.26 Domain Structure effect

In polycrystalline bulk ceramics the pattern of domains is quite different because the domain structure of each grain is formed under elastic clamped conditions by its surrounding neighbors, whereas a single crystal is free [38]. It should be noted that only non-180 domains, i.e. 90 domains (for tetragonal structures) or 71 and 109 domains (for rhombohedral structures), have the potential to reduce elastic energy.
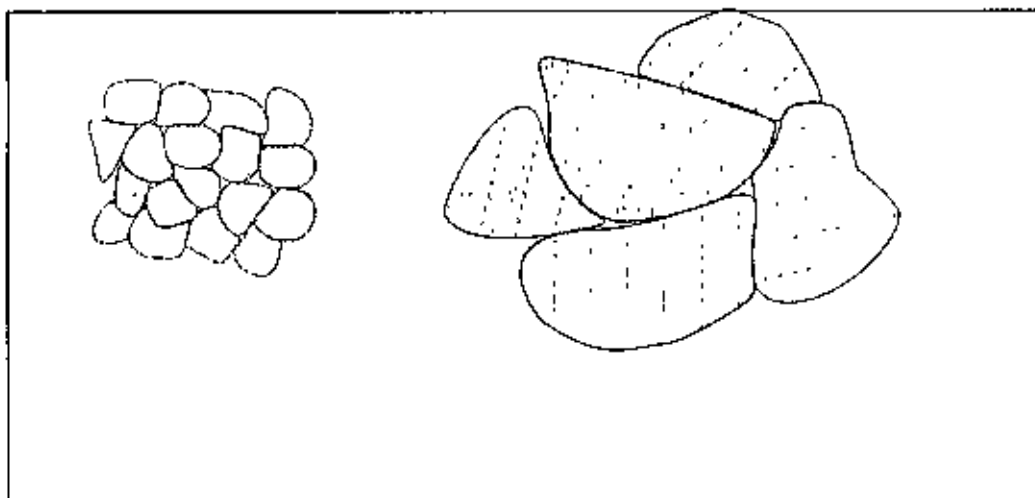
Figure 3-19: Domain pattern of fine grained (left) and coarse grained (right) BaTiO$_3$ ceramic

There exist two types of domain in coarse-grained BaTiO$_3$, called herring bone and square net pattern. The first one is by far the most common in unpoled ceramics. As shown in Fig: 3-19, by decreasing the grain *size* the domain pattern changes from a banded to a laminar structure [8].

3.27 Grain Size Effect

In bulk BaTiO$_3$ ceramics the grain size has a strong effect on the low frequency permittivity for grain sizes below approx. 10 µm as shown in Figure 2-1 7 (a). The permittivity is rising at decreasing grain sizes up to a maximum at grain size
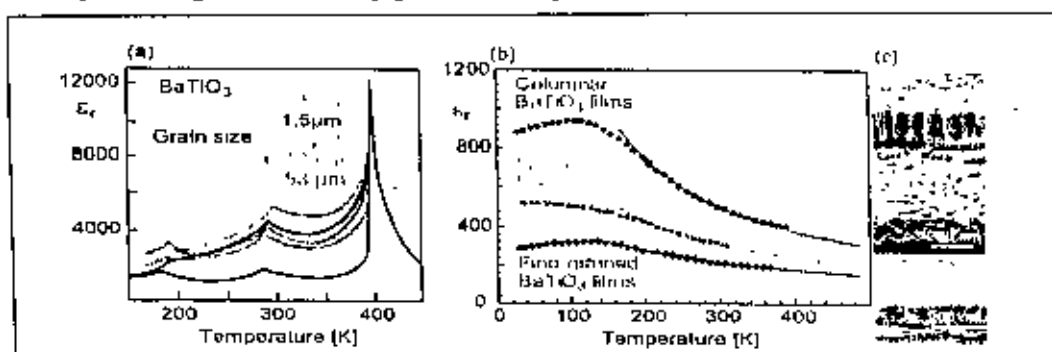
Figure 3-20: Temperature dependency of grain size

~0.7µm [38]. The increase of k' could have caused by internal stresses because each grain is clamped by its surrounding neighbors or by the increase of the number of domain walls contributing to the dielectric constant. Below this grain size the permittivity sharply decreases again in conjunction with a reduction of the tetragonality and of the remnant polarization.

In Figure 3-20 the temperature dependence of the permittivity for (a) bulk ceramics with different grain sizes and (b) thin films with different grain sizes and (c) microstructure of thin films are illustrated. For BaTiO$_3$ thin films a significant increase in the room temperature permittivity from 500 to 900 is observed which was induced by the change in the morphology from a granular to a columnar microstructure (Figure 3-20 (b) and (c)).

In contrast to BaTiO$_3$ bulk ceramics, which exhibit a paraelectric to ferroelectric phase transition with decreasing temperature accompanied by a sharp peak of the permittivity at around 123 only a broad maximum in the permittivity vs. temperature curve is observed for polycrystalline thin films. Additionally, the BaTiO$_3$ thin films do not show a ferroelectric hysteresis at room temperature. While the absence of a remanent polarization is typical for paraelectric material, the grain size dependence indicates a super-paraelectric behavior of BaTiO$_3$ thin films. Compared to bulk ceramics, thin BaTiO$_3$ films of the same average grain size show a significantly lower permittivity, although the grain size dependence is still observed. The difference in the absolute permittivity values may be explained by a combination of thin film effects, which result in a further decrease of the permittivity, as for example film- electrode interfaces and stress effects.

Figure 3-21 shows the variation of dielectric constant with temperature for BaTiO$_3$ ceramics with a fine (<1µm) and coarse (>50µm) grain size. Large grained BaTiO$_3$ (>1µm) shows an extremely high dielectric constant at the Curie point. This is because of the formation of multiple domains in a single grain, the motion of whose walls increases the dielectric constant at the Curie point. For BaTiO$_3$ ceramic with fine grains (<1µm), a single domain forms inside each grain. The movement of domain walls are restricted by

the grain boundaries, thus leading to a low dielectric constant at the Curie point as compared to coarse grained $BaTiO_3$ [39].

The room temperature dielectric constant, k' of coarse grained (>50μm) $BaTiO_3$ ceramics was found to be in the range of 1500-2000. On the other hand, fine grained (~1μm) $BaTiO_3$ ceramics exhibit a room temperature dielectric constant between 3500-6000. The grain size effect on the dielectric constant at room temperature has been explained by the work of Arlt *et. al.* [38] and Buessem *et. al.* [40] coworkers proposed that the internal stresses in fine grained $BaTiO_3$ must be much greater than
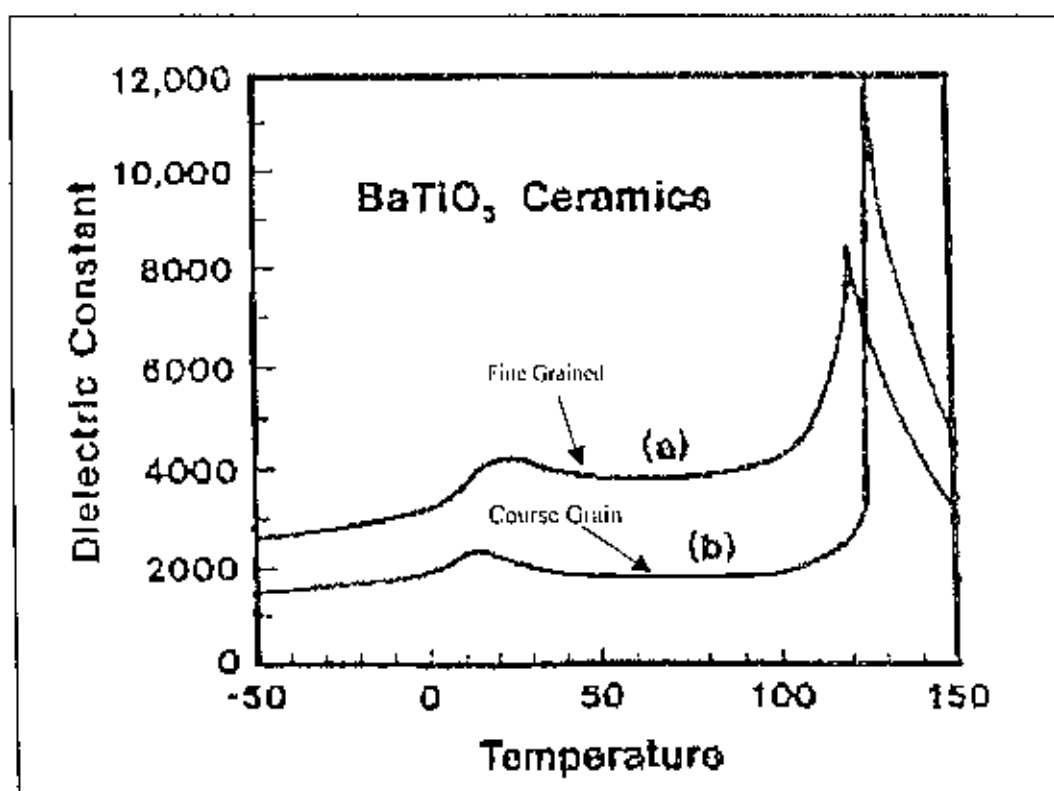
Figure 3-21: Grain size effect on k' of bulk ceramic

the coarse grained ceramic, thus leading to a higher permittivity at room temperature. Arlt studied the domain structures in $BaTiO_3$ ceramics and showed that the room temperature k' reached a peak value at a critical grain size of ~0.7 μm. He concluded that the enhanced dielectric constant was due to the increased 900-domain wall density. The mobility of the 90° domain walls in very fine grained $BaTiO_3$ is hindered and only less than 25 % of the k' was achieved.

As the BaTiO$_3$ ceramics have a very large room temperature dielectric constant, they are mainly used multi layer capacitor applications. The grain size control is very important for these applications.

3.28 Morphology

Dielectric constant strongly depends on the microstructure specially Porosity and other phase present. The effect of grain size discussed earlier. Ideally sintering should provide a ceramic body close to its theoretical density, around 95% or more

Gerson, et al [41] expressed the relation between porosity and k' as

$$Log_{10}(k') = \Sigma_n V_n log_{10}(k'_n) \text{ --- --- } \{21\}$$

where, V_1, V_2....... are volume fraction with k' of k'_1, k'_2`......... Relationship with the experimental data shown in Figure 3-22.

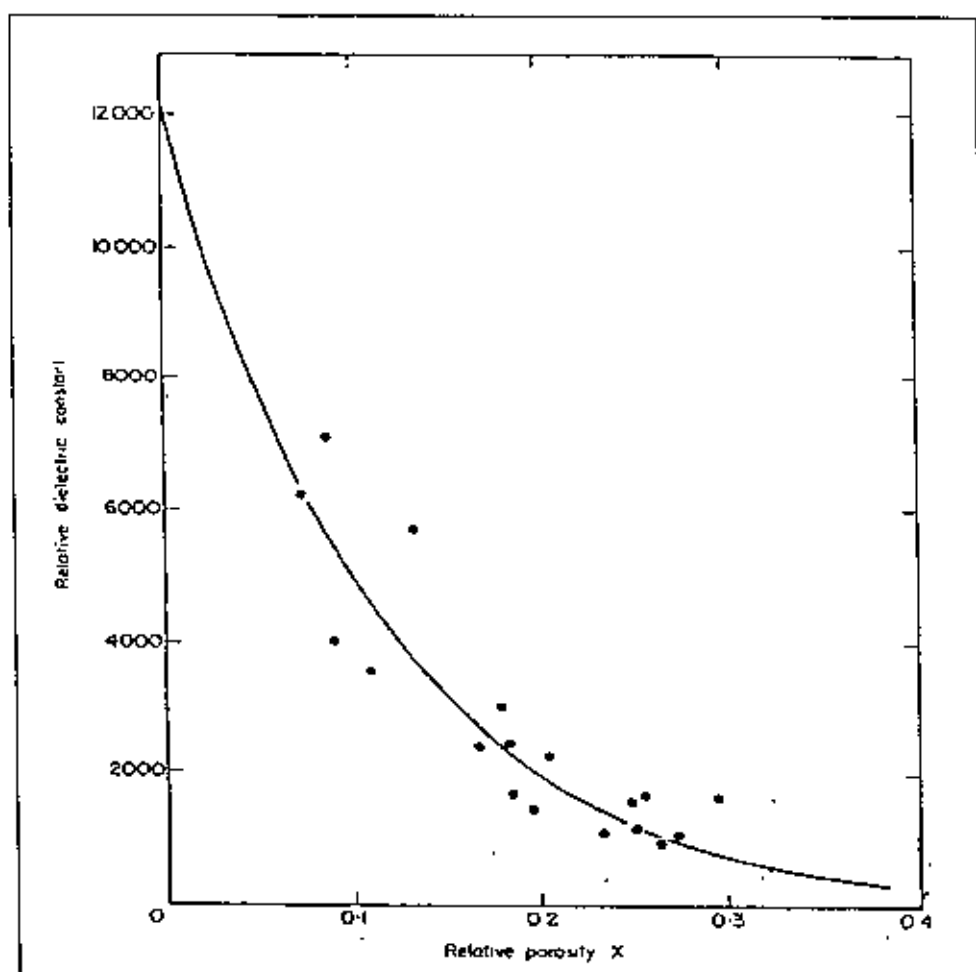Figure 3-22: Dielectric constant relationship with porosity [41]

Another feature of is the core shell structure develops owing to doping and other factors are discussed in section 3.31.

3.29 Doping effect

Various A and B site substitutions in different concentrations have been tried to see their effect on the dielectric and ferroelectric properties of $BaTiO_3$. Sr^{2+} and substitutions to the A site have been found to reduce the Curie point linearly towards room temperature. The substitution of Pb^{2+} for Ba^{2+} raises the Curie point. The substitution of Zr^{4+} tend to decrease T_c but increases other transition temperatures. These effect shown in Figure 3.23 with effect on dielectric property. The simultaneous substitution into both A and B sites with different ions can be used to tailor the
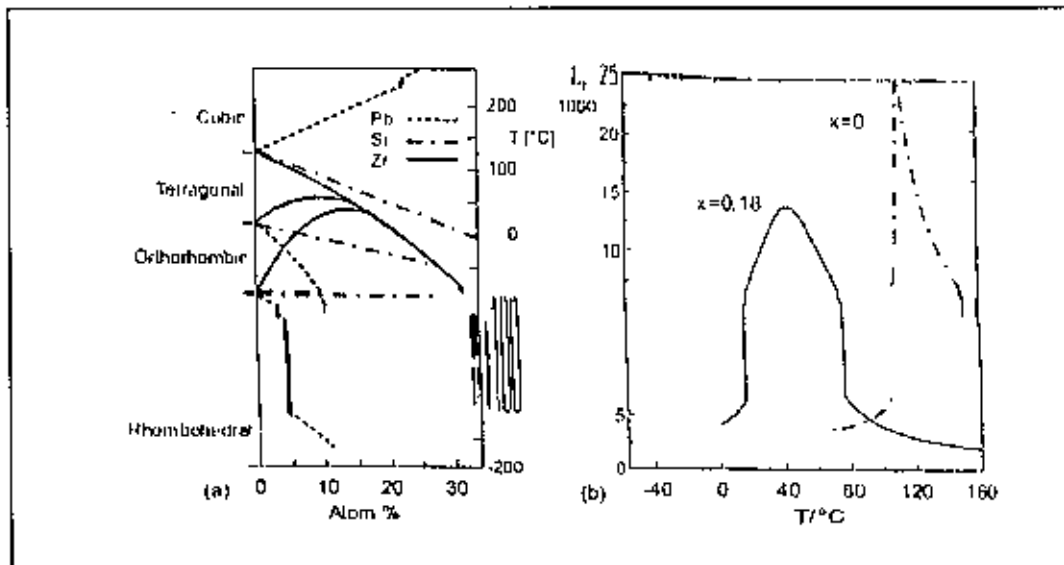
Figure 3-23: Change of transition temperature with dopents and effect on dielectric constant.

properties of $BaTiO_3$. The effects of various isovalent substitutions on the transition temperatures of $BaTiO_3$ ceramic are shown in Figure 3-24.

Doping is necessary to:

-avoid time variations of $k = \varepsilon/\varepsilon_0$

-broaden the k' - T dependence

-decrease T_c to close to room temperature, if maximum k' is   required

If an ion of the perovskite structure $BaTiO_3$ is replaced by a different ion of the same valence, isovalent doping is present, e.g. Ca^{2+} on the Ba^{2+} site $Ba_{1-x}Ca_xTiO_3$. Aliovalent doping exists when donors like La^{3+} on Ba site or Nb^{5+} on Ti-site as well as acceptors like Ni^{2+} or Mn^{3+} on Ti-site are incorporated in the crystal. At least the site occupancy is determined by the size and the valence of the dopant, e.g. Ca^{2+} may be isovalent A-site or acceptor-type on B-site.
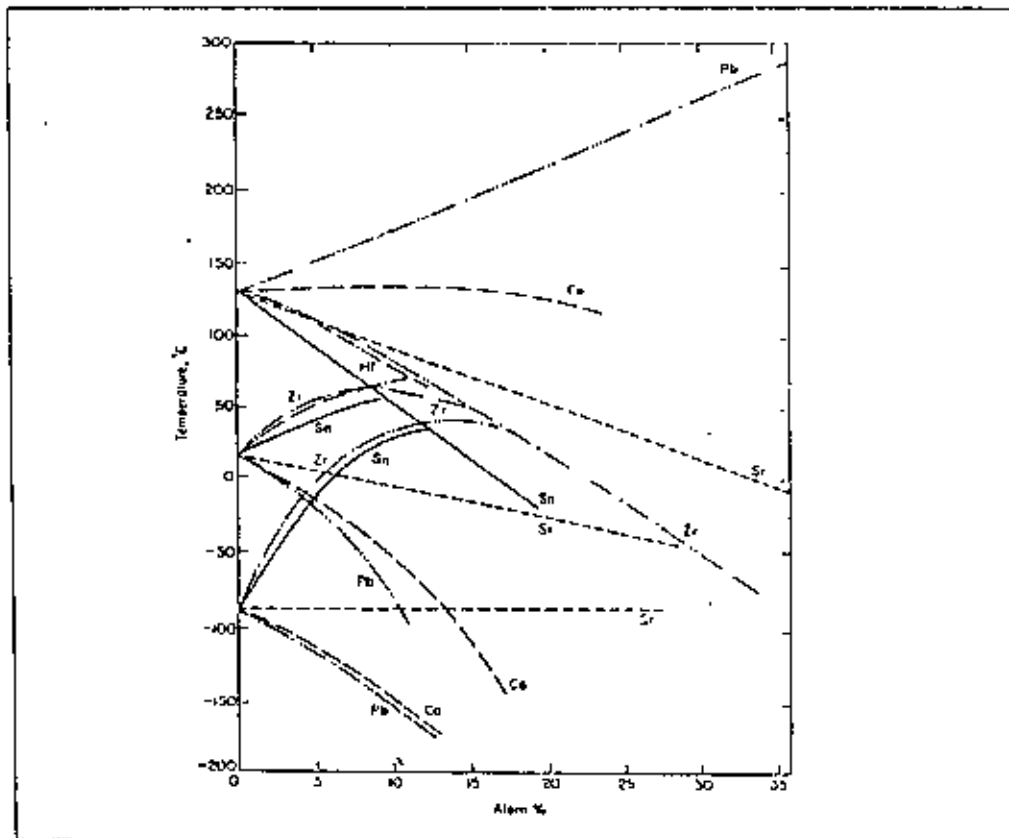
Figure 3-24 The effect of doping on the transition temperatures of $BaTiO_3$ ceramic

Besides Sr, Pb and Zr, Ba can be replaced by Pb, Sr, *Ca*, or *Cd*, and Ti can be replaced by Sn, Hf, Zr, Ce, or Th.

3.30 Commercial formulations

As discussed in detail so far, the permittivity of ferroelectric perovskites shows marked changes with temperature, particularly close to the phase transition. From the device point of view a high dielectric permittivity with stable properties over a wide temperature range is required. There are various commercial specifications, which have to be fulfilled.

Figure 3-25 Commercial formulations and their k′ vs T characteristics [42]

By substitution or doping it becomes possible to tailor the ferroelectric materials to different properties. In Figure 3-25 dielectric constant vs temperature behavior of commercial formulation as illustrated.

3.31 T_c Suppression

Doping generally leads to a shift of the phase transition temperature. In Figure 3-23 and 3-24, the change of the transition temperatures is plotted as function of dopant concentration for different dopants in $BaTiO_3$. It i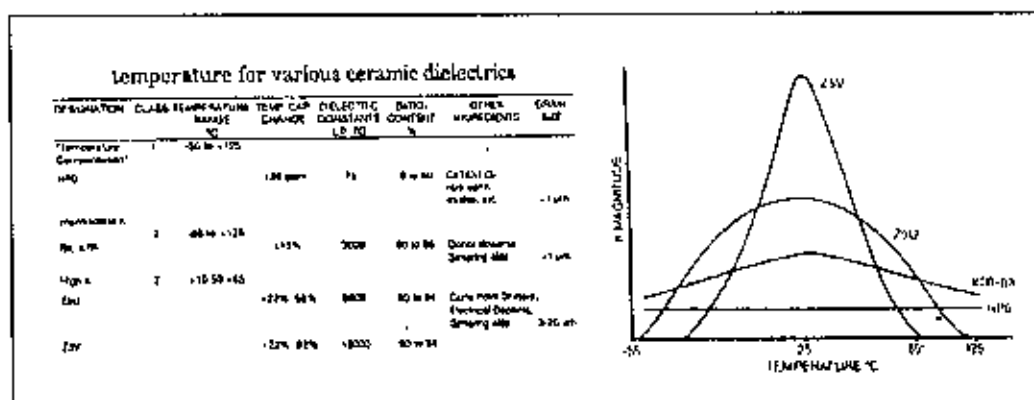s found that Pb-doping stabilizes the tetragonal phase in the sense of their existence over a wide temperature range whereas Sr-doping destabilized the tetragonal phase. This behavior could be understood by the fact that the larger Pb-ions on the A-site form a larger cavity giving the central ion more space for off-center positions than the Sr-ions. In case of high dopant concentrations sequence of the phase transitions in $BaTiO_3$ tends to be suppressed. For $Ba(Zr_xTi_{1-x})O_3$ all phase boundaries meet at a Zr content $x = \sim 0.18$ (Figure 3-23). Because of the superposition of the particular phase transitions the resulting transition becomes diffuse with a broad maximum of the dielectric permittivity as shown in Figure 3-23. Therefore, this composition has the potential as suitable temperature-stable dielectric for ceramic capacitors.

3.32 Core Shell Structure

A different approach to over come the temperature instabilities of the dielectric coefficient is the addition of more complex compositions (than doping with atoms) as $CdBi_2Nb_2O_9$. By controlling the reaction kinetic of the sintering process the microstructure exhibits a grain core-grain shell structure. The core consists of $BaTiO_3$,

and the perovskite material in the shell shows a mixture of $BaTiO_3$ with the complex perovskites $Ba(Bi_5Nb_5)O_3$ and $Ba(Cd_{2/3}Nb_{2/3})O_3$ having an approximate Curie point at T_c 80°c. Figure 3-26 displays schematically the ferroelectric core and the paraelectric shell. The chemical inhomogeneity emerges during a process of reactive liquid phase sintering. Application of too high sintering temperatures leads to uniform distributions of the additives via solid-stated diffusion.
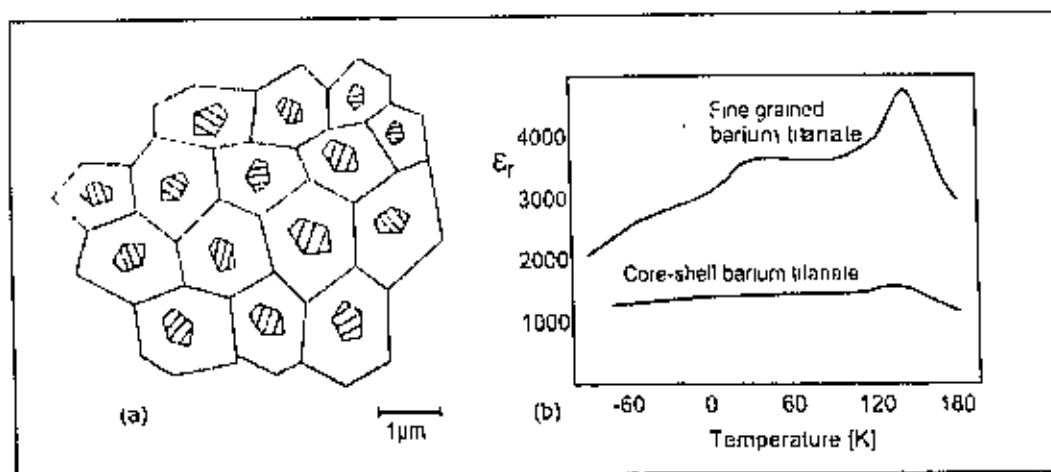

Figure 3-26 : Core Shell structure and its effect on k'

3.33 Relaxor Ferroelectric

These are special type of ferroelectric ceramic in their own right. Strictly, they are neither a derivative of $BaTiO_3$ nor a result of doping effect. The reason of their relevance in this study was to high light few aspects, which was observed in the $BaTiO_3$ samples of this study. Relaxor ferroelectrics are a class of lead based perovskite type compounds with the general formula $Pb(B_1,B_2)O_3$ where B_1 is a lower valency cation (like Mg^{2+}, Zn^{2+}, Ni^{2+}, Fe^{3+}) and B_2 is a higher valency cation (like Nb^{5+} Ta^{5+}, W^{5+}). Pure lead magnesium niobate (PMN or $Pb(Mg_{1/3}Nb_{2/3})O_3$) is a representative of this class of materials with a Curie point at -10°c.

Relaxor ferroelectrics like PMN can be distinguished from normal ferroelectrics such as $BaTiO_3$ and PZT, by the presence of a broad diffused and dispersive phase transition on cooling below the Curie point. Figure 3-27 shows the variation in the dielectric properties with temperature for PMN ceramic. It shows a very high room temperature dielectric constant and a low temperature dependence of dielectric constant. The diffused

phase transitions in relaxor ferroelectrics are due to the compositional heterogeneity seen on a microscopic scale.
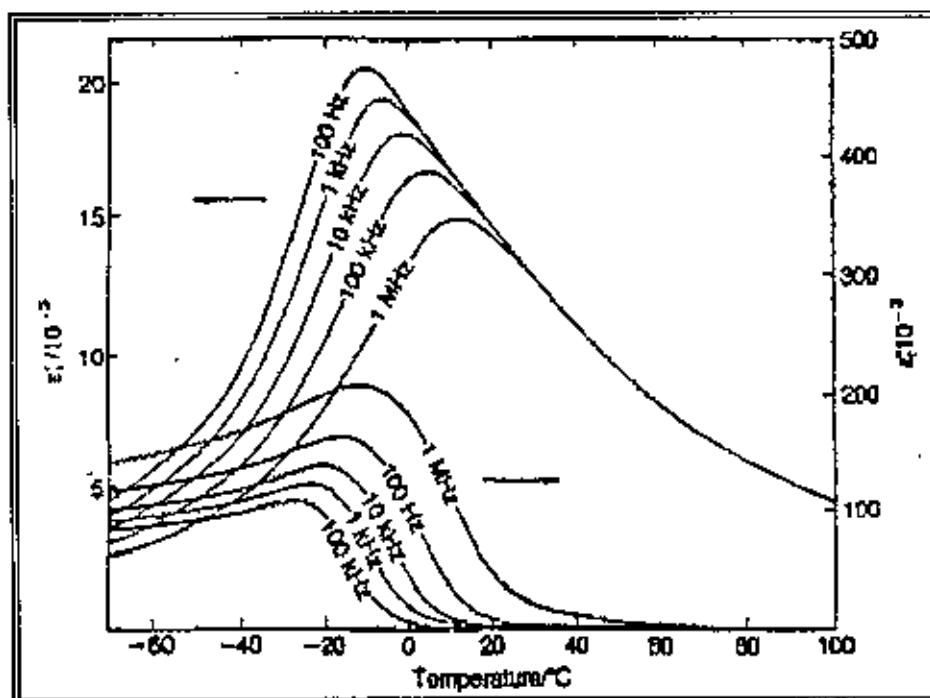

Figure 3-27 Variation of the dielectric properties of PMN with temperature [43]

The relaxors also show a very strong frequency dependence of the dielectric constant. The Curie point shifts to higher temperatures with increasing frequency. The dielectric losses are highest just below the Curie point, T_c Relaxors which give a second order phase transition, the remnant polarization, P_r, is not lost at the Curie point but gradually decreases to zero on increasing the temperature beyond T_c [44]

3.34 Applications

Barium titanate can be regarded as 'role model' of electronic ceramic from application point of view. Its piezoelectric, pyroelectric and ferroelectric properties were successfully applied in many commercial applications. Vast majority of commercially important application are in polycrystalline bulk or film form. In the following sections, property wise applications are briefly discussed. Since dielectric properties of BaTiO$_3$ were studied in this thesis, capacitor application especially MLCC emphasized. Cut-away schematic of MLCC is shown in Figure 2-30 and a actual MLCC shown in Figure 3-31.

3.35Ferroelectric applications as Bulk

Notable application of ferroelectric $BaTiO_3$ is in the manufacture of capacitor for electrical appliances. Basics of capacitor have been discussed in the section 3.2 with example of simple ceramic capacitor. From application point of view MLC capacitors are most important and technologically challenging. The volumetric efficiency (more capacitance from given capacitor size) further enhanced by using multi layer ceramic (MLC) capacitors. As shown in Figure 3-30, the MLC capacitor structure consists of alternate layers of dielectric and electrode material. Each individual dielectric layer contributes capacitance to the MLC capacitor as the electrodes terminate in a parallel configuration.

Hence, the effective equation (cf. equation 5) for capacitance becomes,

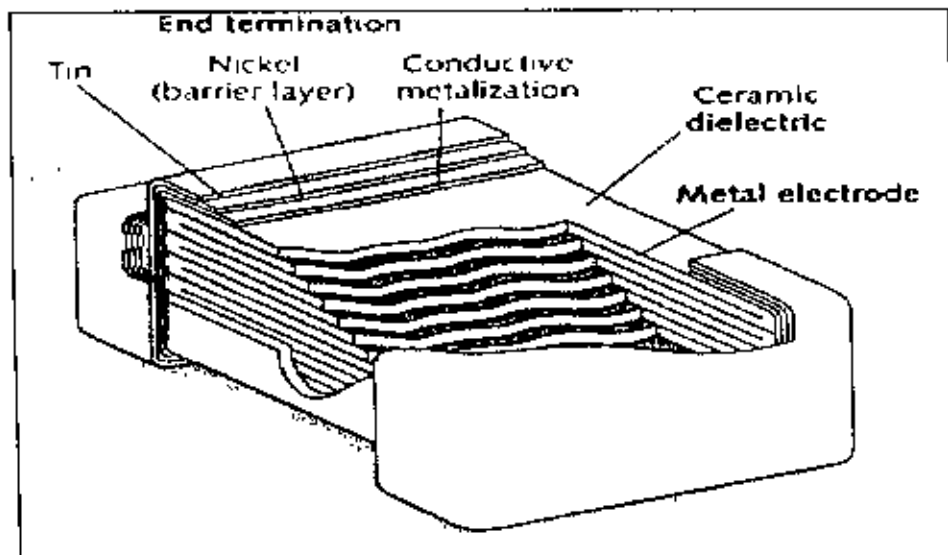$$C = \frac{n\varepsilon_n k'A}{d}$$

Figure 3-28 Schematic of multi layer capacitor

Here, n is the number of dielectric layer. The advances in tape casting technology have made it possible to make dielectric layers <20 μm thick. This, combined with the use of a high dielectric constant ceramic like $BaTiO_3$,
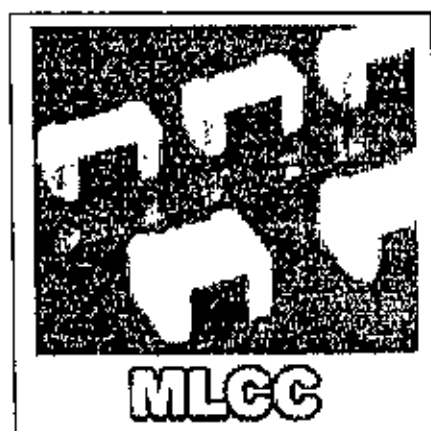
Figure 3-29 MLCC capacitor

allows large capacitance values to be achieved in relatively small volume capacitor devices [43]. MLC capacitors are made by the tape casting process.

3.36 MLCC processing

Slurry with a suitable binder/solvent system is first made from the dielectric ceramic powder. Thin green sheets of the ceramic are then made by the tape casting process. Ink consisting of an electrode (Pd, Ag-Pd, etc.) and organic is screen printed on the dielectric sheets and then hundreds of sheets are stacked one on top of the other. A low pressure at a temperature between 50°C and 70°C is applied to laminate the sheets. These laminates are then diced to form a monolithic green MLC capacitor. The binder removal is accomplished by heating the green body very slowly to a temperature of 300-400°C. The MLC capacitor is then sintered at a high temperature depending on the type of ceramic. After applying the terminations for the internal electrodes of the MLC capacitors, the capacitor is mounted on the electronic substrate by soldering.

The critical steps in the fabrication of the MLC capacitors include the formation of thin uniform green sheets from the ceramic slurry. Any non-uniformity in the thickness could lead to dielectric breakdown during operation of the device. The co-firing of the ceramic tapes and metal electrodes should be compatible and should not lead to any reactions between the two.

3.37 Ferroelectric Thin Films

Ferroelectric thin films have attracted attention for applications in many electronic and electro-optic devices. Beside $BaTiO_3$ other important ferroelectric materials being used for making thin films include the perovskite type materials such as, $Pb(Zr_xTi_{1-x})O_3$ and $Pb(Mg_{1/3}Nb_{2/3})O_3$. Applications of ferroelectric thin films utilize the unique dielectric, piezoelectric, pyroelectric, and electro-optic properties of ferroelectric materials. Some of the most important electronic applications of ferroelectric thin films include nonvolatile memories, thin films capacitors, pyroelectric sensors, and surface acoustic wave (SAW) substrates. The electro-optic devices being studied include optical wave guides and optical memories and displays

3.38 Piezoelectric Applications

In the early days, piezoelectric property of $BaTiO_3$ was used in phonographic pick-ups. Piezoelectric ceramics can be used for both active and passive transducer applications in ultra sound application. In the passive mode the transducer acts as a sound receiver i.e. there is conversion of sound energy into an electrical signal. The converse piezoelectric effect permits a transducer to act as an active sound transmitter.

In the pulse echo mode, the transducer is used to perform both the active and passive functions at the same time. A sound wave is propagated into the medium and a faint echo is received back after a small time gap due to the acoustic impedance mismatch between the interface materials. This principle is used in transducers for ultrasonic medical imaging applications. Other applications are gas igniter, displacement transducer, accelerometers, piezoelectric transformers, impact printer head for dot matrix, etc.

3.39 Other applications

Recently $BaTiO_3$ has been used as in-built thermal switchers on motors. When the temperature rises above a set point, the resistance through the switch increases, shutting off the motor. Also for constant temperature heating devices as the device becomes self-regulating at the set temperature by the increase of resistance. However, in spite of all of this interest, an accurate model of the cause of the PTCR (positive temperature coefficient of resistivity) effect remains a contentious issue. At a particular temperature, which can be tuned by the choice of dopants and the doping level, a rather sharp increase

in resistivity covering several orders of magnitude is observed. The resistance drops normally on either side of this sharp transition. The nature of this PTCR effect occurs in the same temperature range where the sample undergoes a structural phase transition from a tetrahedral to a cubic unit cell. However, the phase transition also occurs in the single crystal sample where no PTCR effect is observed. Apparently, the grain boundary region must be in control of this phenomenon.

CHAPTER 4

Experimental

Disc shape samples were prepared in this experiment. Three sets of samples were prepared with different materials and process variables. Presinter powder processing of the samples and pellets so made were then sintered by hand milling 12 hrs milling and 24 hours milling with zirconia ball.

4.1 Sample preparation

Conventional mixed oxide method was used through out. Appropriate weight of Barium carbonate ($BaCO_3$), Titanium oxide (TiO_2) and doping source of chromium (Cr) strontium (Sr) and Vanadium (V) were mixed and milled by hand and by ball

The doping sources were Cr_2O_3, (chromium oxide) $SrCO_3$ and (Strontium carbonate) and V_2O_5 (vanadium pentaoxide).
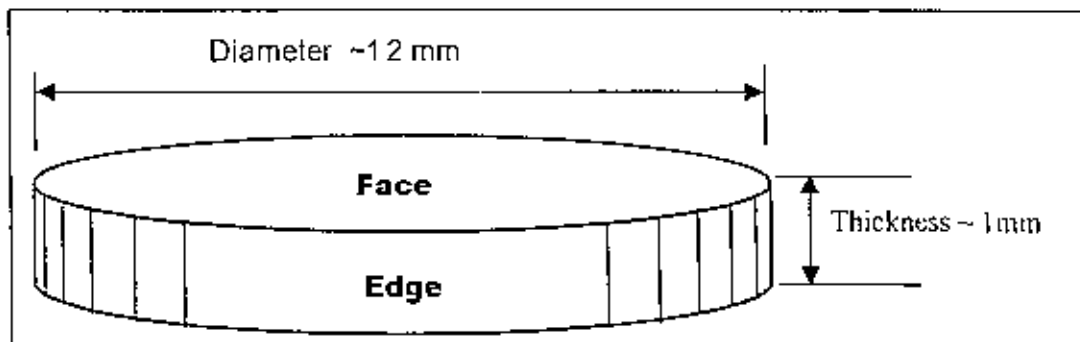
The shape of the sample shown in fig [4.1]

Fig-4.1: Final shape of a sample.

Zirconia ball and acetone were used as media. Typical milling times were 12 hours and 24 hours.

4.2 Calcination

First powder was heated from room temperature to 1100°C in a heating furnace which was set at 1100°C for 24 hours. Then the furnace was turn off and was allowed to cool down to room temperature. When the room temperature was attained, the chunk was taken out and ground until it becomes powder. The above procedure was repeated for

three times. After 72 hours of total calcinations, the chunk was ground again until it becomes fine powder.

4.3 Preparation of pellets

Three sets of milled calcined powder were mixed with polyvinyl alcohol (PVA) before pressed into pellets. Samples were pressed into pellets under uniaxial pressure of 1200-1250 psi using hand pressure machine.

4.4 Sintering

Furnace was used to sinter the pellets in air atmosphere. All the pellets were sintered at 1300°C; the temperature ramp was 10°C/minute. The samples thus obtained were used for dielectric properties measurement.

4.5 Dielectric constant and Dielectric loss

Electrical properties of the sample were measured using Agilent model 4129A impedance analyzer. Dielectric constant k′ was calculated from the capacitance value.

4.6 Microstructure

Sintered samples were polished using conventional ceramographic technique. Concentrated HCl was used as etching agent. The microstructure of samples was examined using scanning Electron Microscope (SEM). Samples were gold sputtered prior to SEM examination. At Materials and Metallurgical Engineering Dept. Phillips XF 30 was used with acceleration voltage of 10kV.

4.7 X-ray Diffraction

Extent of reaction or $BaTiO_3$ formation was examined by XRD in powder form.

Table: XRD operational condition:

X-ray source:	MoK_α	for calculation
current:	20 mA	$Mo\ K_\alpha = 0.710688A°$ used
Degree range:	10°-70°	
Scanning Speed:	1° per second	

CHAPTER 5

Results and Discussions

5.1 X-ray diffraction analysis

To characterize the samples, X-ray diffraction analysis was carried out with an X-ray diffractometer using Molybdenum target. Figure 5.1 shows the X-ray diffraction pattern for all the samples of the series respectively.

The table 5.1 gives the corresponding peak position observed for these samples. The observed position of the diffraction peaks look identical and thus have confirmed the single phase perovskite structure of all the samples with no significant trace of impurity. By changing the doping level of Ba, Ti and Ca, Sr, Cr and V the position of the diffraction peak does not change significantly which also indicates that the crystal structure remains unchanged.

Table 5.1: X-ray diffraction peak position for various doped BaTiO$_3$ sample.

| Samples	1st Peak	2nd Peak	3rd Peak	4th Peak	5th Peak	6th Peak
BaTiO$_3$	14.00°	17.20°	20.00°	24.80°	32.40°	38.80°
Ba(Ti$_{.975}$Cr$_{.025}$)O$_3$	14.00°	17.20°	20.00°	24.80°	32.40°	38.80°
Ba$_{.9}$Sr$_{.1}$(Ti$_{.975}$Cr$_{.025}$)O$_3$	14.00°	17.20°	20.00°	24.80°	32.40°	38.80°
Ba$_{.8}$Ca$_{.1}$Sr$_{.1}$(Ti$_{.975}$Cr$_{.025}$)O$_3$	14.00°	17.20°	20.20°	24.80°	32.40°	38.80°
Ba(Ti$_{.975}$V$_{.025}$)O$_3$	14.00°	17.20°	20.20°	24.80°	32.40°	38.80°
Ba$_{.9}$Sr$_{.1}$(Ti$_{.975}$V$_{.025}$)O$_3$	14.00°	17.00°	20.20°	25.00°	32.60°	38.80°
Ba$_{.8}$Ca$_{.1}$Sr$_{.1}$(Ti$_{.975}$V$_{.025}$)O$_3$	14.20°	17.20°	20.00°	25.00°	32.60°	38.80°
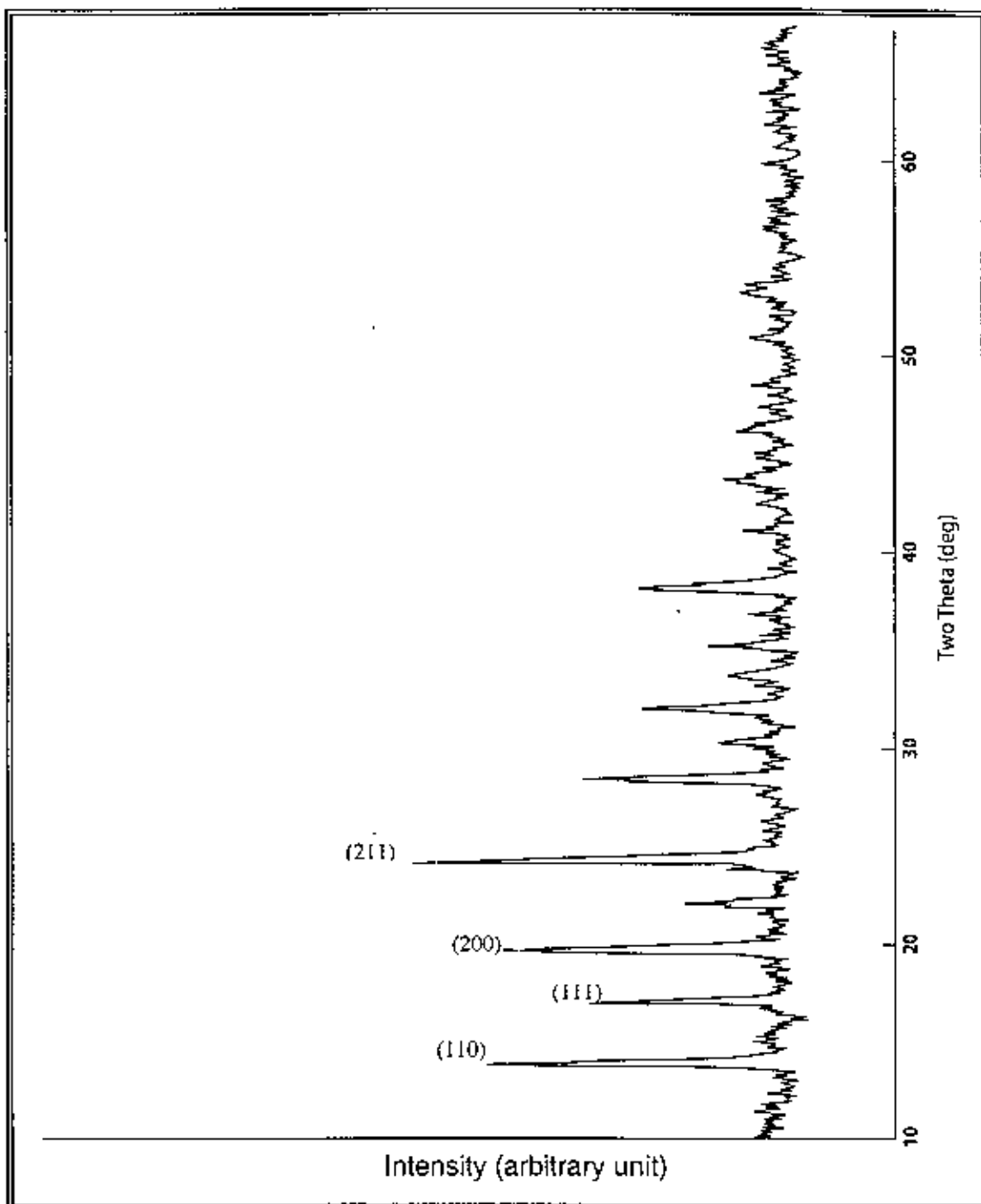
Figure-5.1: X-Ray diffraction pattern of BaTiO₃
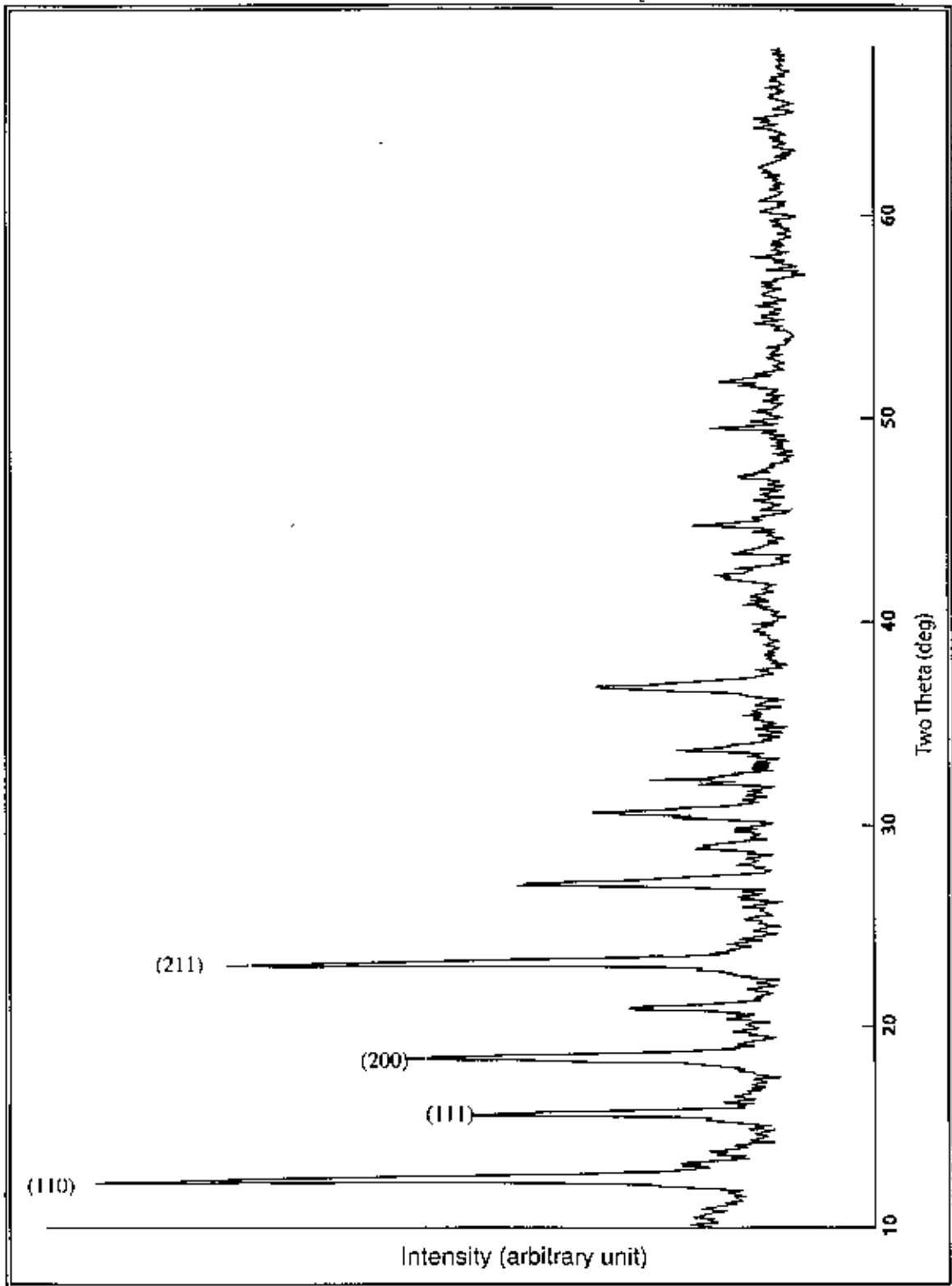
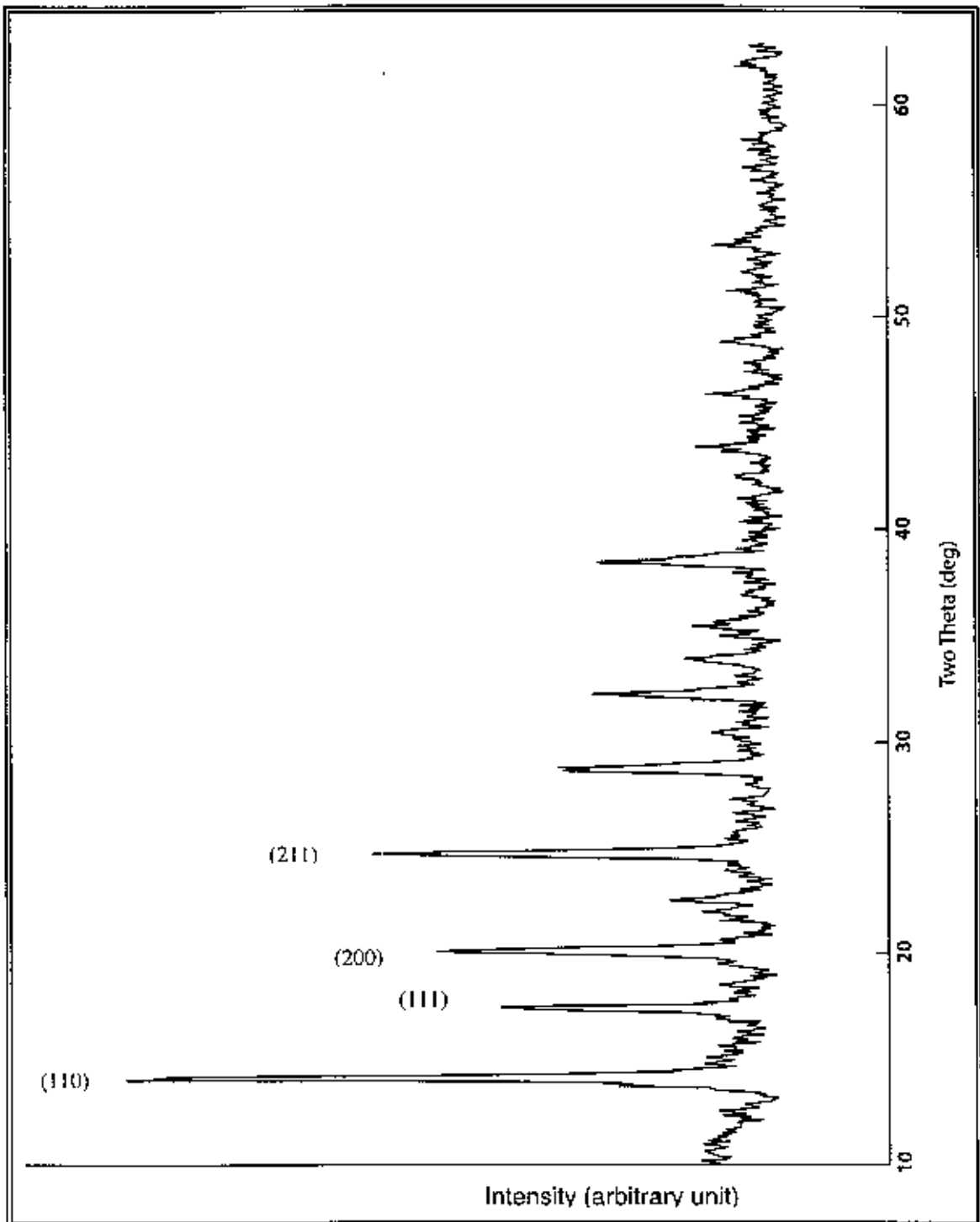Figure-5.2: X-Ray diffraction pattern of Ba(Ti$_{.975}$Cr$_{.025}$)O$_3$

Figure-5.3: X-Ray diffraction pattern of $Ba_{.9}Sr_{.1}(Ti_{.975}Cr_{.025})O_3$
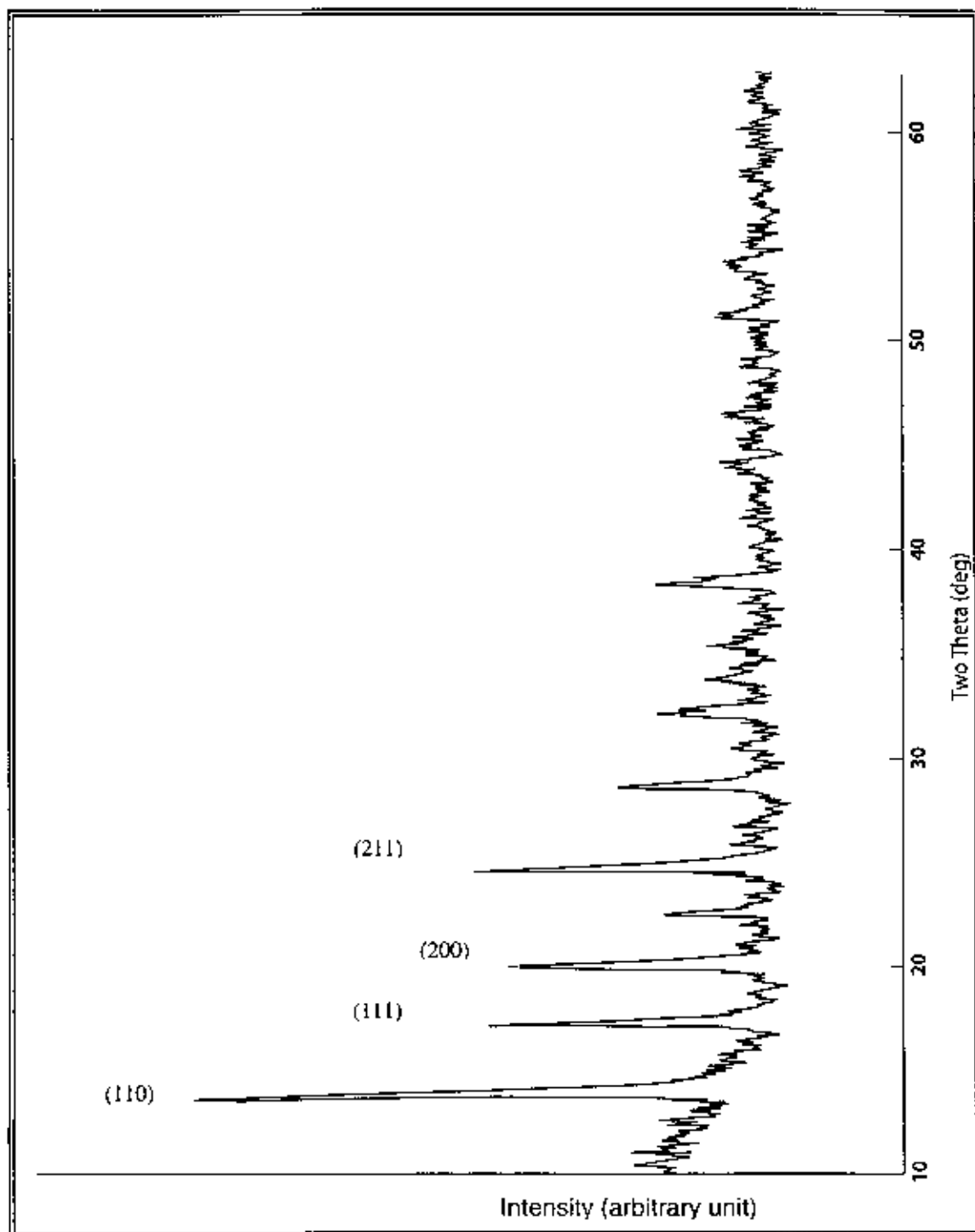
Figure-5.4: X-Ray diffraction pattern of $Ba_{.8}Ca_{.1}Sr_{.1}(Ti_{.975}Cr_{.025})O_3$
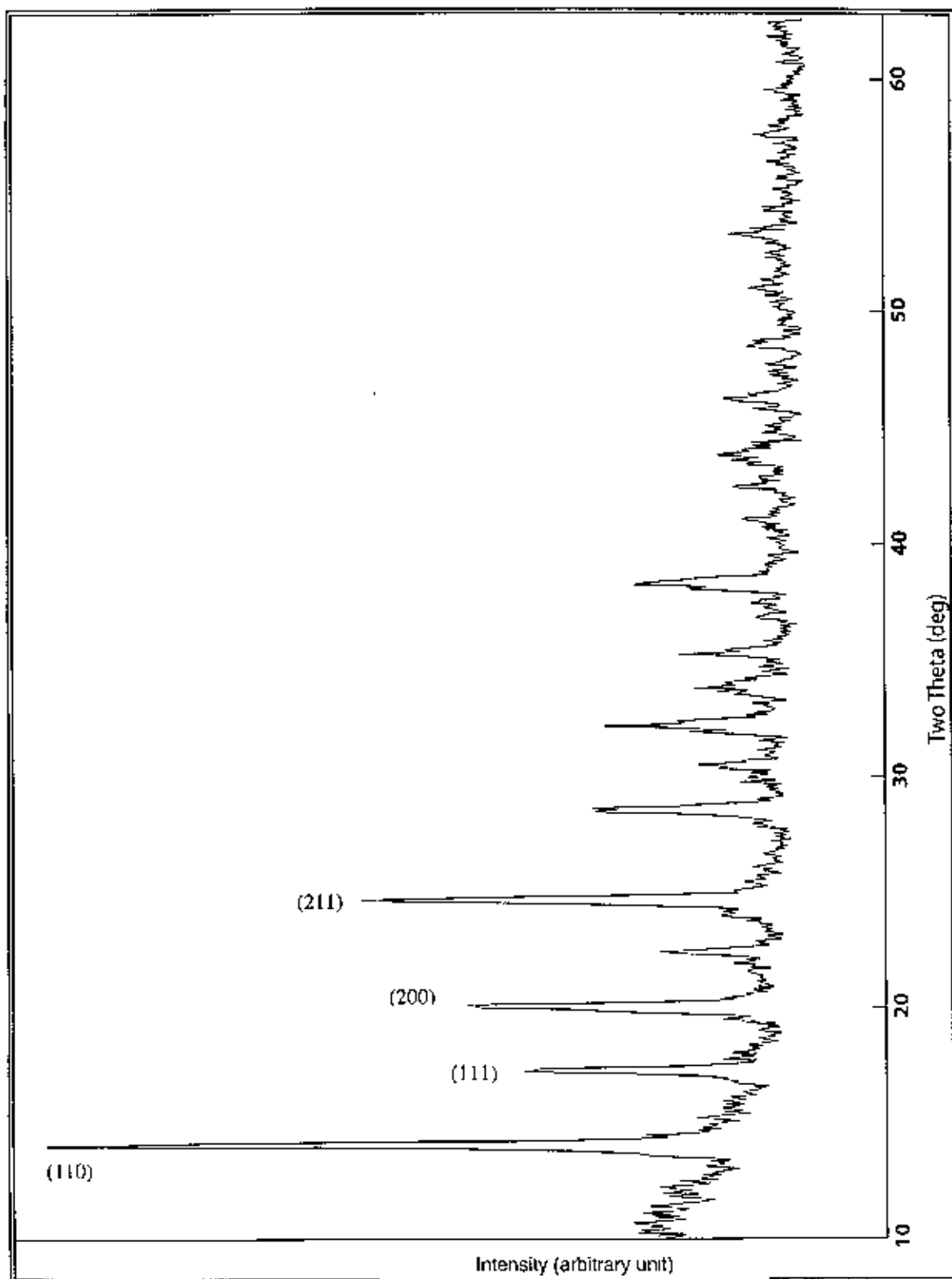
Figure-5.5: X-Ray diffraction pattern of Ba(Ti.975V.025)O3
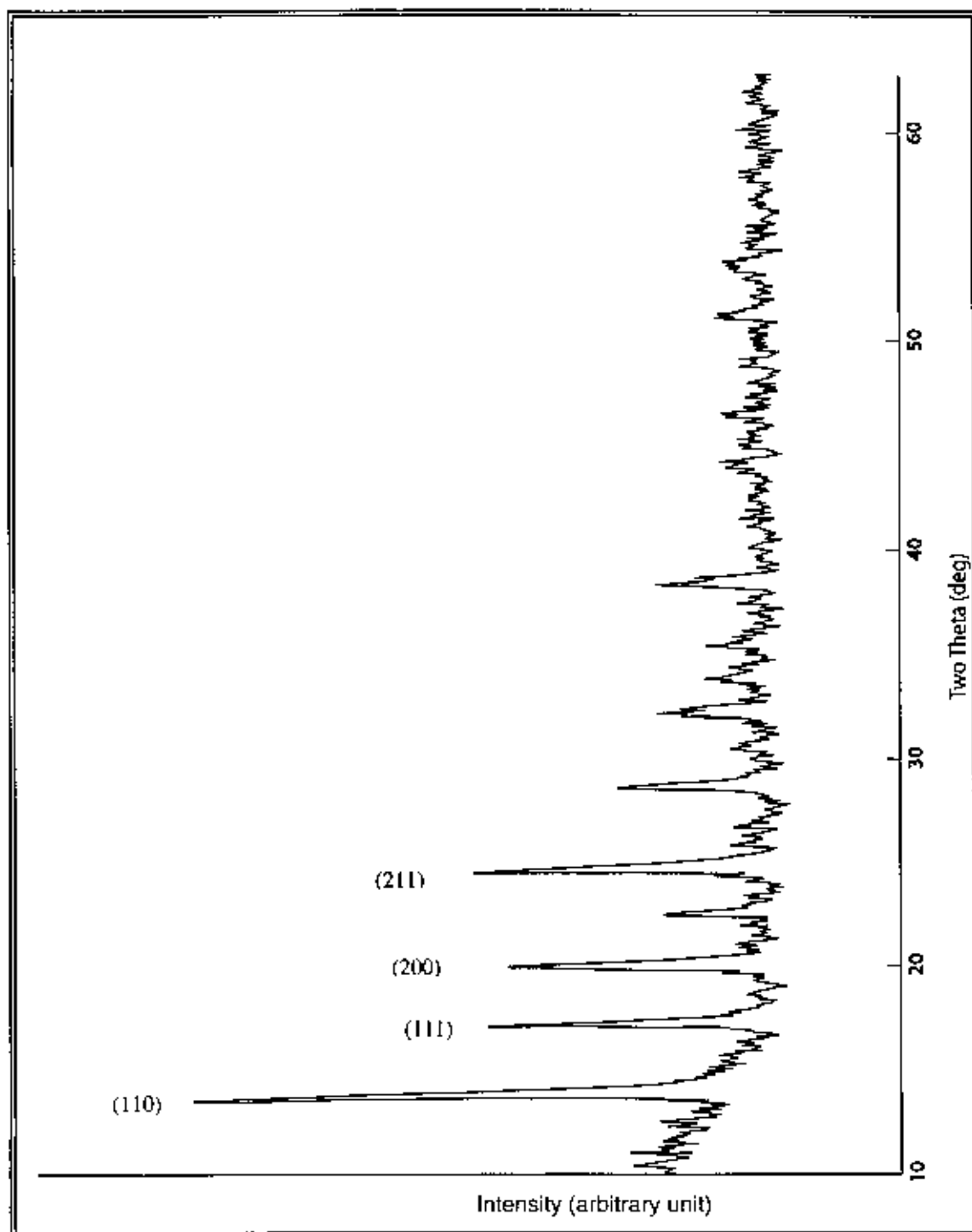
Figure-5.6: X-Ray diffraction pattern of Ba$_{.9}$Sr$_{.1}$(Ti$_{.975}$V$_{.025}$)O$_3$
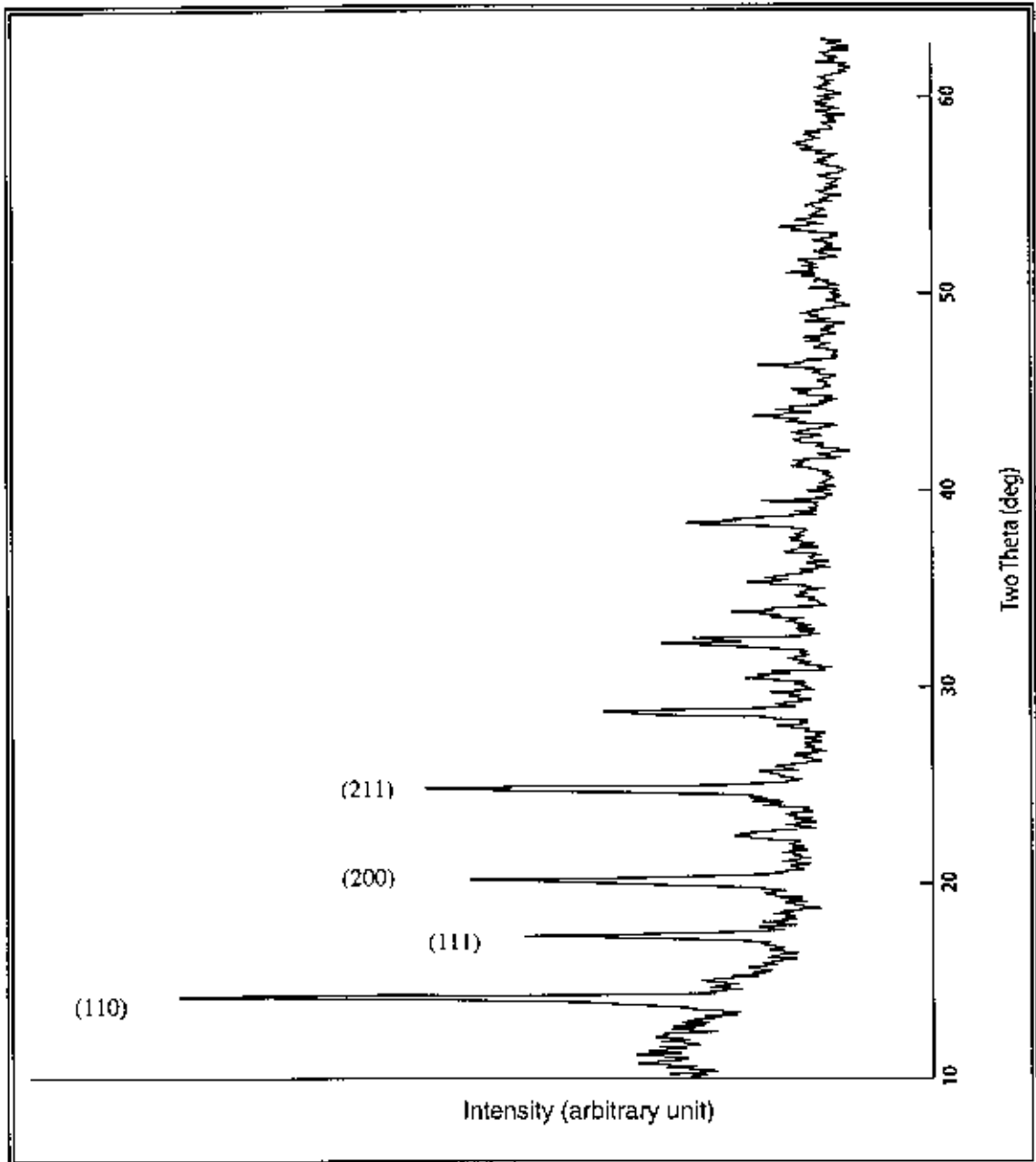
Figure-5.7: X-Ray diffraction pattern of $Ba_{.8}Ca_{.1}Sr_{.1}(Ti_{.975}V_{.025})O_3$
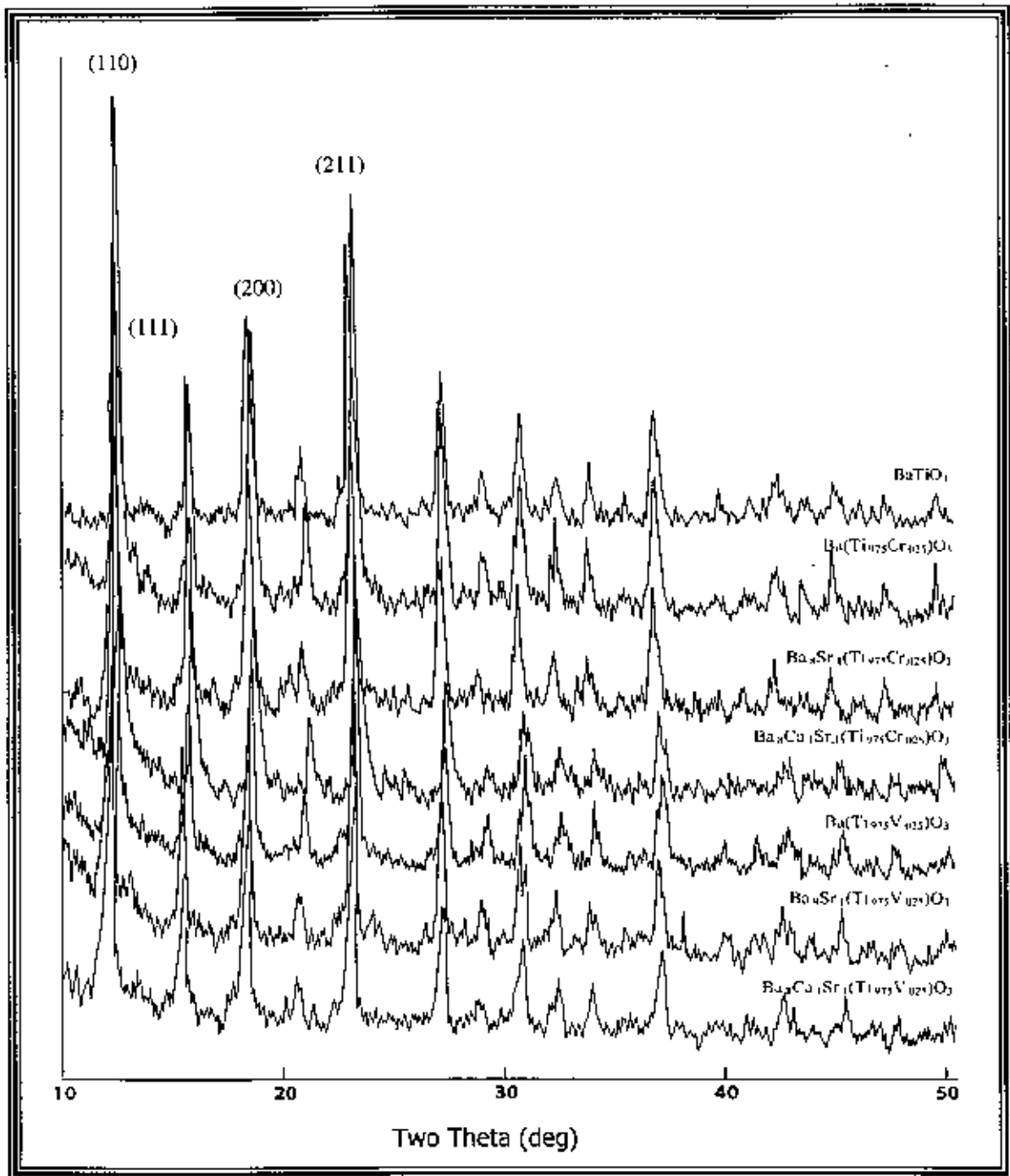
Figure· 5.8: X-ray Diffraction patterns of the samples BaTiO$_3$, Ba(Ti$_{.975}$Cr$_{.025}$)O$_3$, Ba$_{.9}$Sr$_{.1}$(Ti$_{.975}$Cr$_{.025}$)O$_3$, Ba$_{.8}$Ca$_{.1}$Sr$_{.1}$(Ti$_{.975}$Cr$_{.025}$)O$_3$, Ba(Ti$_{.975}$V$_{.025}$)O$_3$.
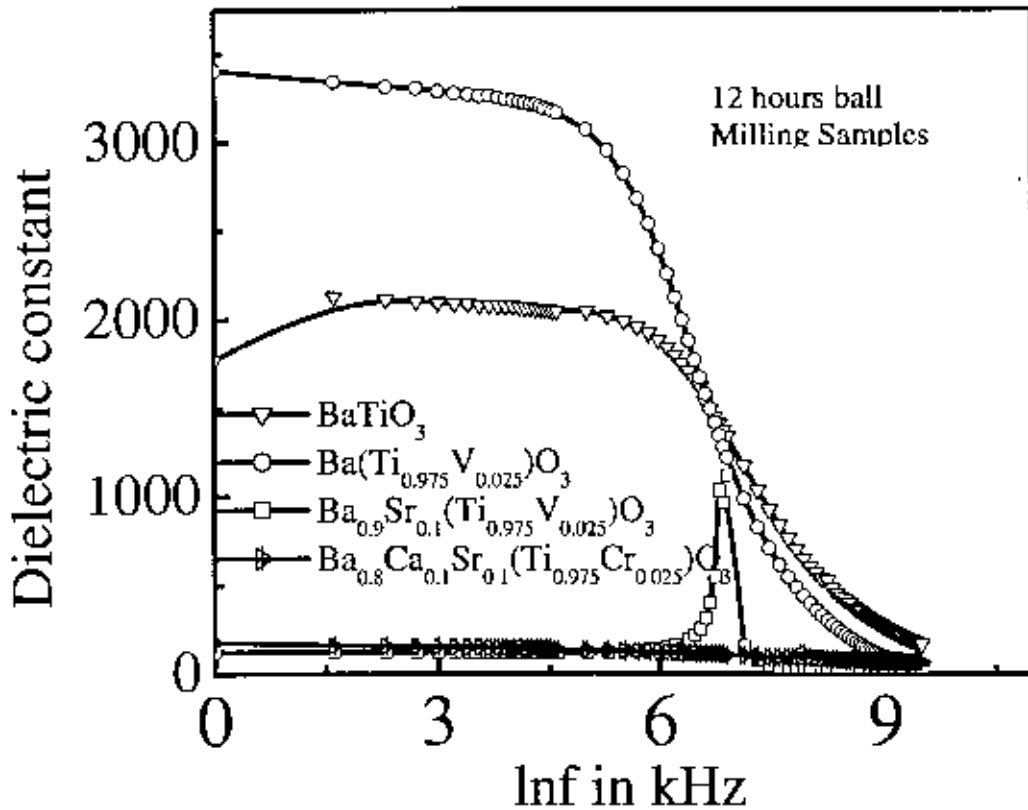
Figure-5.9: Dielectric constant as a function of frequency

Figure 5.9 indicates that for the sample $Ba(Ti_{.975}V_{.025})O_3$ the dielectric constant increases but for sample $Ba_9Sr_1(Ti_{.975}V_{.025})$ and $Ba_8Ca_1Sr_1(Ti_{.975}V_{.025})O_3$ the dielectric constant decreases. In Sample Ba $(Ti_{.975}V_{.025})O_3$ titanium is replaced by 0.025 mole fraction vanadium. Vanadium has larger ionic radius and electronic polarizibility. The dielectric constant increases in this case due to the ionic radius and electronic polariazbility. In Sample $Ba_9Sr_1(Ti_{.975}V_{.025})O_3$ barium is replaced by 0.1 mole fraction strontium. Strontium has smaller ionic radius and electronic polarizability than barium. The dielectric constant decreases in this case due to the smaller ionic radius and electronic polarizability. In Sample $Ba_8Ca_1Sr_1(T_{1.975}V_{.025})O_3$ barium is also replaced by 0.1 mole fraction calcium. Calcium has smaller ionic radius and electric polarizability than Barium. The dielectric constant decreases in the same manner due to the ionic radius and electronic polarizibility.
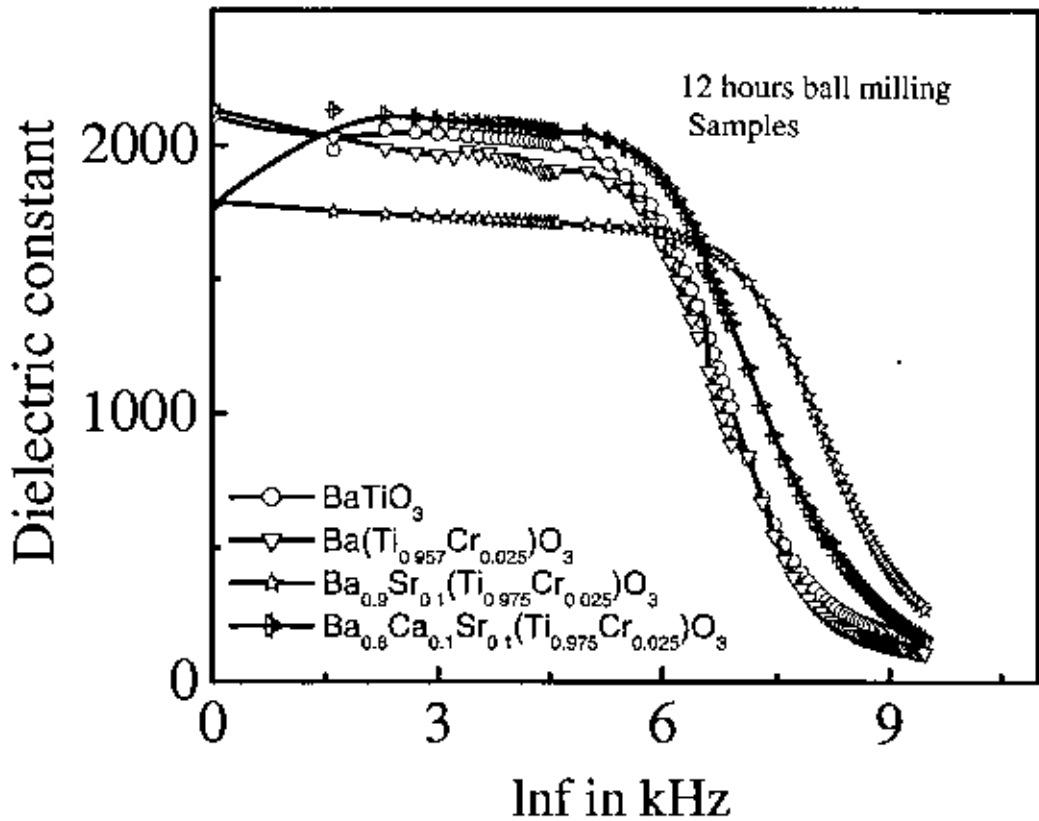
Fig-5.10: Dielectric constant as a function of frequency

Figure- 5.10 indicates that in sample $Ba(Ti_{.975}Cr_{.025})O_3$ and $Ba_{.9}Sr_{.1}(Ti_{.975}Cr_{.025})O_3$ The dielectric constant decreases slightly. In sample $Ba_{.8}Ca_{.1}Sr_{.1}(Ti_{.975}Cr_{.025})O_3$ the dielectric constant increases slightly. In sample $Ba(Ti_{.975}Cr_{.025})O_3$ titanium is replaced by 0.025 mole fraction chromium. Chromium has smaller ionic radius and electronic polarizability than titanium. Dielectric constant decreases in that case due to the smaller ionic radius and electronic polarizibility. In sample $Ba_{.9}Sr_{.1}(Ti_{.975}Cr_{.025})O_3$ Barium is replaced by 0.1 mole fraction strontium. strontium has smaller ionic radius and electronic polarizability than barium, The dielectric constant decreases in that case due to smaller ionic radius and electronic polarizability. In sample $Ba_{.8}Ca_{.1}Sr_{.1}(Ti_{.975}Cr_{.025})O_3$ barium is again replaced by 0.1 mole fraction calcium. In sample $Ba_{.8}Ca_{.1}Sr_{.1}(Ti_{.975}Cr_{.025})O_3$ the doping of calcium has positive effect for increasing dielectric constant.
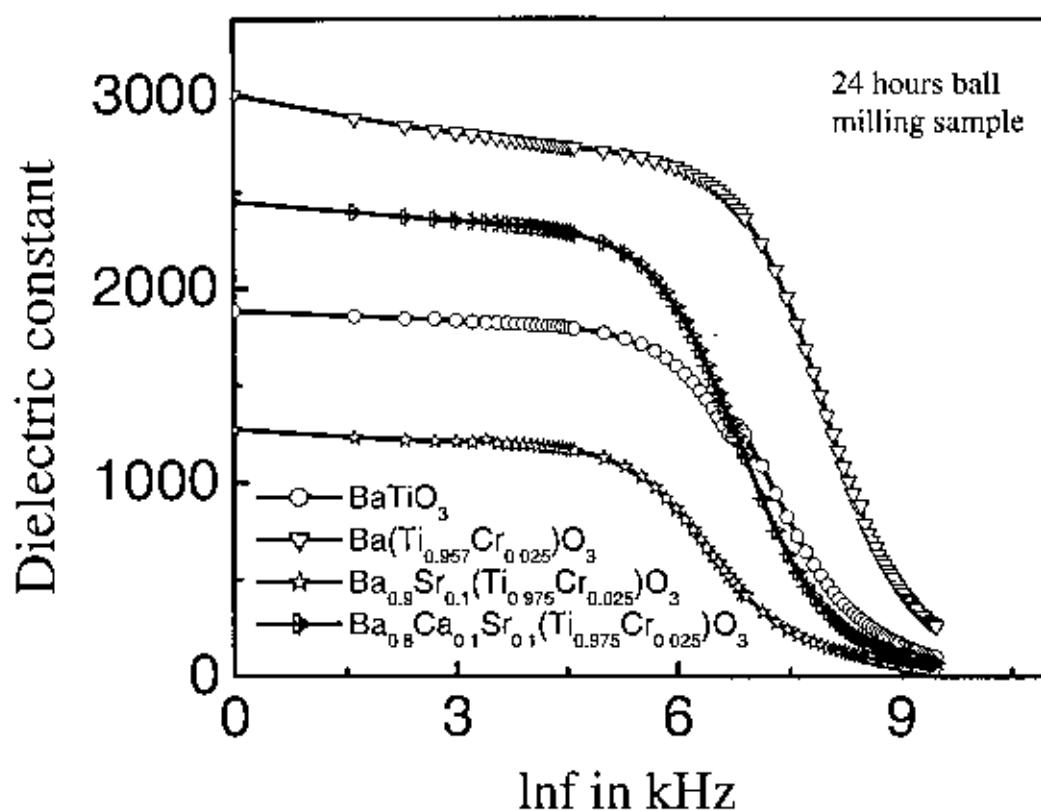
Fig-5.11: Dielectric constant as a function of frequency

Figure-5.11:   indicates the dielectric constant of 24 hours milling samples as a function of frequency. From figure-5.11, it can be seen that in the sample $Ba(Ti_{.975}Cr_{.025})O_3$ the dielectric constant increases more high. In the sample $Ba_{.8}Ca_{.1}Sr_{.1}(Ti_{.975}Cr_{.025})O_3$ the dielectric constant also increases. But in the sample $Ba_{.9}Sr_{.1}(Ti_{.975}Cr_{.025})O_3$ the dielectric constant decreases. In sample $Ba(Ti_{.975}Cr_{.025})O_3$, titanium is replaced by 0.025 mole fraction cromium. Cromium has smaller ionic radius and electronic polarizbility than titanium. Due to the smaller ionic radius and electronic polarizibility dielectric constant should be decreased, but in that case dielectric constant increased. The dielectric constant increases in that case due to the outer shell configuration of Cromium. In sample $Ba_{.9}Sr_{.1}(Ti_{.975}Cr_{.025})O_3$. Barium is replaced by 0.1 mole fraction strontium. Strontium has smaller ionic radius and electronic polarizability than barium. The dielectric constant decreases in that case due to smaller ionic radius and electronic polarizability.In sample $Ba_{.9}Ca_{.1}Sr(Ti_{.975}Cr_{.025})O_3$ barium is again replaced by 0.1 more fraction calcium. It can be also seen that the doping of calcium has positive effect for increasing dielectric constant.
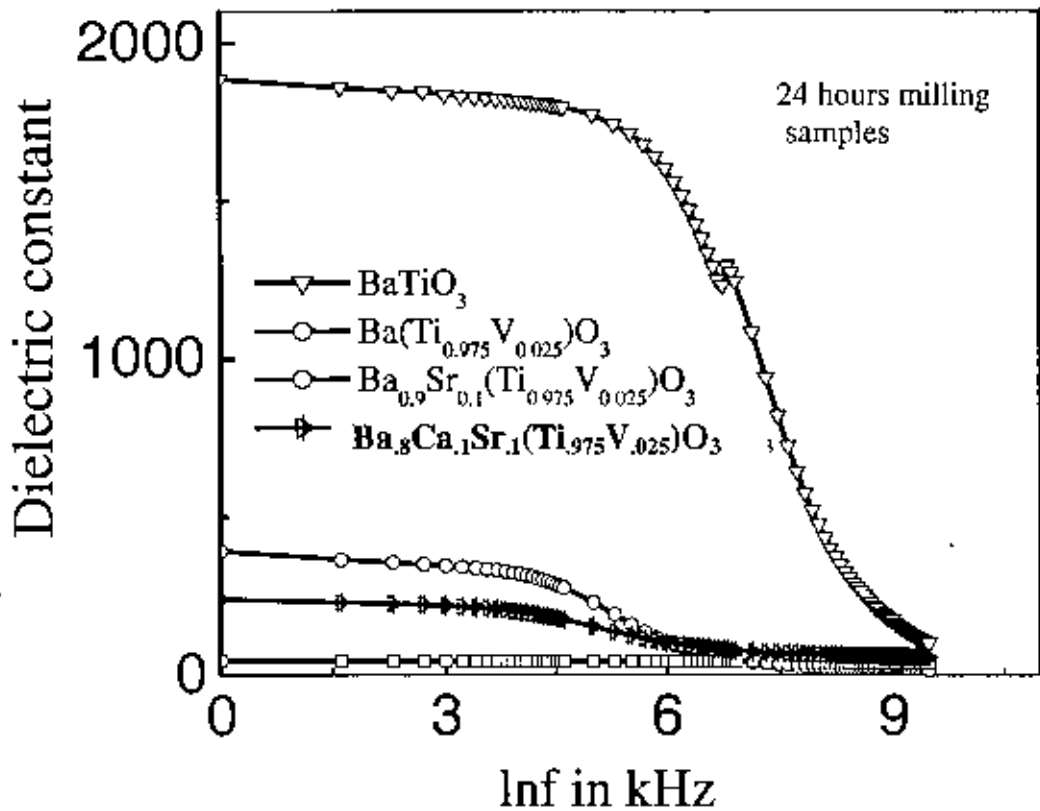
Fig-5.12: Dielectric constant as a function of frequency

Figure 5.12 indicates the dielectric constant of 24 hours ball milling samples as a function of frequency. For the sample $Ba(Ti_{0.975}V_{.025})O_3$ the dielectric constant decreases. For sample $Ba_{.9}Cr_{.1}(Ti_{.975}V_{.025})O_3$ and for the sample $Ba_{.8}Ca_{.1}Sr_{.1}(Ti_{.975}V_{.025})O_3$ the dielectric constant also decreases. In sample $Ba(Ti_{.975}V_{.025})O_3$ titanium is replaced by 0.025 mole fraction vanadium. The vanadium has larger ionic radius and electronic polarizability than titanium. The dielectric constant should be increased in that case. But dielectric constant decreases. The outer shell electron configuration of vanadium and titanium might have cause the decrease of dielectric constant. Other reasons for decrease of dielectric constant is also porosity and increase of electrically conducting grain and decrease of insulating grain boundaries. In sample $Ba_{.9}Sr_{.1}(Ti_{.975}V_{.025})O_3$ barium also is replaced by 0.1 mole fraction strontium. Strontium has smaller ionic radius and electronic polarizability than barium. The dielectric constant decreases and has no significant effect due to smaller ionic radius electronic polarizability. In sample $Ba_{.8}Ca_{.1}Sr_{.1}(Ti_{.975}V_{.025})O_3$, barium is replaced by 0.1 mole fraction barium. It can also he seen that for sample $Ba_{.8}Ca_{.1}Sr_{.1}(Ti_{.975}V_{.025})O_3$ the doping of calcium has positive effect.

Fig-5.13: Dielectric constant as a function of
temperature at fixed frequency 1000kHz
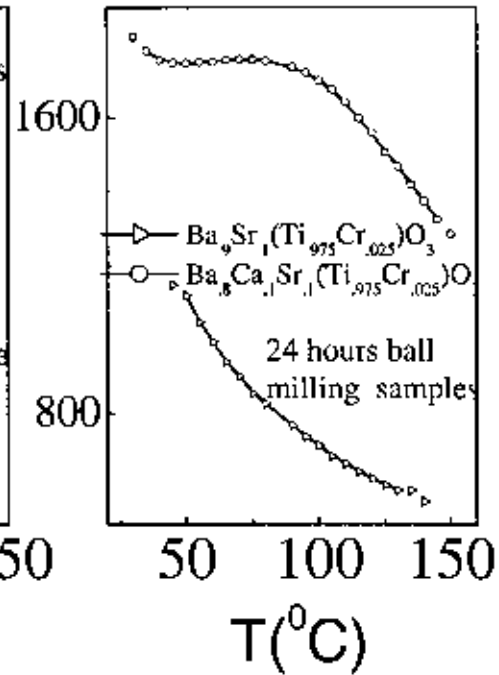
Fig-5.14: Dielectric constant as a function of
temperature at fixed frequency 1000kHz

Figure 5.13 and 5.14 indicates the dependence of dielectric constant as a function of temperature at a fixed frequency of 1000 kHz. These figures indicate that the dielectric constant of the sample $BaTiO_3$, $Ba(Ti_{.975}Cr_{.025})O_3$, $Ba_{.9}Sr_{.1}(Ti_{.975}Cr_{.025})O_3$ $Ba_{.8}Ca_{.1}Sr_{.1}(Ti_{.975}Cr_{.025})O_3$ increases with increasing temperature until reaching a maximum then decreases with further increase in temperature. This can be explained by the relaxation time. The relaxation move to higher temperature and the number of successful ion jump per second and also increases with increasing temperature.
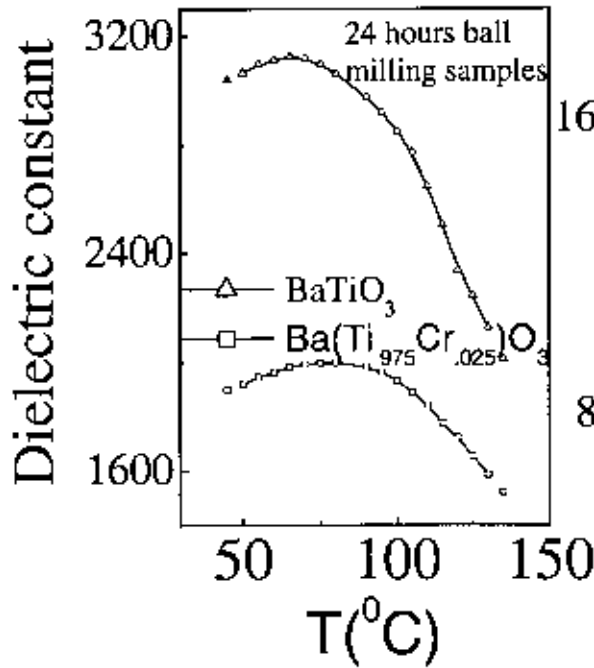
Fig-5.15: Dielectric constant as a function of temperature at fixed frequency 1000kHz
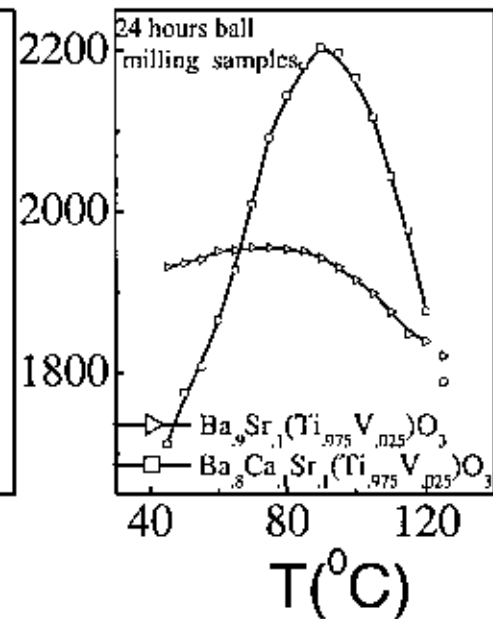
Fig-5.16: Dielectric constant as a function of temperature at fixed frequency 1000kHz

Form Figure 5.15 it can be seen that the dielectric constant for the samples $Ba(Ti_{.975}V_{.025})O_3$ and $Ba_{.9}Sr_{.1}(Ti_{.975}V_{.025})O_3$ are high particularly at low temperature and decreases as temperature is increased.

Form Figure 5.16 it can be seen that the dielectric constant for the sample $Ba_{.8}Ca_{.1}Sr_{.1}(Ti_{.975}V_{.025})O_3$ the dielectric constant increases slightly and steady with increasing temperature and then decreasing with increasing temperature.

That can be also explained by the relaxation time and number of successful ion jump per second. In this case the relaxation also moves to higher with increasing temperature.
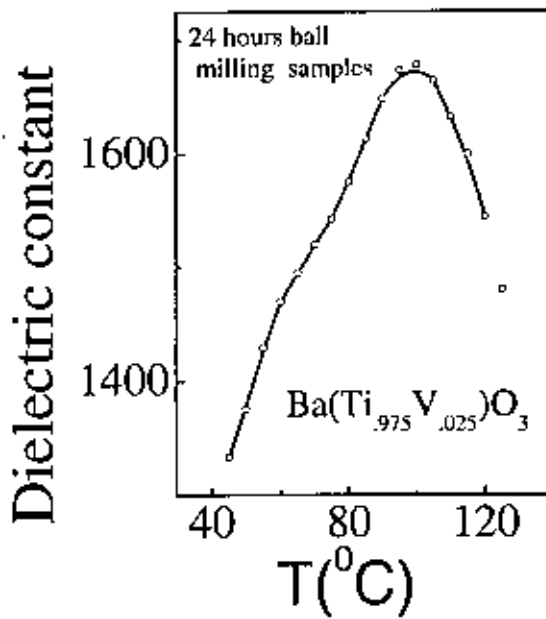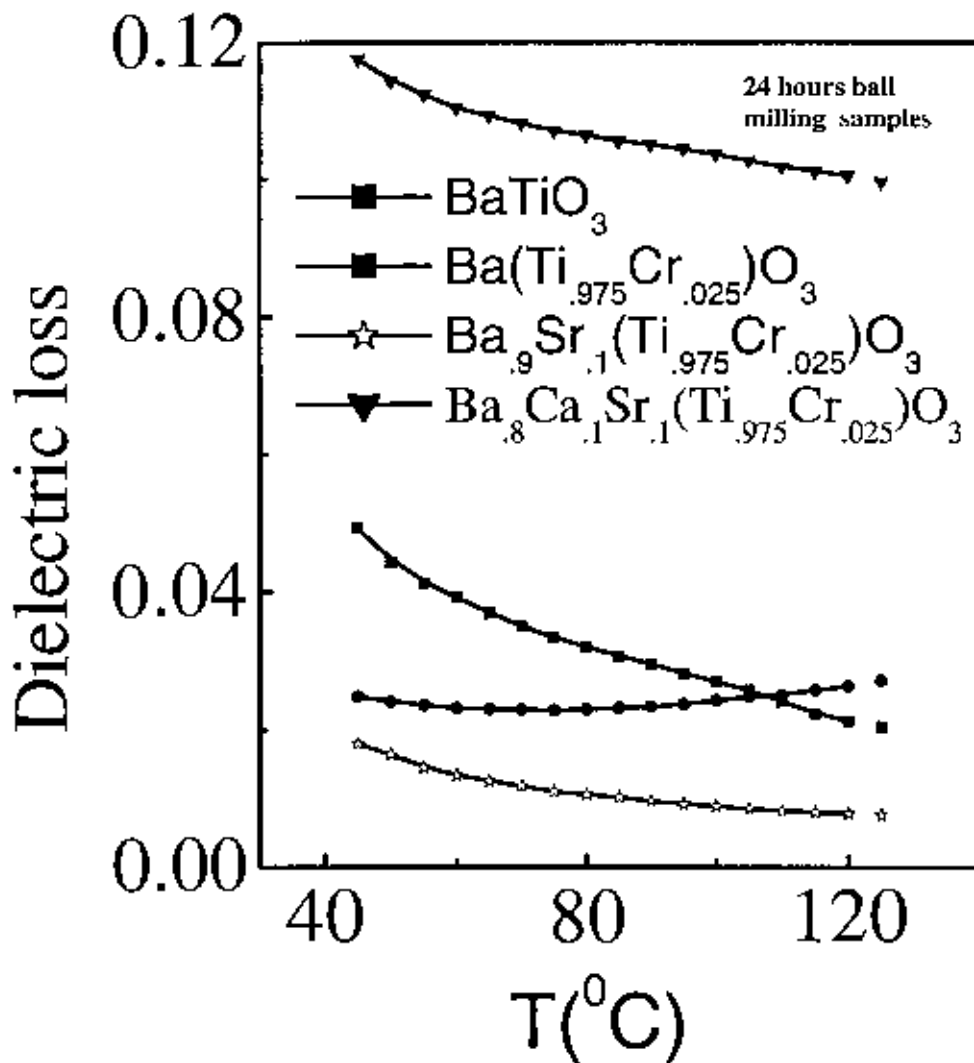
Fig-5.17: Dielectric loss as a function of temperature at fixed frequency 1000kHz

Figure-5.17. Shows the Dielectric loss as a function of temperature for the samples $BaTiO_3$, $Ba(Ti_{.975}Cr_{.025})O_3$, $Ba_{.9}Sr_{.1}(Ti_{.975}Cr_{.025})O_3$ and $Ba_{.8}Ca_{.1}Sr_{.1}(Ti_{.975}Cr_{.025})O_3$

Figure-5.17 indicates that the sample $Ba_{.8}Ca_{.1}Sr_{.1}(Ti_{.975}Cr_{.025})O_3$ dielectric loss increases and decreases with the increasing temperature. For the sample $Ba(Ti_{.975}Cr_{.025})O_3$ dielectric loss increases with the increasing temperature and for sample $Ba_{.9}Sr_{.1}(Ti_{.975}Cr_{.025})O_3$ dielectric loss decreases with the increasing temperature.
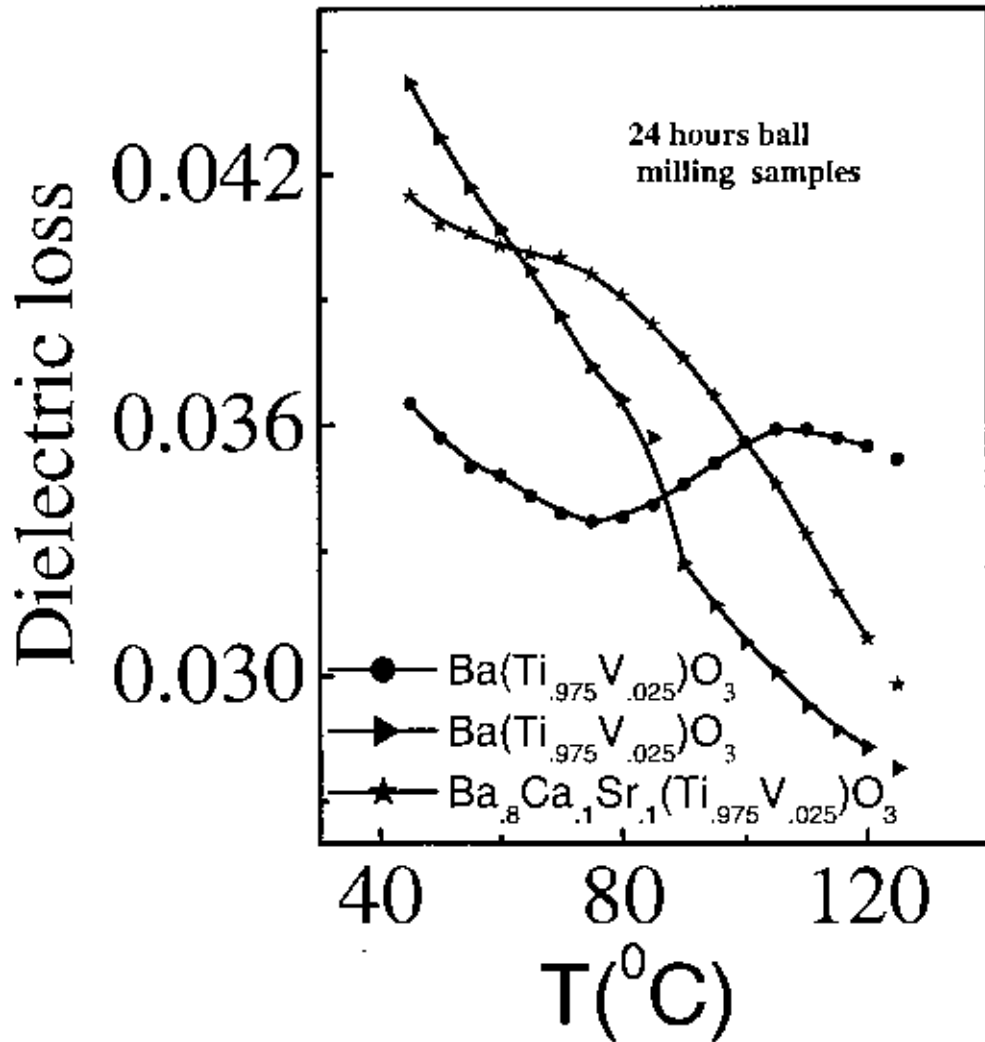
Fig-5.18: Dielectric loss as a function of temperature

Figure 5.18 indicates that for the sample $Ba(Ti_{.975}V_{.025})O_3$ the dielectric loss decreases with increasing temperature. For the sample $Ba_{.9}Sr_{.1}(Ti_{.975}V_{.025})O_3$ and $Ba_{.8}Ca_{.1}Sr_{.1}(Ti_{.975}V_{.025})O_3$ the dielectric loss decreases with increasing temperature.
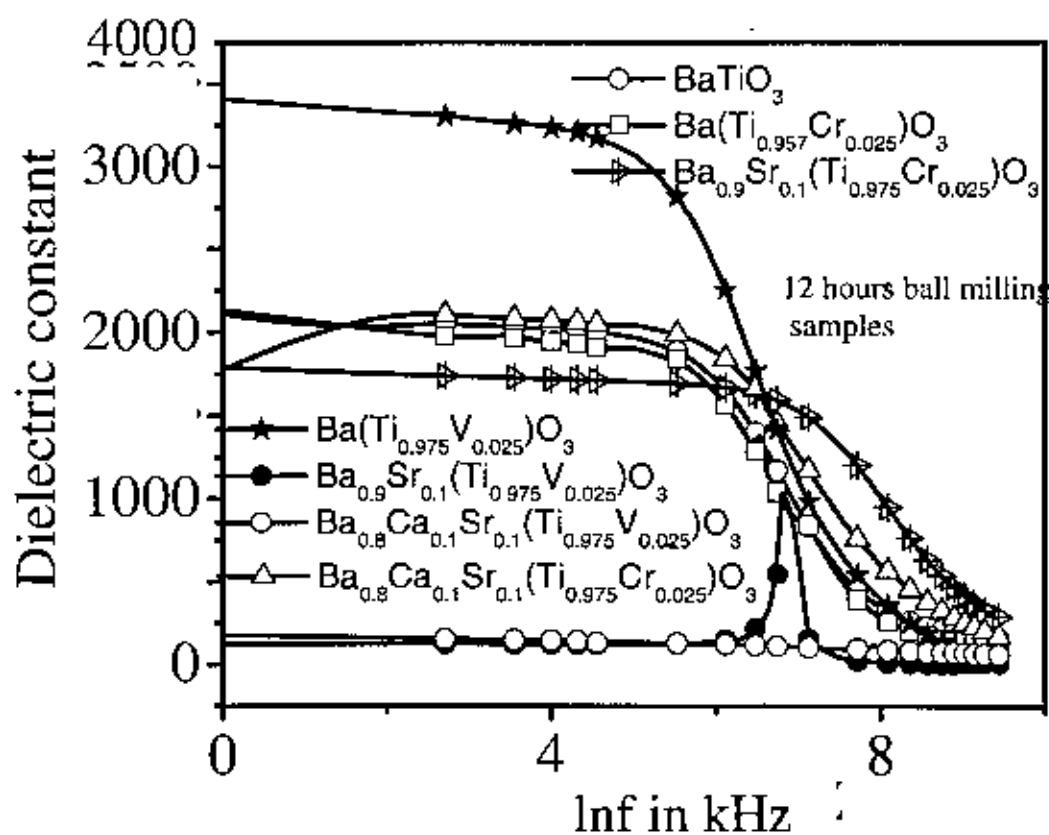
**Figure-5.19: Dielectric constant as a function of frequency
for the samples ball milling for 12 hours**

Figure 5.19 indicates the dielectric dielectric constant as a function of frequency for the samples ball milling for 12 hours.

Fig-5.20: Variation of Dielectric constant as a function of frequency (hand milling, 12 hours milling, 24 hours milling) for sample - BaTiO₃ at room temperature

Figure-5.20 indicates that dielectric constant increased dramatically for the milling behavior. Dielectric constant rapidly increased with increasing milling time. Dielectric constant of the sample BaTiO3 ball milling for 12 hours is more than the hand milling sample. Again the dielectric constant for the sample milling for 24 hours is more than the sample ball milling. This behavior can also be explained by the grain size effect. In that case milling was carried out to reduce the partial size of the powder to micron range. Particle size was reduced by the action of impact and friction of balls with powder. Fine grained samples exhibits higher dielectric constant than course grained samples.

Figure-5.21: Variation of Dielectric constant as a function of frequency hand milling, 12 hours milling, 24 hours milling for sample - $Ba(Ti_{.975}Cr_{.025})O_3$ at room temperature.

Figure 5.21 indicates that the dielectric constant also increased for the milling behavior. Dielectric constant of sample $Ba(Ti_{.975}Cr_{.025})O_3$ ball milling for 12 hours is more than the hand milling sample. Dielectric constant ball milling for 24 hours is move than the sample ball milling for 12 hours. The dielectric constant increased in later case also due to the effect of grain size.
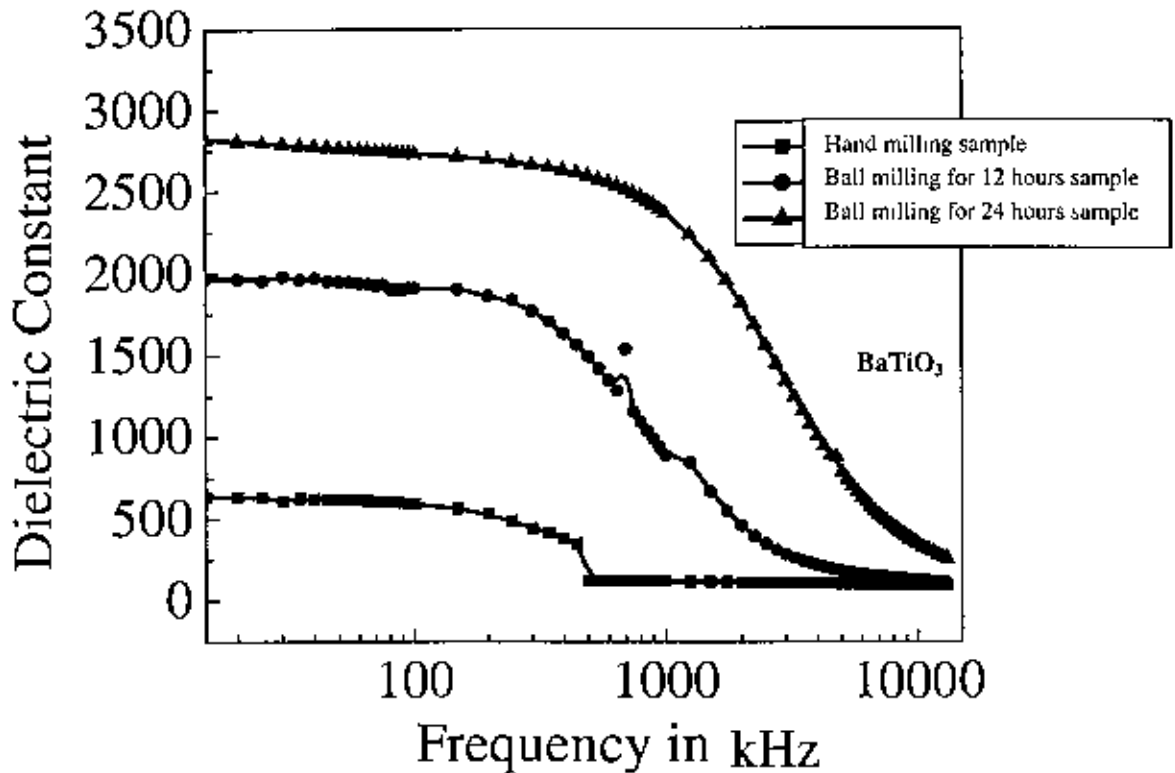
Fig: 5.22: Variation of Dielectric constant as a function of frequency (hand milling, 12 hours milling, 24 hours milling) for sample - $Ba_{.9}Sr_{.1}(Ti_{.975}Cr_{.025})O_3$ at room temperature.

Figure 5.22 indicates the dielectric constant increased for the milling behavior. Dielectric constant of sample $Ba_{.9}Sr_{.1}(Ti_{.975}Cr_{.025})O_3$ ball milling for 12 hours is more than the sample again the dielectric constant for the samples ball milling for 24 hours is more than the sample ball milling for 12 hours. The increase of dielectric constant is also due to effect of grain size

Fig-5.23: Variation of Dielectric constant as a function of frequency (hand milling, 12 hours milling, 24 hours milling) for sample - $Ba_8Ca_1Sr_1(Ti_{975}Cr_{025})O_3$ at room temperature.

Figure 5.23 indicates the dielectric constant as a function of frequency. Dielectric constant of sample $Ba_8Ca_1Sr_1(Ti_{975}Cr_{025})O_3$ ball milling for 12 hours is more than the hand milling sample. Dielectric constant ball milling for 24 hours is also more than the sample milling 12 hours. The increases of dielectric constant also due to the effect of grain size as mentioned earlier.

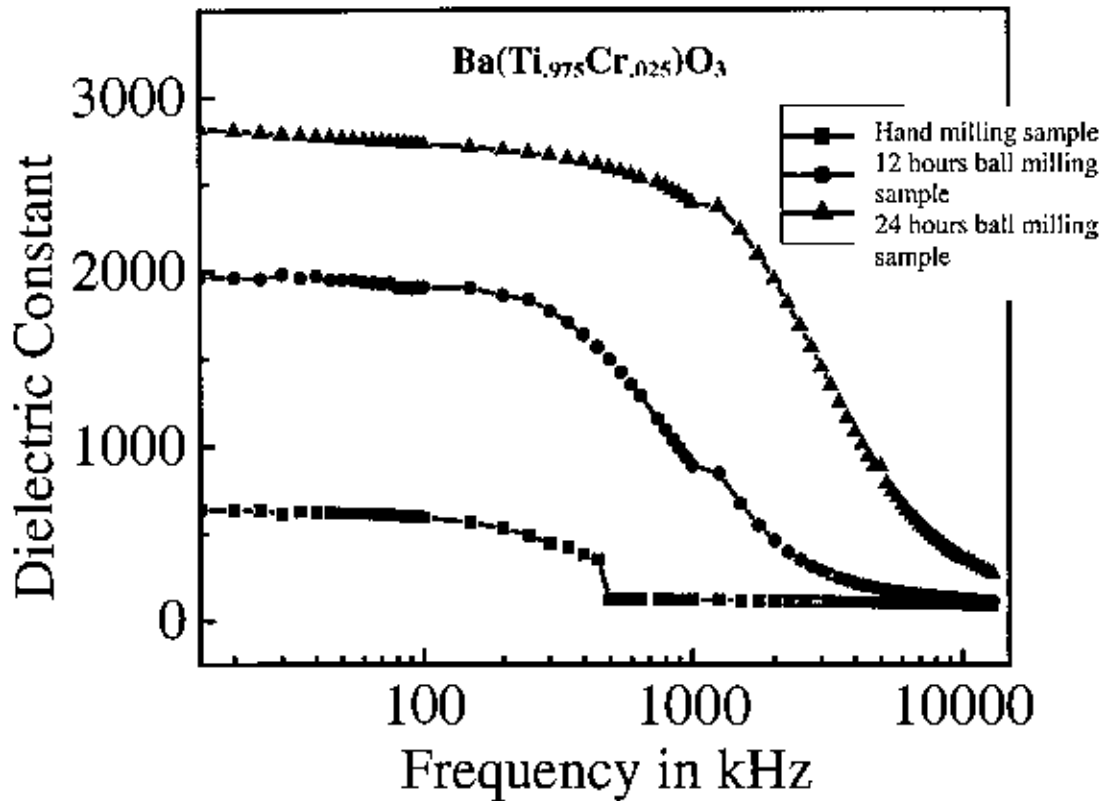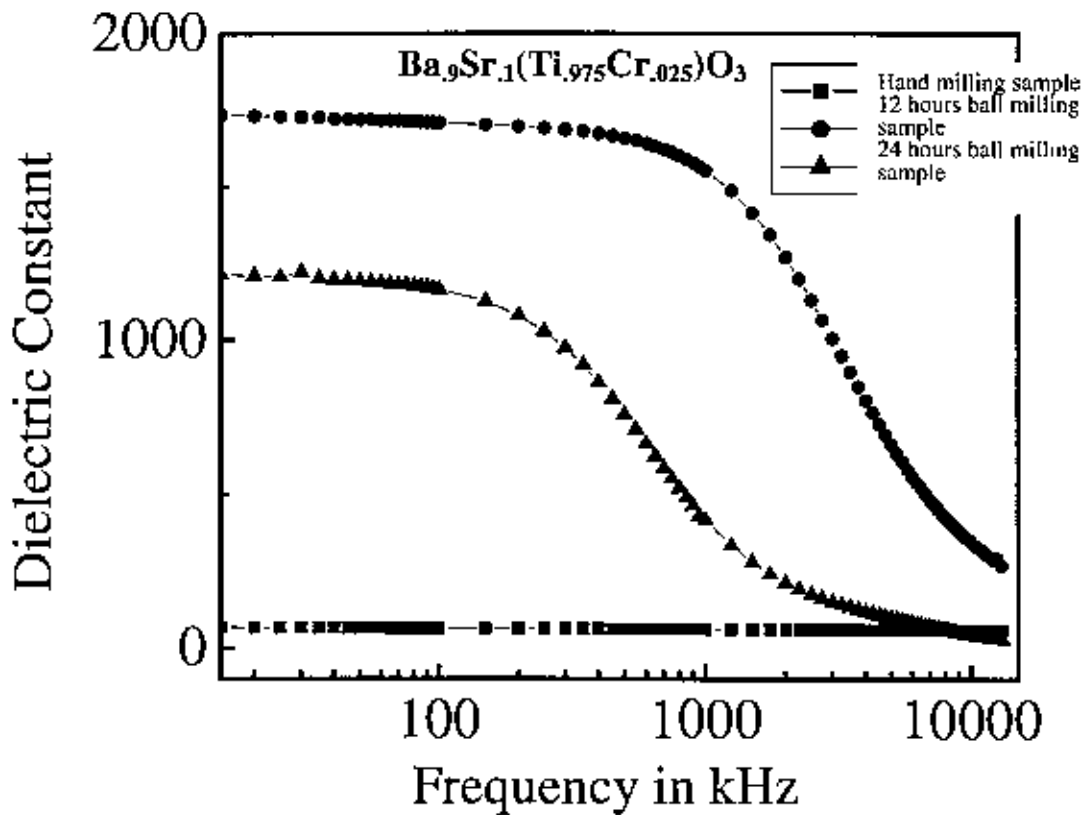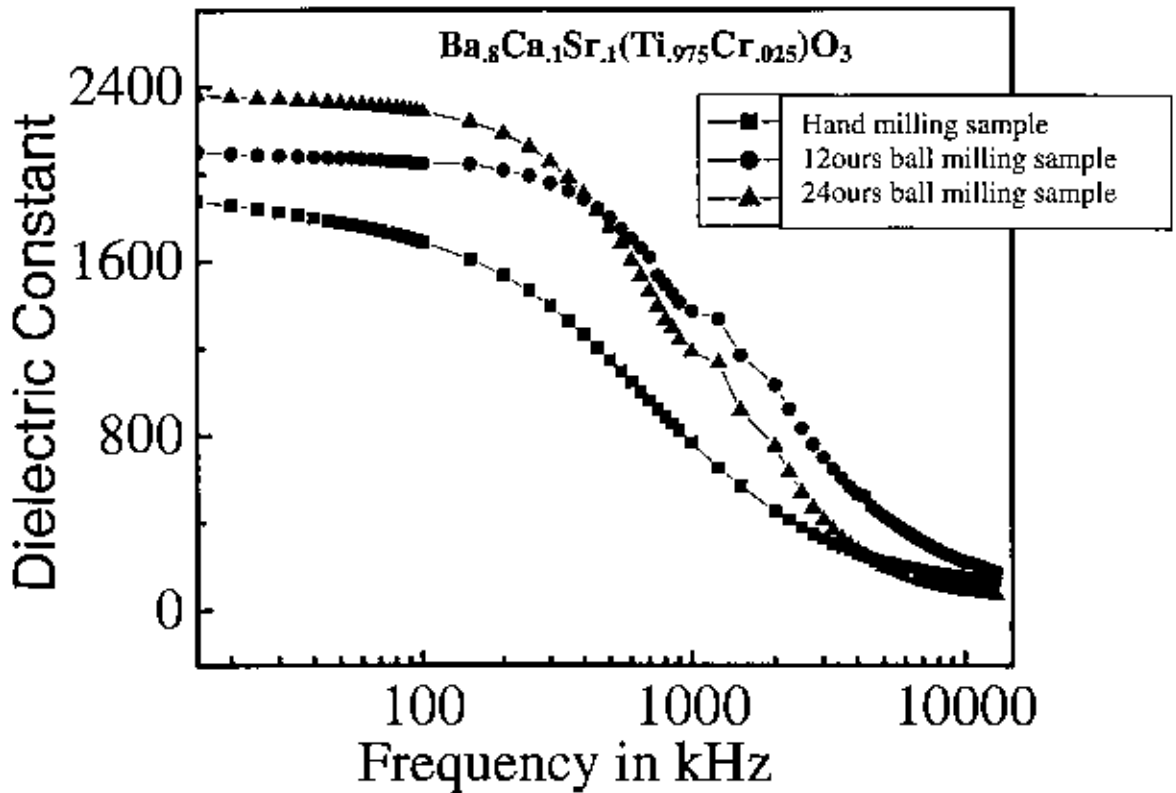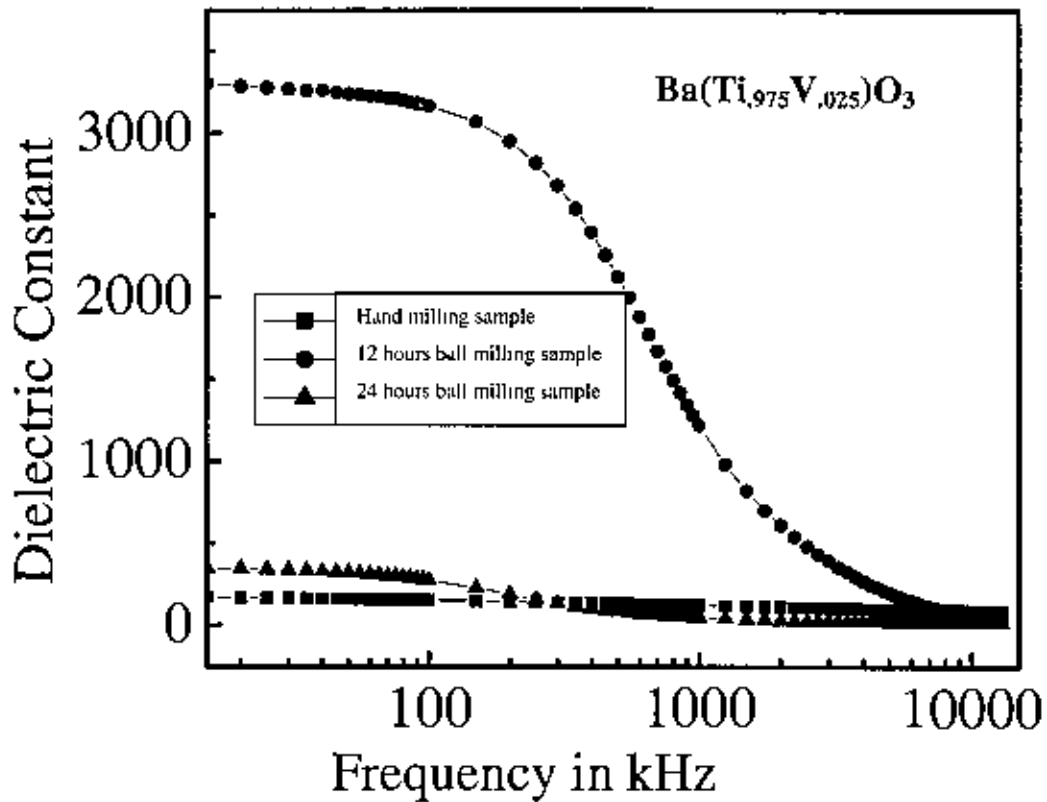**Fig-5.24: Variation of Dielectric constant as a function of frequency (hand milling, 12 hours milling, 24 hours milling) for sample - Ba(Ti$_{.975}$V$_{.025}$)O$_3$**

Figure 5.24 indicate that dielectric constant dose not increases for the milling time. The dielectric constant of sample Ba(Ti$_{.975}$V$_{.025}$)O$_3$ ball milling for 12 hours is higher than the hand milling sample. Again the dielectric constant ball milled for 24 hours is lower than the sample ball milled for 12 hours and slightly higher than the hand milled sample or almost the same. The dielectric constant for the sample ball milled for 24 hours should be higher than the sample ball milled for 24 hours. In that case dielectric constant decreased and almost same as hand milled sample. In this case for the 24 hours ball milling does not carried out to reduce the particle size. But for the 12 hours ball milling reduces the size of the powder to the micron range. In that case the size of the grain increased instead of decreased.
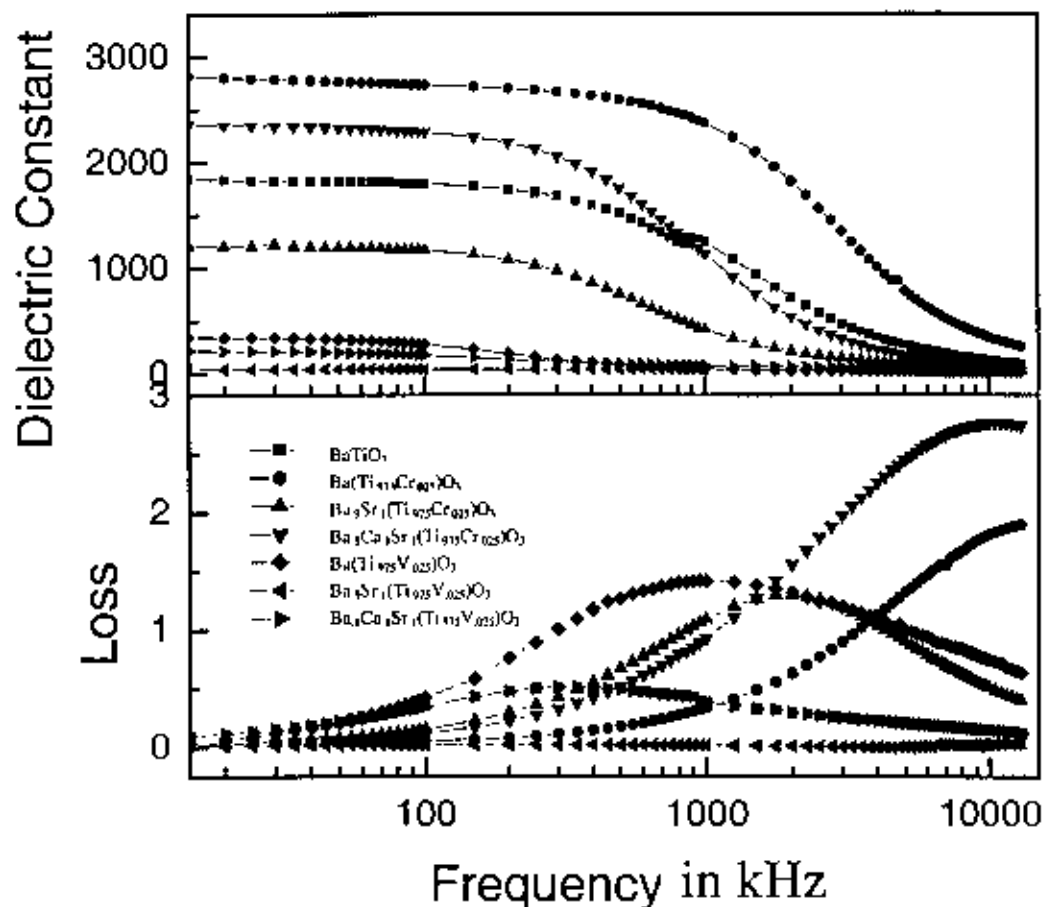
Figure-5.25: Variation of Dielectric Constant and dielectric loss as a function of frequency for all 24 hours ball-milling samples at room temperature.

Figure 5.25 shows the dielectric constant and dielectric loss for all the samples ball milling for 24hours as a function of frequency.

Table 5.25:Dielectric constant for various doped BaTiO₃ samples in frequency range .5kHz to 1000kHz.

Samples	Dielectric Constant	
	Frequency 0.5kHz~100kHz	Frequency 100kHz-1000kHz
$BaTiO_3$	1179	396
$Ba(Ti_{.975}Cr_{.025})O_3$	2300	1230
$Ba_{.9}Sr_{.1}(Ti_{.975}Cr_{.025})O_3$	488	1078
$Ba_8Ca_1Sr_{.1}(Ti_{.975}Cr_{.025})O_3$	2729	2351
$Ba(Ti_{.975}V_{.025})O_3$	304.33	86
$Ba_{.9}Sr_{.1}(Ti_{.975}V_{.025})O_3$	25.57	15
$Ba_8Ca_1Sr_1(Ti_{.975}V_{.025})O_3$	155.78	62

5.2 Calcination

Analysis of data and microstructure study do suggest three major factors calcination thermal profile, particle size of milling product and sintering thermal profile. The principal aim of calcination is to form desired phase through solid-state reaction. This kind of reaction is very sluggish and time consuming. SEM micrograph of sample $Ba(Ti_{.975}Cr_{.025})O_3$, $Ba_{.9}Sr_{.1}(Ti_{.975}Cr_{.025})O_3$, $BaTiO_3$ sintered at 1300°C are shown in figure [5.26], [5.27] and [5.28]. Sample $Ba(Ti_{.975}Cr_{.025})O_3$ seems to contain acceptable level of porosity. Close examination of the pore suggests that these pores were result of gas escape and unreacted powder that did not coagulate.

These gas escape holes might have formed due to CO_2 formation from the reaction of unreacted particles that did not form TiO_3 during calcinations. Close up of such pore shown in figure [5.26]
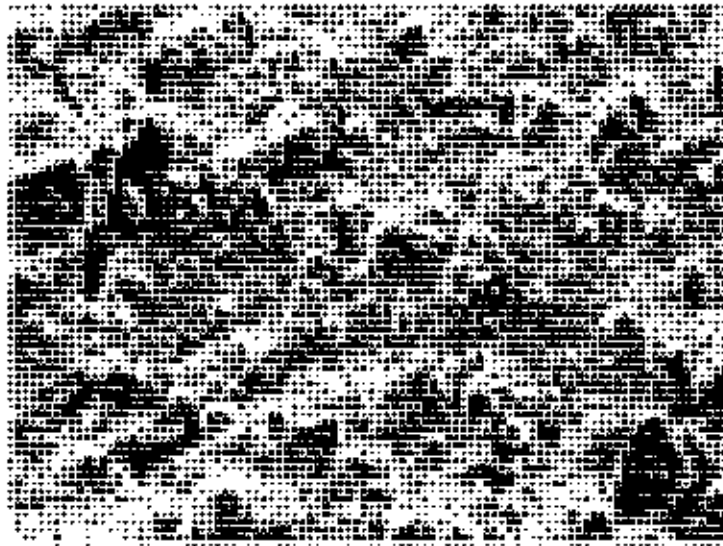
Figure-5.26: SEM micrograph of a pore for $Ba(Ti_{.975}Cr_{.025})O_3$

Fully sintered grains are surrounded by loose particles that make up the pores. Un reacted powder might be BaO and Ba_2TiO_4.
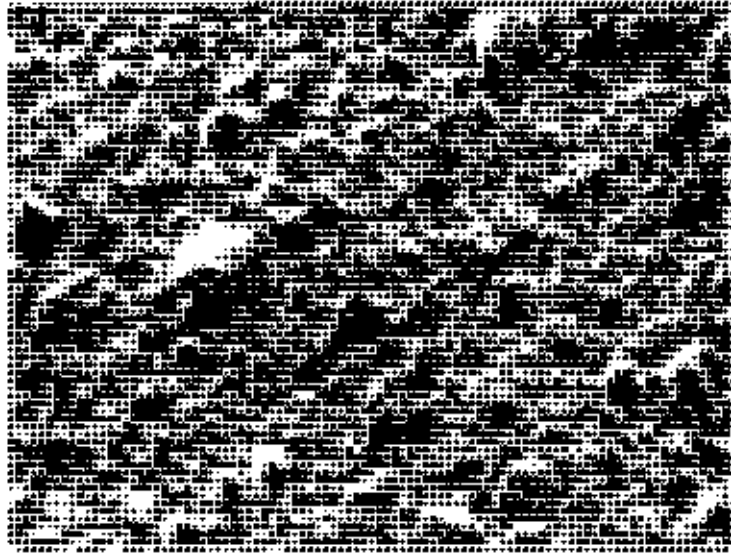
Figure-5.27: SEM micrograph of $Ba_8Sr_1(Ti_{.975}Cr_{.025})O_3$

The SEM micrograph of etched sample $Ba(Ti_{.975}Cr_{.025})O_3$ and $Ba_9Sr_1(Ti_{.975}Cr_{.025})O_3$ illustrated in figure [5.26] and [5.27] also indicate the presence of different phases and flaky morphology of the sample.
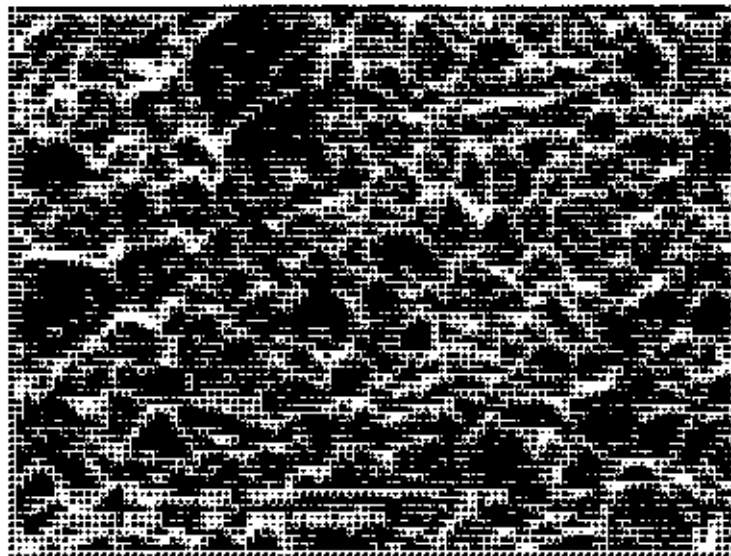
Figure-5 28: SEM micrograph of $BaTiO_3$

Figure [5.28] indicates the formation of different sizes grain and grain boundary.

Form these figures we can also see that the dielectric constant increases with increasing temperature as accepted for the semiconducting behavior until reaching a maximum, then decreases with further increases in temperature. All the figures show the temperature dependence of dielectric loss at selected frequencies. Dielectric loss is related to the homogeneity of the material.

CHAPTER 6

Conclusions

In the present study we have investigated the dielectric properties of doped $BaTiO_3$ ceramics. The dielectric constant and dielectric loss of the above doped $BaTiO_3$ have been studied as a function of frequency in the frequency range of 0.5 kHz to 13 MHz at room temperature. The dielectric constant as a function of temperature has been studied at fixed frequency 1MHz. The dielectric constant decreases in regular fashion with the increase in temperature in the range of 30 to 150°C.

No peaks were observed in the dielectric constant versus temperature range of 30 to 60°C for $BaTiO_3$ sample. The dielectric constant for $BaTiO_3$ ball milling for 24 hours was found 1179 at 100 kHz The highest value of the dielectric constant for the above sample was found 2729 for sample $Ba(Ti_{.975}Cr_{.025})O_3$.

The lowest value of the dielectric constant for the above sample was found 14.57 for the sample $Ba_{.9}Sr_{.1}(Ti_{.975}V_{.025})O_3$. The highest value of the Curie temperature was found 110°C for the sample $Ba(Ti_{.975}V_{.025})O_3$. The dielectric constant almost constant in the frequency range of 0.5 kHz to 100 kHz. The highest dielectric loss was 2.74 for the sample $Ba_{.8}Ca_{.1}Sr_{.1}(Ti_{.975}Cr_{.025})O_3$. The dielectric loss increases with increasing frequency then decreases with increasing frequency for all the sample except for the sample $Ba_{.8}Ca_{.1}Sr_{.1}(Ti_{.975}Cr_{.025})O_3$ and $Ba(Ti_{.975}Cr_{.025})O_3$.

The dielectric properties of the doped $BaTiO_3$ ceramics are affected by the grain size. The major factors, the size of the ionic radius, electronic polarizability and the outer shell electron configuration control the electrical properties. Doping variables seems to effect the density, sintering and flattening of k' peak, peak at T_c; Possibly shifting of T_c as well.

The relatively high values of the dielectric constant at low frequencies are due to the polarization ensuring that the samples can be finally considered as formed of electrically conducting grains and insulting grain boundaries. Flaky morphology of the SEM may affect the dielectric properties of the materials.

References

1. Ashok K Ganguli, PikaJha, Tokeer Ahmad and Padam R Arya "Nanometer-sized dielectric oxides: synthesis and properties" Indian J. Phys. **78A(1)** 13-17 (2004).

2. B. Jaffe, W.R. Cook and H. Jaffe "Piezoelectric Ceramic", Academic Press Limited (1971).

3. J. Nowotny and M. Rekas: pp: 1-144 in Electronic Ceramic materials Edited by J Nowotny. Tran Tec, Zurich, Switzerland, 1992.

4. Valasek, J. Phys. Rev **17**, 422-3(1921).

5. Thurnauer, H. The Rochester Engineer **21**, 74-5,77 (Nov. 1942).

6. Thurnauer, H. and Deaderick, J., U.S. Patent 2, 429, 588, Octc. **21**, 1947; field oct. 2, 1941.

7. Goldschmidt, V. M. Shrifter Norske Videnskaps. Akad. Oslo, I, Mat. Naturv. Kl. No 2, 8. (1926).

8. W.J.Merz, Phys. Rev. **91**, 513 (1953).

9. J.C. Burfoot, Ferroelectrics. Von Nostrand, New York (1963).

10. M. Saifi, B. Dubois, E.M. Vogel, J. Mater. Res, **1**, 452, (1986).

11. J.C. Chen, K. C. Lee, S. P Lin, Jpn. J Appl. Phys **39**, 1812-1814, (2000).

12. T.J. Yang. V. Gopalan, P.J. Swart, U. Mohideen, Phys. Rev. Lett **82**, 4106(1999).

13. M. Muller, E. Soergel, M.C. Wenger, K Buse, Appl. Phys; B., **78**, 367-370(2004).

14. Z. Wang, J.E. Blendell, G.S. White, Q. Jiang, Smart Mater. Struct **12**, 217-222, (2003).

15. A Panupath, Ph. D Thesis, 1999.

16. A. Von. Hippel, Rev. Modern Phys. **22**, 221 (1950).

17. D.P Cameron, IBM. Journal, **January** 1957.

18. J.A. Hooton and W.J. Merz, Phys. Rev **98**, 409 (1955).

19. U. Bottger, "Polar Oxides. Properties Characterization and Imaging". Wiley-VCH, Weinheim, **2005.**

20. J. P. Remeika, J. Am. Ceram. Soc. **76**, 940 (1954).

21. J.K. Lee, K.S. Hong and J. W. Jang, J. Am. Ceram. Soc., **84** (9) 2001-2006, (2001).

22. R.E. Newnham, "structure- Property Relations", Springer-Verlag, New York, 1957.

23. R. E. Nettleton, Ferroelectrics, 1, 3, 87 207,221 (1970).

24. R. E. Nettleton, Ferro electrics, 2, 5, 77 93 (1971).

25. R.E Newnham, L. J. Bowen, et al., Matl. Engg., 2 107 (1980).

26. F.S. Galasso, Structure- Property Relations, Springer-Verlag, 1975.

27. H.D. Megaw, Acta Cryst., **7**, 187-94 (1954).

28. C. Kittel, Introduction to solid state Physics, Wiley, New York, 1996.

29. T. Izuhar, et al., Appl. Phys. Lett. **82**, 616-618, (2003).

30. Z. C. Chen, T. Ring, J. Lematre, J. Am. Ceram. Soc. , **75**, 3201-208, (1992).

31. A. Bauger, J. Mutin, J. C. Nic pec, Mater. Sci. , **18**, 3548, 1943.

32. I. K. Templeton, J. A. Pask, J. Am. Ceram, Soc. , **42**, 212 (1959).

33. W. Maison, et. al., Science Asia, **27**, 239-243, (2001).

34. J. C. Burfoot, Ferroelectrics, Von Nostrand, New York, (1969).

35. G. Arlt, D. Hennings and G. De with, J. Appl. Phys, **58** (4), 1619-25, (1985).

36. M. A. Omar, Elementary Solid State Physics, Perason Education, Inc., (1999).

37. W. D. Kingery, Introductions to Ceramics. Jhon Wily & Sons. (1975).

38. W. R. Buessem, L. E. Cross, A. K. Goswami, J. Am. Ceram. Soc., **75**, 2927 (1996).

39. R. Gerson, J.M Peterson, D.R. Rote, J. Appl. Phys., **34**, 3242-5, (1963).

40. M. Khan, Technical Information-Multilayer Ceramic Capacitors Materials and Manufacture AVX Corporation, USA.

41. J.P. Remeika, J. Am. Cheram. Soc., **76**, 940-1 (1954).

42. T.R. Shrout, J. P. Doughery, J. Am. Ceram. Soc., **57**, (1990).

43. C. Miranda, M.E.V. Costa, M. Avdeev, A.L. Kholkin, J.L. Baptista "Relaxor Properties of Ba-based layered perovskites" J. Eur. Ceram. Soc., Vol. **21** (10-11) 1303-1306 (2001).

44. Viktor Bovtun, Jan Petzelt, Viktor. Porokhonskyy, Stanislav. Kamba, Yuri Yakimenko "Structure of the dielectric spectrum of relaxor Ferroelectrics'', J. Eur. Ceram. Soc., Vol;**21** (10-11) 1307-1311(2001).

45. Milan Marvan, Andrew K. Jonscher, Jaromir Fahnrich "Electro caloric effect as a cause of dielectric loss" J. Eur. Ceram. Soc., Vol: **21** (10-11), 1345-1348(2001).

46. M. Pereira, A.G. Peixoto, M.J.M. Gomes "Effect of Nb Doping on the micro structural and electrical properties of the PZT ceramics.''J. Eur. Ceram.Soc., Vol: **21** (10-11), 1353-1356(2001).

47. You-Ming. Tsau, Yi-Chun Chen, Hsiu-Fung Cheng, I-Non Lin, "Ferro electric (Ba,Sr) TiO_3 and $Pb(Zn,Ti)O_3$ thin films prepared by pulsed laser deposition.'' J. Eur. Ceram. Soc., Vol : **21** (10-11) 1561- 1564(2001).

48. K. Kakimoto, H. Kakemoto, A. Baba, S. Fujita, Y. Masuda "Synthesis and dielectric properties of $Sr_xBa_{1-x}Nb_2O_6$ formed by YAG Laser ablation" J. Eur. Ceram. Soc., Vol: **21** (10-11), 1569-1572(2001).

49. R.C. Buchanan, R, Palan, A. Ghaffari, K. Tran, J.E Sundeen, "Orientation effects on polarization and pyroelectric properties of ferroelectric thin films on Si," J. Eur. Ceram. Soc., Vol: **21** (10-11) 1577-1580(2001).

50. Satoshi Kazuta, Yasuo Cho, Hiroyuki Odagawa "Determination of crystal properties of peizoelectric thin film using scanning non linear dielectric microscopy." J. Eur. Ceram.Soc., Vol: **21** (10-11), 1581-1584(2001).

51. K. Reichmann, T. Schneller, S. Hoffmann-Eiffert, U. Hasenkox, R. Waser, "Morphology and electrical properties of $SrTiO_3$ films on conductive oxide films" J. Eur. Ceram. Soc., Vol: **21** (10-11), 1597-1600(2001).

52. Youichi Mizuno, Tomoya, Hagiwara, Hirokazu, Chazono, Hiroshi, "Effect of milling process on core shell micro structure and electrical properties for $BaTiO_3$-based Ni MLCC," J. Eur. Ceram. Soc., Vol: **21** (10-11) 1649-1652(2001).

53. Jae-Ho. Jeon, Yoo-Dong Hahn, Hai-Doo Kim, " Micro structure and dielectric properties of barium-strontium titanate with a functionally graded structure." J. Eur. Ceram. Soc., Vol: **21** (10-11), 1653-1656(2001).

54. S. Rodewald, J. Fleig, J. Maier, "The distribution of grain boundary resistivities in $SrTiO_3$ polycrystals: a comparison between spatially resolved and microscopic measurements" J. Eur. Ceram. Soc., Vol: **21** (10-11) 1749-1752(2001).

55. C. Hofer, U.Weber, R. Waser, "Electrical characterization of grain boundary decorated $SrTiO_3$ Ceramics." J.Eur. Ceram. Soc., Vol: **21** (10-11), 1753-1757(2001).

56. F. Zimmermann. M. Voigts, C. Weil, R. Jakoby, P. Wang, W. Menesklou, E. Ivers-Tiffee, " Investigation of barium strontium titanate thick films for tunable phase shifters" J. Eur. Ceram.Soc., Vol: **21** (10-11). 2019-2023 (2001).

57. Arlt, G. Hennings, D. and de with G., Dielectric properties of fine grained barium titanate Ceramics. J. Appl. Physic., **48(4)**, 1619-1624(1985).

58. Zhou, L. Vilarinho, P.M. and Bapita, J.L., Dependence of the structural and Dielectric properties of $Ba_{1-x}Sr_xTiO_2$ Ceramic solid solutions on raw material processing. J. Eur. Ceram. Soc., 2015-2020 (1999).

59. Lemanov, V. V., Smirnova, E.P., Syrnikov, P.P. and Tarakanov, E. A., Phase transitions and glass like behavior in $Ba_{1-x}Sr_xTiO_3$. Phy s. Rev. B 54 (5), 3151-3157 (1996).

60. C.J. Peng and H. YLa, "Compensation effect in Semi conducting Barium Titanate," J. Am. Ceram. Soc **71[1]** C-44-C-46 (1988).

61. N. Hirose and A. R. West, "Im pedance Spectroscopy of Undoped. BaTiO$_3$ Ceramics" J. Am. Ceram. Soc **79[6]** 1633-41 (1996).

62. Freer, "Micro wave Dielectric Ceramics – An overview," Silli. Ind, 9/10, 191-97 (1993).

63. Ceramic Transactions, Vol 53, Materials and processes for wireless Communications by T. Negas and H. Ling. American Ceramic Society. Westerville. OH. 1995.

64. M. Maeda, T. Yamamura, and T. I. Keda, "Dielectric Characteristics of several Complex Oxide Ceramics at Microwave frequencies" Jpn. J. Appl. Phys. Suppl, **26** 76-79 (1987).

65. W. S. Lee. D. F. K. Hennings and T. Y. Tseng "Effect of calcination temperature and $\frac{A}{B}$ Ration on Dielectric properties of (Ba, Ca) (Ti, Zr, Mn) O$_3$ Multilayer Capacitors with Ni Electrodes" J. Am. Ceram. Soc 83.1402-406 (2000).

66. K. S. Mazdiyasni, R.T. Dollof J. S. Smith II. Preparation of High Purity submicron BaTiO$_3$ Powder. J. Am. Ceram. Soc **52.** 521 (1969).

67. F. Kulcsar " A micro-structure study of Barium Titanate Ceramics" J. Am. Ceram. Soc., **39[13]** 13-17(1956).